LATE QUATERNARY PALEOCEANOGRAPHY OF THE NORTHERN INDIAN OCEAN

Thesis submitted

to

Goa University

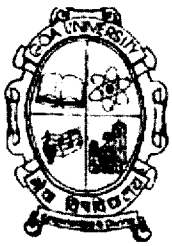

for the award of degree of

DOCTOR OF PHILOSOPHY

in

Marine Sciences

by

Pawan Govil

National Institute of Oceanography,

Dona Paula – 403 004, Goa, India.

2008

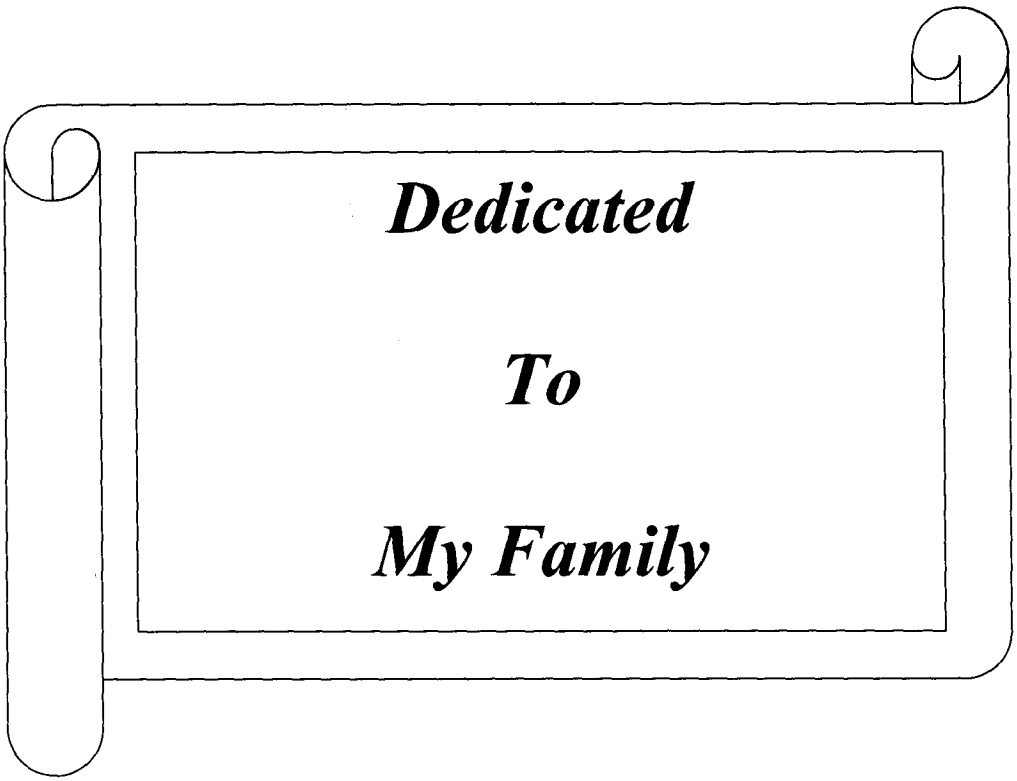
Dedicated
To
My Family

DECLARATION

I, hereby state that the present thesis entitled ***"Late Quaternary Paleoceanography of the Northern Indian Ocean"*** is my original contribution and the same has not been submitted on any previous occasions. To the best of my knowledge, the present study is the first comprehensive work of its kind from the area mentioned.

Literature related to the problem investigated has been cited. Due acknowledgements have been made wherever facilities and suggestions have been availed of.

Pawan Govil

PAWAN GOVIL

राष्ट्रीय समुद्र विज्ञान संस्थान
national institute of oceanography

Dr. P. Divakar Naidu
Scientist 'F'

February 7th 2008

CERTIFICATE

As required under the university ordinance OB-9.9, I certify that the thesis entitled ***"Late Quaternary Paleoceanography of the Northern Indian Ocean"***, submitted by **Shri Pawan Govil** for the award of the degree of doctor of philosophy in Marine Science is based on his original studies carried out by him under my supervision. The thesis or any part thereof has not been previously submitted for any other degree or diploma in any university or institution.

(P. Divakar Naidu)
Research Guide

All the suggestions made by the examiners are incorporated.

(P.K. Saraswati)
I/T. Bombay.
7.05.2008

दोना पावला, गोवा 403 004, भारत
DONA PAULA, GOA - 403 004, India

☎ : 91-(0)832-2450 450
fax : 91-(0)832-2450 602/03

e-mail : ocean@nio.org
URL : **http://www.nio.org**

Regional Centres
Mumbai, Kochi, Visakhapatnam

Contents

CHAPTER 1

Introduction

CHAPTER 2

Material and Analytical Methods

CHAPTER 3

Quantification of plaeo sea surface temperature and sea surface salinity in the Bay of Bengal: Implication on monsoon fluctuations

CHAPTER 4

Quantification of paleo sea surface temperature and sea surface salinity over last 68,000 years in the Arabian Sea: Response of evaporation–precipitation budget

CHAPTER 5

Productivity Changes in the Arabian Sea and Bay of Bengal over last 70 Kyr

CHAPTER 6

Changes of depositional environment in the Indus Fan during Late Quaternary

CHAPTER 7

List of Figures

List of Figures

List of Tables

PREFACE

The summer monsoon is the dominant climatic feature of the Indian Ocean tropics and the adjacent continent. Boreal summer is characterized by high solar radiation that causes intense sensible and latent heating over northern India and Tibet Plateau. This pattern of heating causes ascending air flow and the development of an intense low pressure cell that is centered over Asia around 30°N. The atmospheric pressure gradient between the Asian Continent and the cooler southern Indian Ocean induces large scale meridional over turning with the lower circulation limb being the strong low-level southwesterly summer monsoon winds of the western Indian Ocean. The convergence of these air masses and their uplift due to heating and orographic steering causes seasonal monsoon rains. By contrast, the winter season of the Asian sector is characterized by low solar radiation, cold temperature, and northeasterly winds, which flow from the cold Asian continent towards the Arabian Sea. These continental winter monsoon winds carry little moisture and have relatively low velocity. Thus, the unique monsoon circulation in the Indian Ocean and associated rainfall over Asia has a fundamental impact on socio-economic and agricultural development in the densely populated Asian countries as well as on the biogeochemistry of the Indian Ocean sediments.

Previous monsoon reconstructions mainly from the Arabian Sea have shown that the strength of the Indian monsoon varied significantly over decades to ice ages, in some cases, for well-established reasons such as the precessionally forced variations in summer insolation. On century to millennial time scales, high-resolution monsoon records from the Arabian Sea demonstrate that the monsoon variability is strongly linked to temperature variations in the North Atlantic region (Schulz *et al.*, 1998). The most likely mechanism for this connection indicates that the Indian monsoon is changing in response to high northern latitude temperature. Probably the initial cause of high-latitude climate change could still lie with in the tropics (Clement *et al.*, 1999). Such global teleconnection is supported by the relationship between El Nino Southern Oscillation (ENSO) activity and monsoon established both through observational and paleoclimatological data (Ivanochko *et al.*, 2005 and reference there in). In this context, the proposed research is aimed to understand the Late Quaternary Paleoceanography of the Northern Indian Ocean with the following specific objectives.

- To understand the high-resolution variability of monsoon from both the Arabian Sea and Bay of Bengal.
- To reconstruct the Sea Surface Temperature changes at selected core sites from the Arabian Sea and Bay of Bengal and to evaluate the relationships between monsoon and high latitude climate changes.
- To study the productivity changes of Bay of Bengal over last 30 kyr and compare these changes with the productivity records of the Arabian Sea.
- To understand the changes of terrigenous material supply from the Indus River during the Late Quaternary in order to understand the depositional history of Indus Fan.

This thesis comprises 7 chapters:

Chapter 1 contains general introduction to paleoclimate and impact of climate on the ancient civilization. Physiographic features of the Arabian Sea and Bay of Bengal and introduction about monsoons mechanisms. Discussed about circulation patterns of the Indian Ocean during the southwest (SW) and northeast (NE) monsoons, and changes of sea surface temperature and sea surface salinity during SW and NE monsoons. Also, introduced various proxies used in this study.

Chapter 2: This chapter deals with material and methods. To achieve the proposed objectives, detailed work has been carried out on four cores, SK218/1 and SK157/20 from western and central Bay of Bengal respectively. AAS-9/21 from the eastern Arabian Sea and Ocean Drilling Program Site 720A from northwestern Arabian Sea, Accelerator Mass Spectrometer radiocarbon ^{14}C dates was used to establish the chronology in all the cores. Magnesium/Calcium (Mg/Ca) ratios of planktonic foraminifera (*Globigerinoides ruber*) were used to reconstruct the sea surface temperatures (SST). Oxygen isotopic ratios of planktonic foraminifera (*Globigerinoides ruber*) and SST derived from the Mg/Ca were used to reconstruct the oxygen isotopic values of sea surface water. $\delta^{13}C$ and organic carbon data were used as proxies of productivity in selected cores. Geochemical elements such as Al, Ti, clay mineral and grain size analysis have been used to study the depositional history of Indus Fan during Late Quaternary.

Chapter 3: In this chapter, the results of SK-218/1, SK-157/20 were presented and discussed the role of monsoon on high latitude climate changes. In recent years a growing body of evidence has been pouring in mainly from marine records, supporting the hypotheses that temperature changes in the Arctic and Greenland steer the intensity of the Asian Monsoon (Schulz *et al.*, 1998; Kudrass *et al.*, 2001). However, the physical link between the high latitude climate and monsoons are still elusive. Therefore, here main emphasize is laid on the reconstruction of monsoon variability on centennial scale and compared these changes with Greenland Ice Core records (GISP) to explore the robust relationships between monsoon and Greenland temperatures.

The foraminiferal $\delta^{18}O$ record ($\delta^{18}Oc$) from the Bay of Bengal shows striking similarities with the GISP ice core $\delta^{18}O$ record which essentially represents changes of air temperature in the high latitudes of the northern hemisphere from 65 to 12 kyr. However, from 12 kyr to present day the Bay of Bengal $\delta^{18}O_C$ record shows rapid fluctuations as compared to the GISP $\delta^{18}O$ record. However, the isolated monsoon signal i.e. oxygen isotopic values of surface water ($\delta^{18}Osw$) of Bay of Bengal shows D-O events 1, 2, 3 and 4 very prominently with a shift of 0.54‰, 0.31‰, 0.37‰ and 0.55‰ respectively, but the timing of $\delta^{18}O_{SW}$ shifts (events) differs as compared to the GISP data set, all four events in Bay of Bengal record lead that of D-O events noticed in the GIPS core. Therefore, this suggests that the monsoon could initiate the start of millennial scale abrupt climate changes through the shifts of the Intertropical Convergence Zone (ITCZ) and associated convection, water vapor supply to the troposphere and latent heat penetration.

Chapter 4: This chapter contains sea surface temperature and sea surface salinity changes over the last 67,000 years in the eastern Arabian Sea. Here sea surface temperature and sea surface salinity changes and evaporation and precipitation (E-P) variability between glacial and interglacial were discussed. About 4.5^0C temperature change is noticed over last 67,000 years in the eastern Arabian Sea, the minimum SST of 24.5^0C during last glacial maximum and a maximum of 29^0C during the Holocene is documented. Strikingly during Marine Isotope Stage (MIS) 4 higher SST are noticed as compared to MIS 3. Similarly, the $\delta^{18}Osw$ also show higher values during MIS 4 than the MIS3, therefore, higher SST during MIS 4 would be caused the higher

evaporation in the eastern Arabian in association with less precipitation which results in higher δ^{18}Osw along the eastern Arabian Sea. The δ^{18}O record as well as SST data shows that deglacial warming was initiated around 18 cal kyr BP in the eastern Arabian Sea. Further more during the deglacial transition two episodes warm events (ASW2 and ASW1) are noticed. The comparison of δ^{18}O and SST records from the eastern and western Arabian Sea reveals that the SST and δ^{18}O shifts between last glacial maximum and Holocene show a wide contrast between these two basins. Furthermore, SST shift of 4.5^{0}C between Holocene and last glacial maximum was noticed along the eastern Arabian Sea, where as 2^{0}C SST shift documented in the western Arabian Sea. In this chapter a detailed comparison on SST and δ^{18}O changes over last 25 cal kyr BP between the eastern and western Arabian Sea were discussed.

Chapter 5: This chapter deals with paleoproductivity changes of the Bay of Bengal and Arabian Sea. Monsoons play a dominant role in controlling the regional climate, biological productivity and particulate flux supply to the sediment in the northern Indian Ocean. Sediment trap experiments have demonstrated that the biological productivity and terrigenous supply in the Arabian Sea is strongly linked to the intensity of monsoon. It is generally understood that the summer monsoon was stronger during interglacials than glacials (Prell *et al.*, 1992 and references there in). Nevertheless, the productivity proxies behave differently in different regions of the Indian Ocean, leading to contradictory conclusions on the relationship between productivity and monsoon strength (Clemens *et al.*, 1991; Naidu and Shankar 1999; Agnihotri *et al.*, 2003), most of these studies were carried out in the Arabian Sea. In this study an attempt has been first time to study the productivity changes in the Bay of Bengal and made comparison with the Arabian Sea records. The δ^{13}C data and organic carbon data from the Bay of Bengal show greater values during Holocene than in the last glacial maximum which reflects that productivity of Bay of Bengal is higher during Holocene as compared to the last glacial period. In way the productivity patterns of Bay of Bengal are very similar with that of the western Arabian Sea and the productivity changes are highly coupled with the strength of the SW monsoon.

Chapter 6: This chapter deals about the depositional history of Indus Fan during Late Quaternary and specific events of turbidity flows into the Indus Fan system. The

primary source of sediments to the Indus Fan is derived from the Indus River, which drains the arid to semi-arid western Himalaya Mountains, with headwaters at elevations greater than 4000 m and a catchment area of c. 1 X 10^6 km^2. Peak discharge occurs during the summer months as a result of seasonal glacier melting and the increased runoff generated by the summer monsoon rainfall (Milliman *et al.*, 1984). This chapter deals about how the terrigenous material supply through the Indus River to the Indus Fan varied during glacial and interglacial during Late Quaternary and also addresses the turbidity events in the Indus Fan system.

High values of calcium carbonate associating with low values of Al and Ti from 0 to 375 ka and low values of calcium carbonate along with high values of Al and Ti from 375 to 525 ka represent two distinct sedimentary sequences. The sediments deposited from 525 to 375 ka correspond to turbidite sequences, characterized by a high terigenous input of coarse-grained sediments mostly composed of sand and silt. The sediments deposited from 375 ka to the present day comprise pelagic sequences, consisting of pelagic material and clay. The major turbidity flow between 375 and 525 ka resulted in the greatest development of the Indus Fan during the Late Quaternary Period. Most of the active channels were buried by 375 ka, followed by the deposition of mainly pelagic sequences since then. The higher concentration of an Indus-derived Himalaya clay mineral assemblage (illite and chlorite) in both the turbidite and pelagic sequences reveals that the source and supply of clay minerals to the Indus Fan was the same during pre- and post- turbidite deposition.

Chapter 7 deals with summary and conclusions on the role of monsoon on the global climate, initiating of deglacial warming in the Indian Ocean, productivity variations of Bay of Bengal and the Arabian Sea and dispositional history of Indus Fan.

ACKNOWLEDGEMENTS

It was my guide, ***Dr. P. Divakar Naidu, Scientist 'F', Geological Oceanography Division, National Institute of Oceanography*** (NIO) who aroused the interest for foraminiferal research in me. With his knowledge and experience he kept paving my path without letting me stray away from my goals. It has been from his guidance, encouragement and persistence throughout the course of my research that my efforts have borne fruits and my thesis has taken shape, for which I shall ever be indebted to him.

I express my sincere gratitude to my co-guide ***Prof. G. N. Nayak, Head, Department of Marine Sciences, Goa University*** for his kind support.

I am very grateful to ***Dr. S. R. Shetye, Director, NIO*** and ***Shri. Rasik Ravindra, Director, National Center for Antarctica and Ocean Research (NCAOR)*** who have been very kind in providing all necessary facilities in their respective institutes.

I feel greatly obliged by the honorable members of the "Faculty Research Committee" – Prof. P. V. Desai Dean, Faculty of Life Sciences & Environment, Prof. G. N. Nayak, Former Dean, Faculty of Life Sciences & Environment and Head, Department of Marine Sciences, Goa University, Prof. D. J. Bhat, Former Dean, Faculty of Life Sciences & Environment, Goa University and Dr. Rajiv Nigam, Scientist, NIO. Their contribution has been invaluable especially in terms of their help and guidance during my Ph.D. registration at the Goa University, consistent monitoring of the progress of my work and offering many valuable suggestions during the course of study.

I owe deep gratitude to ***Dr. Rajiv Nigam*** for giving his moral guidance to me throughout my stay at NIO. I express my sincere thanks to him as a vice chancellor nominee from Goa University for my Ph.D.

I greatly thankful to subsequent in-charges of the Human Resource Development Group of NIO, Dr. R. Sharma, Dr. V. K. Banakar and Shri. Krishna Kumar, Member of HRDG for making the atmosphere at NIO conducive for this study.

I truly appreciate the help extended for my Ph.D. work under DAAD fellowship by Dr. Stefan Mulitza and Dr. Henning Kuhnert, Bremen University, Bremen, Germany for giving me place in their office and in the lab under this fellowship. I am also thankful to Dr. G. wefer, Director, MARUM, Bremen University, Bremen, Germany to give moral support during my stay in Germany. I gained a lot through my visit to Germany. Not only did I get an excellent exposure to the Dutch work system but my 6 months working experience on oxygen and carbon isotopes and Mg/Ca elemental ratios from planktonic foraminiferal species was indeed a great part and help to me in the field of past climate modeling during my thesis.

Obtaining Radio Carbon Dates to substantiate my data would have not been possible without the expertise and kind co-operation from Kiel University, Kiel, Germany. Their contribution is acknowledged. I especially thank Dr. B. R. Rao for making me to understand the XRD peaks of clay minerals and Dr. A. L. Paropkari for providing the AAS-9/21 core samples.

I will fail in my duty if I do not acknowledge the contributions of a few senior scientists from NIO namely, Drs. V. Ramaswamy, O. S. Chauhan, V. K. Banakar, D. V. Borole, R. Banerjee, M. Shyamparasad, S. D. Iyer, G. Ranade, M. V. Ramanna, A. R. Gujar, B. Ingole, M.V.S.N. Guptha, S. Prasanna Kumar S/Shri M. C. Pathak, K. L. Kotnala. I thank one and all for their help and encouragement. I am also thankful to Dr. M. P. Tapaswi, Documentation Officer, NIO and his staff for helping me procure certain books and journals as per the demands of my research.

I express my sincere thanks to my colleague Dr. Abhijit Mazumder for generously devoting his valuable time at the eleventh hour. I owe much to Dr. Rajeev Saraswat for his advice, constructive criticism and help during various stages of this work. I am indebted to Mrs. Sujata Kurtakar Raikar, Rajani Panchang Dhumal, Kum. Linshy V. N. and Shri. Sanjay Singh Rana, D. H. Shanmukha for their full support for computational and graphical work, and Kum. Swati Bhonsle, Lea Baretto processing samples used in this study.

I have given finalization of my thesis writing in National Centre for Antarctic and Ocean Research, Goa, with moral support from all senior scientists. Few friends from NCAOR made my way easier during final stages of thesis and tried their level best to keep my head cool, namely Dr. S. Saini, Kamlesh Verma, Lalit Ahirwar, Rajshree, Rekha.

I take this opportunity to thank my friends Dr. P. V. Bhaskar, Dr. Jaysankar De, Pranab Das, Mandar Nanajakar, Sanjay Singh, Anand Jain, Ravi Naik, Vishwas Patil, Chetan Gaonkar, Ram Meena, Dr. Tomchu Singh, Dr. Sameer Damre, Varda Damre, Radhika, Sree S. Nair, Shamina D'Silva, Priya D'Costa for helping me in my tough times.

The present work is a part of the NIO's institutional project [MLP0003] on Paleoclimate.

My acknowledgement is incomplete without a special mention of my parents and my family members who have been most supportive throughout the duration of my research. Without their love, blessings and encouragement, this thesis would not have materialized.

CHAPTER 1

Introduction

1.1 Global Climate:

The average weather condition over a long period (a minimum of 30 years) is known as climate. Climate varies on different time scales ranging from interannual to millions of years, as well as from region to region. Climatic fluctuations on different time scales are forced by both internal and/or external mechanisms that operate at different frequencies. For example, glacial and interglacial changes on time scales of thousands of years are the most conspicuous climate fluctuations noticed in the Earth's History during the Quaternary. James Croll was the one who proposed that glacial–interglacial cycles are related to the variations in the orbital configuration of the Sun and Earth (Croll 1867). The hypothesis was later elaborated by Milankovitch (1941) and more recently by Berger (1977).

The changes in orbital configuration of the Sun and Earth include variation in the position of equinoxes and solstices with respect to the perihelion, the obliquity of the Earth's ecliptic, and the eccentricity of the Earth's orbit with average periodicities of approximately 23,000, 41,000 and 100,000 years, respectively. These orbital variations are termed as Milankovitch cycles, after Milutin Milankovitch. The Earth's Eccentricity which is defined as the shape of the Earth's orbit around the Sun and varies from circular to elliptical, over a period of about 100,000 years. Obliquity (Axial tilt), is the inclination of the Earth's axis with respect to its plane of revolution around the Sun. Change in the degree of Earth's axial tilt occurs on a periodicity of 41,000 years from 21.5 to 24.5 degrees. Precession, which is defined as the Earth's slow wobble back and forth on its spin axis. The precession has a periodicity of 23,000 years. The combined effect of these three parameters (Eccentricity, Obliquity and Precession) is semi-annual insolation variation. This insolation variation has an approximate periodicity averaging about 41,000 years in the middle and high latitudes, and 21,000 years in the low latitudes. Beside these long-term changes, solar insolation also varies over decadal to centennial scales thus affecting various biotic and abiotic processes and components of the Earth including human beings.

1.2 Role of Climate on Ancient Civilizations:

Climate has played an important role to establish the evolutionary human life and the domestication of plants and animals. Recent archeological evidences from Yana River, Siberia indicate that the human adaptation to harsh and frigid climate began around 27,000 years ago (Pitulko *et al.*, 2004). Likewise, humans adapted to arid condition in Thar and Sahara desert in the late Holocene and subsequently several human civilizations adapted to the rapid shift in climate. Evidences also exist that the collapse of human civilizations caused due to abrupt climate changes, for example collapse of Maya, Akkadian, Mochika and Tiwanaku were attributed to comparatively rapid change in climatic conditions (deMenocal 2001; Haug *et al.*, 2003). The Indus Valley Civilization was at the height of its glory during the period when Egyptian, Babylonian and Mesopotamian Civilizations were existing in the present day Middle East. Archaeologists believe that the Indus Valley Civilization belonged to the period between 3500 BC and 2800 BC. The decline of Indus Valley Civilization from 3500 years BP was ascribed to the onset of arid climate (Naidu 1996; Gupta 2004). As climatic changes disrupted the agriculture which was the main occupation of the Indus Valley people (crops such as wheat, barley, peas and bananas were grown). As the agriculture was heavily monsoon dependent, changes in monsoon pattern lead to the failure of different crops and thus the collapse of the civilization.

1.3 Monsoon:

The word "monsoon" is derived from the Arabic word mausim, which means season. Wind blows from ocean to land during the summer and from land to ocean during the winter in the Indian Ocean. This seasonal reversal of the wind direction between summer and winter drives the southwest and northeast monsoons in the Indian Ocean and precipitation in the South Asia. Upliftment of the Himalaya and the Tibetan Plateau occurred coeval with the increase in strength of the Indian Monsoon, thus the evolution of Indian Monsoon has direct bearing with the uplifment of Himalayas (Prell *et al.*, 1992). The evolution of Indian Monsoon started in the late Miocene, at about 9.5 Million years (Ma). Between 9.5 and 5.0 Ma the monsoon increased noticeably in strength. The fundamental mechanism of the monsoons is: (1) the differential heating of the land and ocean and the resulting pressure gradient that drives the winds from high pressure to low pressure, (2) the swirl introduced to the

winds by the rotation of earth, and (3) moist processes that determine the strength, vigor, and location of the major monsoon precipitation by storing, redistributing, and selectively releasing, in the vicinity of the heated continents, the solar energy arriving over most of the tropics and subtropics (Webster 1987). The combined effect of these three mechanisms produces the monsoon's characteristic reversals of high winds and precipitation.

1.3.1 Southwest (Summer) Monsoon:

The summer monsoon is the dominant climatic feature of the tropical Indian Ocean and the adjacent continent. Boreal summer is characterized by high solar radiation that causes intense sensible and latent heating over northern India and Tibet Plateau. This pattern of heating causes ascending air flow and the development of an intense low pressure cell that is centered over Asia at around 30°N and high pressure over relatively cold southern tropical Indian Ocean (Fig. 1.1).

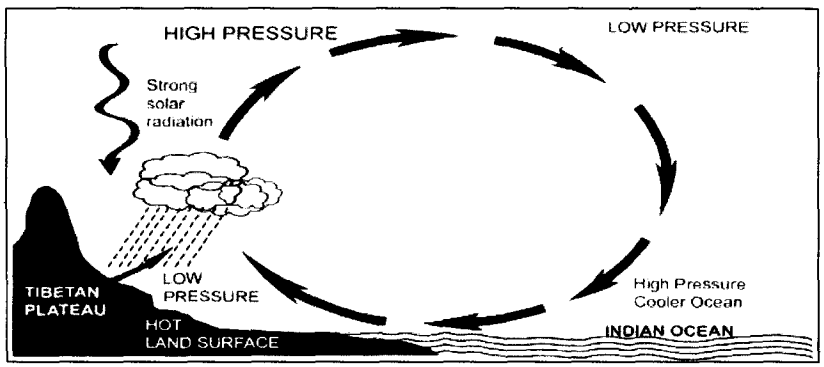

Figure 1.1 The climate model controlled by summer monsoon.

The atmospheric pressure gradient between the Asian continent and the cooler southern Indian Ocean induces large-scale meridional overturning with the lower circulation limb being the strong low-level southwesterly summer monsoon winds of the western Indian Ocean. The convergence of these air masses and their uplift due to heating and orographic steering causes seasonal monsoon rains.

1.3.2 Northeast (Winter) Monsoon:

During northern hemisphere winter season, Central Asia, Tibet and the Himalayas are covered by snow and ice. Most of the solar insolation during these

months is reflected by the high albedo of snow which results in significant loss of heat causing cooling of air in the tropospheric region and sinking to the ground, forming a high pressure cell over Asia (from Siberia to northern India). On the other hand, warm sea surface temperature of the tropical Indian Ocean result in ascent of warm air to the troposphere and thus development of low pressure region (Fig. 1.2).

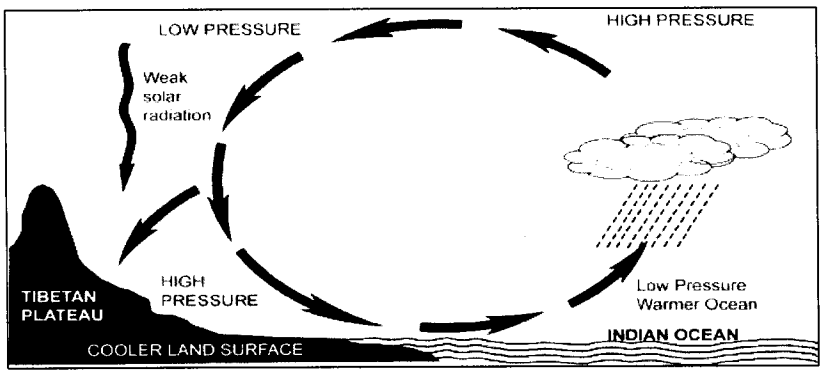

Figure 1.2 The climate model is controlled by winter monsoon.

The development of such pressure gradient between the cool land and warm oceans sets in northeasterly winds, which flow from the cold Asian continent towards the Arabian Sea. These continental winter monsoon winds carry little moisture and have relatively low velocity.

1.4 Indian Ocean Circulation:

1.4.1 Southwest Monsoon:

During southwest (SW) monsoon the surface low level southeasterly trade winds of the Southern Hemisphere extend across the equator to become southerly or southwesterly in the Northern Hemisphere. The frictional stresses of these south-westerly winds in turn drive the Somali Current (SC) flowing northward as western boundary current, the westward flowing South Equatorial Current (SEC) and east ward flowing monsoon current (MC) (Wyrtki 1973). In the eastern Arabian Sea, the West Indian Coastal Current (WICC) including Laccadive Low (LL) flows south during the SW monsoon and joins Southwest Monsoon Current (SMC) which moves eastward (Fig. 1.3).

East Indian Coastal Current (EICC) bifurcates in the Bay of Bengal, which is supplied by SMC from south of the Sri Lanka. Off Sumatra, the monsoon currents cross the equator and turn in to the SEC. These three currents, viz. monsoon current,

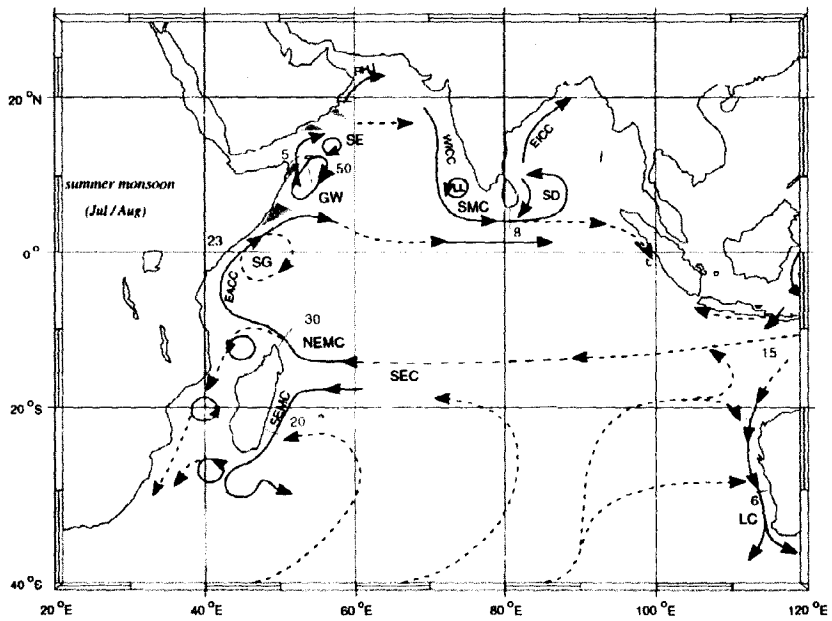

Figure 1.3 Circulation pattern of the Southwest Monsoon. Current branches indicated are the South Equatorial Current (SEC), South Equatorial Countercurrent (SECC), Northeast and Southeast Madagascar Current (NEMC and SEMC), East African Coast Current (EACC), Somali Current (SC), Southern Gyre (SG) and Great Whirl (GW) and associated upwelling wedges, Socotra Eddy (SE), Ras al Hadd Jet (RHJ) and upwelling wedges off Oman, West Indian Coast Current (WICC), Laccadive High and Low (LH and LL), East Indian Coast Current (EICC), Southwest and Northeast Monsoon Current (SMC and NMC), South Java Current (JC) and Leeuwin Current (LC). From Schott and McCreary (2001).

South Equatorial Current and Somali Current, form a very strong wind driven gyre in the equatorial Indian Ocean (Wyrtki 1973).

The more vigorous atmospheric and oceanic circulation during the SW monsoon not only develops the strong western boundary current, the Somali current, but also intense upwelling along the coasts of Somalia and Oman. The upwelling along the coast of Somalia and Oman generates a summer primary productivity bloom that produces approximately 200 g Carbon/m^2/Y and 70-80 % of the flux of organic matter to the sediments, considered as highest in the world's ocean (Nair *et al.*, 1989). The upwelling along the coast is the most intense between 5° N to 11° N, where the entire warm surface layer is removed and subsurface water with temperature well below 20° C reaches the sea surface (Warren 1966).

1.4.2 Northeast Monsoon:

Indian Ocean circulation during northeast (NE) monsoon is relatively weak and characterized by the North Equatorial Current (NEC), an eastward flowing Equatorial Counter Current (EEC) (Fig. 1.4). The East African Coastal Current (EACC) meets southward flowing near surface Somali Current (SC) in a zone of 2-4° S, and the two flows then supply the eastward-flowing South Equatorial Countercurrent (SECC) (Wyrtki 1973; Schott and Mc Creary 2001).

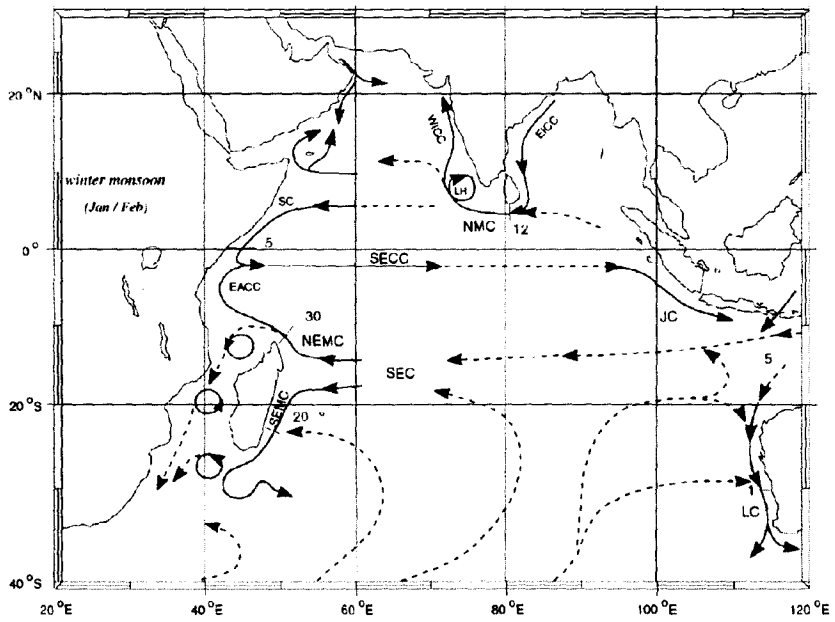

Figure 1.4 Circulation pattern of the Northeast Monsoon. Current branches indicated are the South Equatorial Current (SEC), South Equatorial Countercurrent (SECC), Northeast and Southeast Madagascar Current (NEMC and SEMC), East African Coast Current (EACC), Somali Current (SC), Southern Gyre (SG) and Great Whirl (GW) and associated upwelling wedges, Socotra Eddy (SE), Ras al Hadd Jet (RHJ) and upwelling wedges off Oman, West Indian Coast Current (WICC), Laccadive High and Low (LH and LL), East Indian Coast Current (EICC), Southwest and Northeast Monsoon Current (SMC and NMC), South Java Current (JC) and Leeuwin Current (LC). From Schott and McCreary (2001).

The winds blowing from the northeast during the winter months are dry because they have lost the moisture on the Asian landmass. As these winds approach the southern tip of India, the state of Tamil Nadu, they do pass over the Bay of Bengal and pick up moisture. Tamil Nadu then receives most of its rainfall during these months. During the NE monsoon, water movements to the north of the Equator are from east to west, forming the Northeast Monsoon Current (NMC). This flow starts

from November, reaches its highest in February and subsides in April. NMC low salinity water mass flows to the north and reaches west coast of India in November to January. In Arabian Sea off Somalia most of its water turns south, crosses the equator and forms the Equatorial Countercurrent (Fig. 1.4). During NE monsoon, the surface flow does not appear to penetrate beyond the thermocline. Thus upwelling in Indian Ocean does not occur during NE monsoon season, except along eastern shore of Andaman Sea and in the northern part of Arabian Sea off Karachi (Wyrtki 1973).

Ship-drift data (Defant 1961; Rao *et al.,* 1989) and surface-drifter data (Molinari *et al.*, 1990; Shenoi *et al.*, 1999) shows broad westward or southeastward flows across the Arabian Sea during the winter monsoon. Towards late spring and early summer, the weather is hot and dry over most of the subcontinent (Wyrtki 1973).

1.5 Water Masses:

Northern Indian Ocean has two different water masses. A high salinity water mass is formed in the Arabian Sea due to excess evaporation and the subsurface flow of Persian Gulf and Red Sea water (Wyrtki 1973). A low salinity water mass is formed in the Bay of Bengal by excess precipitation and abundant river runoff. During SW monsoon high precipitation in the Bay of Bengal and more fresh water discharge from Ganges, Brahmaputra, Irrawadi and Godavari forms a north-south salinity gradient in the Bay of Bengal, ranging from 26 to 34 psu (Levitus *et al.*, 1994) (Fig. 1.5).

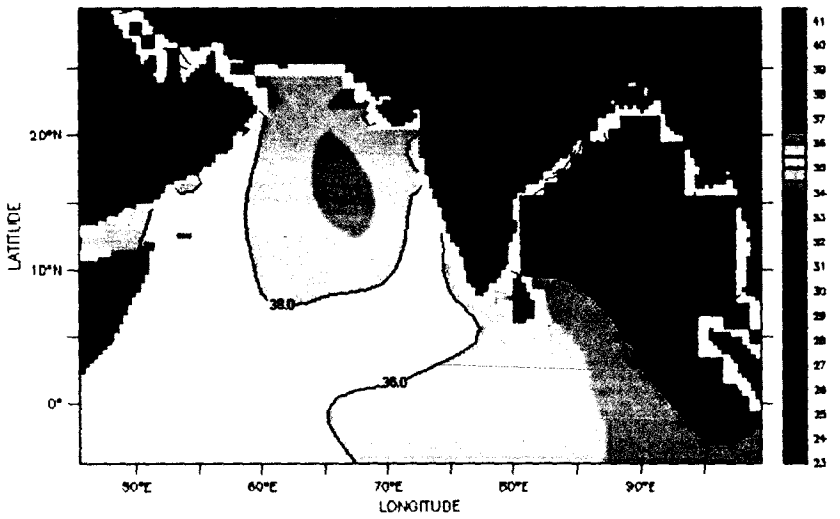

Figure 1.5 Average sea-surface salinity in the northern Indian Ocean during the SW monsoon (Levitus *et al.*, 1994).

By contrast, in the Arabian Sea, salinity decreases north to south, with highest salinity (38 psu) in the northern Arabian Sea and low salinity (36 psu) in the southern Arabian Sea (Levitus *et al.*, 1994) (Fig. 1.5).

More evaporation and less river discharge and precipitation during NE monsoon increase the salinity of Bay of Bengal. During NE monsoon low salinity surface water of Bay of Bengal moves westward of the South Equatorial Current. The salinity of Bay of Bengal surface water increases north to south from 30 psu to 34 psu (Fig 1.6). Sea surface salinity varies from 36 to 38 psu in the Arabian Sea (Fig. 1.6). High salinity surface waters of the Arabian Sea spreads southwest into off Somalia during NE monsoon and is drawn into Equatorial Counter Current.

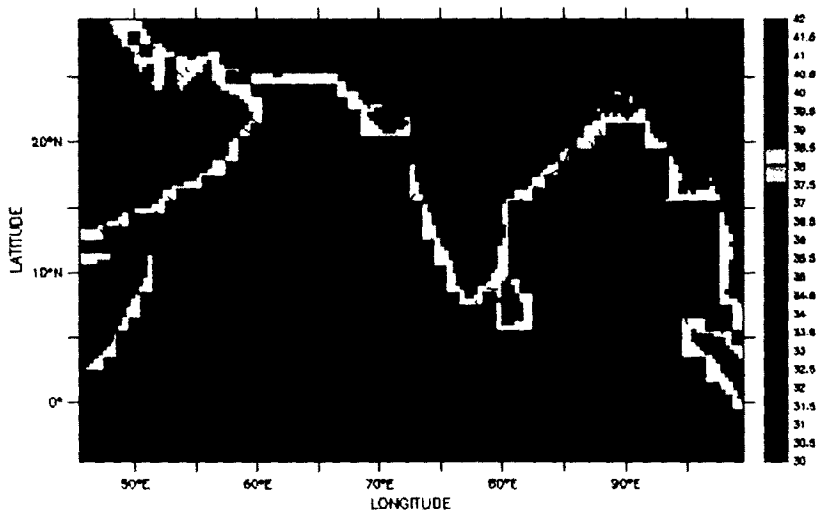

Figure 1.6 Average sea-surface salinity in the northern Indian Ocean during the NE monsoon (Levitus *et al.*, 1994).

Whereas during SW monsoon it spreads in south and then turns to the east. High salinity surface water penetrates deeper up to the thermocline and forms subsurface high salinity water. In addition to the evaporation in the Arabian Sea, two other high salinity water masses affect the subsurface water, the water from the Persian Gulf and Red Sea at the depth of 300 m in Gulf of Oman and 800 m depth in Gulf of Aden, respectively.

In contrast to the salinity pattern in the northern Indian Ocean, variation in sea-surface temperature (SST) is minor (Fig. 1.7). Much of the regional temperature variation is due to upwelling of cooler subsurface waters in the western Arabian Sea

during the SW monsoon. This creates an east-west temperature gradient ranging from 25.0° C to 28.2° C in the Arabian Sea (Fig. 1.7).

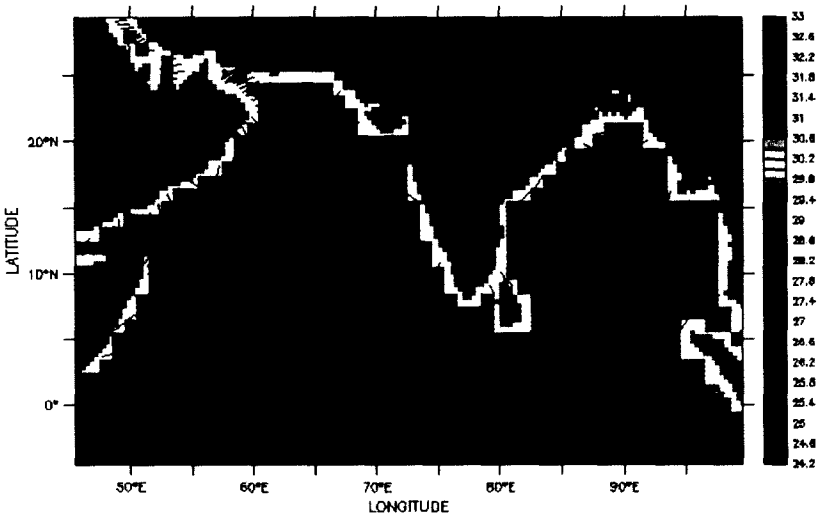

Figure 1.7 Average sea-surface temperatures in the northern Indian Ocean during SW monsoon (Levitus and Boyer 1994).

During the SW monsoon, SST of the Bay of Bengal varies from 28.0° C to 28.6° C (Levitus and Boyer 1994) with a weak east-west gradient (Fig. 1.7). During the NE monsoon, equatorial Indian Ocean surface water remain between 28.0° C to 28.5° C, a weak north-south gradient in the Bay of Bengal (Fig. 1.8) and weak NW-SE gradient occurs in the Arabian Sea (Fig. 1.8).

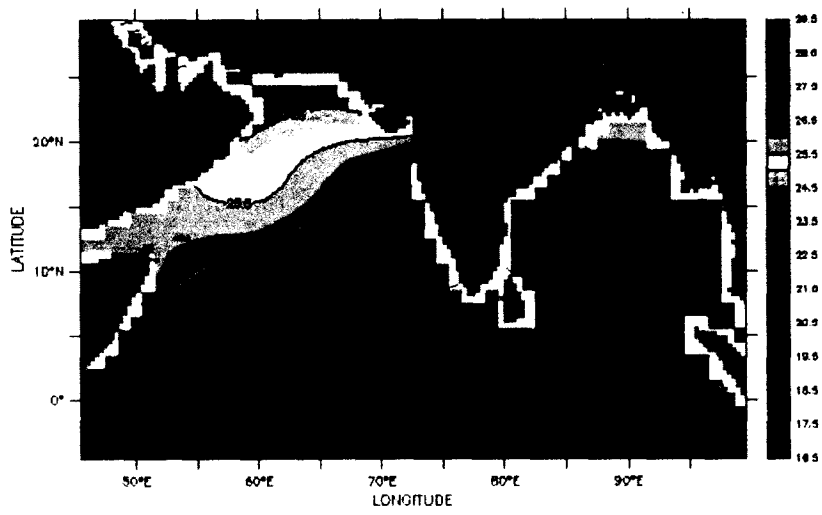

Figure 1.8 Average sea-surface temperatures in the northern Indian Ocean during NE monsoon (Levitus and Boyer 1994).

1.6 Physiographic Features of the Northern Indian Ocean:

Northern Indian Ocean has two major submarine fans, the Indus Fan in the Arabian Sea and the Bengal Fan in the Bay of Bengal (Fig. 1.9). The Arabian Sea covers an area of about 3,863,000 km^2, and is surrounded by arid landmasses to the west and north and by coastal highlands of western India to the east. Three main major rivers discharge fresh water and sediment into the Arabian Sea, viz. Indus, Narmada and Tapti.

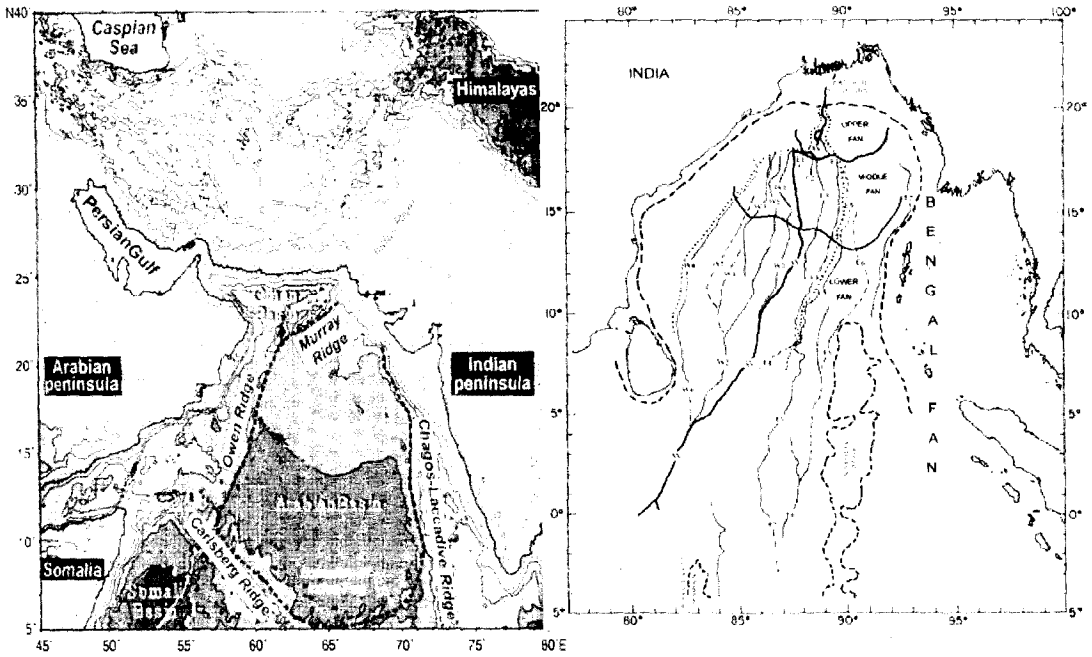

Figure 1.9 Arabian Sea and Bay of Bengal sub marine fans.

The Indus Fan is the second largest fan and is the most extensive physiographic feature of the Arabian Sea in the northwest Indian Ocean Covering an area of approximately 1.1-1.25 million km^2, with a length of 1600 km and a maximum width of 1000 km,. The Indus Fan is bounded by the continental margin of India-Pakistan and Chagos-Laccadive Ridge on the east, by the Owen and Murray Ridges on the west and north, and by the Carlsberg Ridge on the south. The sediments in the Indus Fan are mainly brought by Indus River. The Narmada and Tapti Rivers drain the peninsular shield of India also contribute sediments to the eastern Arabian Sea.

The Bengal Fan is one of the largest deep-sea fans in the world oceans, covers an area of ~3.0 x 10^6 sq. km with length of ~3000 km and maximum width of 1430

km and massive sediments of 20 km thickness. The sediments of the fan are largely eroded from the Himalayas and transported by the Ganges-Brahmaputra River system. The sediments making up this deep-sea fan at times were deposited at a rate of 35 cm/1000 yr, a rate comparable to that of deposition in shallow shelves (20-30 cm/1000yr).

1.7 Aims and Objectives of Proposed Research:

The proposed research was aimed to understand the Late Quaternary Paleoceanography of the Northern Indian Ocean with the following specific objectives:

- To understand the high-resolution variability of monsoon from both the Arabian Sea and Bay of Bengal.
- To reconstruct the Sea Surface Temperature changes at selected core sites from the Arabian Sea and Bay of Bengal and to evaluate the relationship between monsoon and high latitude climate changes.
- To study the productivity changes of the Bay of Bengal over last 30 kyr and compare these changes with the productivity records of the Arabian Sea.
- To unravel the changes of terrigenous material supply from the Indus River during the Late Quaternary, in order to understand the depositional history of the Indus Fan.

1.8 Proxies:

To reconstruct the paleoceanographic variations in the northern Indian Ocean, various proxies were used. The following section mainly deals with various proxies used in the present study.

- Planktonic Foraminifera
- Oxygen and carbon isotopes
- Magnesium/Calcium ratios in Biogeochemical elements in planktonic foraminiferal species
- Paleoproductivity proxies

1.8.1 Planktonic Foraminifera:

Most of the interpretations in this thesis are based on the oxygen and carbon isotopic ratios and Magnesium and Calcium ratios of selected planktonic foraminiferal species. Foraminifers are marine microorganism with a hard outer skeleton, mainly made up of calcium carbonate ($CaCO_3$). Foraminifera, which belong to Protista Kingdom, can be broadly divided into two groups, viz. planktonic foraminifera which floats near the surface (0-200 m) and benthic foraminifera which live on the seafloor (bottom dwelling). Planktonic foraminifera build calcite exoskeleton (tests or shells), of which the physical and chemical composition reflects the sea water condition in which they are formed. After the death of these organisms many of these skeletons pile up on the seafloor, so that deep sea cores from most ocean basins contain millions of these foraminiferal tests. There are about 30-40 recent planktonic foraminiferal species and each species has its preference regarding depth, season and food source. Therefore, the distribution of various modern planktonic foraminifera is controlled by the surface water hydrography (Be 1960; Zhang 1985), water mass properties (Be and Tolderlund 1971; Vincent 1976), and upwelling (Kroon and Ganssen 1989). Hence, the qualitative analyses of variation in faunal composition and morphological characteristics of planktonic foraminifera (Nigam 1990; Naidu and Malmgren 1996) preserved in marine sediments provide the necessary information to study the oceanic processes in the past.

Application of planktonic foraminifera to micropaleontological, paleoceanographic and paleoclimatic research has enjoyed more than 160 years of activity. During the first century, foraminifera were used primarily for biostratigraphic analysis. Although fossil shells were recognized from beach sands and deep sea sediments as early as 1826 (d'Orbigny 1826; Parker and Jones 1865), it was until Owen (1867) and the scientific results of the challenger expedition (Brady 1884) that the planktonic life habitat of these marine protozoon's was clearly established. Applications of planktonic foraminifera in the field of paleoceanography and paleoclimate substantially increased through the pioneering work by Schott (1935). Since then several researchers have been using planktonic foraminifera as primary tool to study the paleoceanography in the world oceans.

1.8.2 Oxygen Isotopes ($\delta^{18}O$):

Oxygen has three stable isotopes, ^{16}O, ^{17}O and ^{18}O. The most common isotope is ^{16}O, which constitutes ~99.7% of all oxygen on the earth and another stable oxygen isotope that is often used in paleoclimate studies is ^{18}O which constitute about 0.2% and the least abundant (0.04%) stable isotope of oxygen is ^{17}O. These isotopes have slightly different physical properties, for instance ^{16}O evaporates faster than ^{18}O from the water and when they fall out as rain ^{18}O releases faster than ^{16}O. This phenomenon has several specific effects as rain clouds loose their ^{18}O first and with continuing rain the precipitation becomes increasingly enriched in ^{16}O (Rozanski *et al.*, 1992). This process leads to rainfall being increasingly depleted in ^{18}O further from source and becomes more depleted further inland, therefore, precipitation in the polar regions are depleted with ^{18}O and enriched with ^{16}O. Thus oceans become depleted with ^{16}O during glacials because most of the ^{16}O gets locked up in the ice sheets when the ice caps are maximum in size. Measuring the $^{18}O/^{16}O$ ratios in sea water would provide information about how much ice was stored on the continents and how the ocean water is affected by the evaporation and precipitation balance and riverine influx.

Another important application of stable oxygen and carbon isotopes in the field of paleoceanography comes through the fractionation of oxygen and carbon isotopes between the calcium carbonate crystallization (i.e. foraminifera) and ambient sea water, the fraction processes is temperature dependent. If temperature increases the incorporation of ^{16}O increases and ^{18}O decreases and vice versa in the foraminifera. Urey was the first to demonstrate that the fractionation of oxygen isotopes in the carbonate-water system is a measurable function of temperature and suggested that this can be useful as a geological thermometer. He noted that, "calcium carbonate of organism is in equilibrium with the water depth in which it lives, and the shell sinks to the bottom of the sea. It is only necessary to determine the ratio of the isotopes of oxygen in the shell today in order to know the temperature at which the organism lived" (Urey 1948). Subsequent research at the University of Chicago (McCrea 1950; Epstein *et al.*, 1953; Emiliani 1954, 1955) have steered the study of oxygen isotope ratios in planktonic foraminifera into the forefront of fields studying climate changes and ocean history.

1.8.2.1 Oxygen Isotope as a Stratigraphic Tool in Paleoceanography:

Oxygen isotopic studies on planktonic and benthic foraminiferal species have been carried out on important cores from different parts of world ocean (Shackleton 1977). The study of oxygen isotopic ratios relative to PDB standard calcite shows the synchronous pattern through geological past. Variation in oxygen isotopic composition in the ocean sediment taken a consideration of mixing of ocean water (< 1000 years) and as isotopic composition is controlled by amount of water stored in continent ice (Shackleton and Opdyke 1973) suggest that the variation in isotopic composition record are synchronous in ocean sediment from any region. Ice sheet extent and melting of glaciers effects the sea level globally, it plays a major role in consideration to establish the chronostratigraphy based on marine sediment. These synchronous variations enable to correlations to be made between cores that may be thousands of kilometers apart (Bradley 1999; Pisias *et al.*, 1984; Prell *et al.*, 1986). Based on the isotopic signals from marine sediments from all over World Ocean, universally recognizable isotopic stages can be defined (Bradley 1999; Pisias *et al.*, 1984; Emiliani 1955, 1966). Nevertheless, even after establishing the chronology based on the isotopic composition; have to add the dating techniques to make the absolute chronostratigraphy by using the ^{14}C radiocarbon, U-series dating and paleomagnetism. Many investigators have shown the correlation between the climatic variability based on orbital tuning and in isotopic signals in marine sediment as a change in sedimentation rate (Hays *et al.*, 1976; Kominz *et al.*, 1979; Martinson *et al.*, 1987) and created a well-controlled chronostratigraphy. Warmer periods (Interglacial or Interstadials) are assigned odd numbers and colder (glacial) periods are assigned even numbers.

Marine Isotopic Stages (MIS) have been used extensively to reconstruct the time frame of marine sediment cores from the world oceans (Prell *et al.*, 1986; Bassinot *et al.*, 1994). By Using the orbital time scale tuning to the $\delta^{18}O$ record it has been established the chronology of MIS up to 2.5 Ma (Shackleton *et al.*, 1990).

Oxygen isotope values of foraminifera depend on local variation of salinity and temperature and globally with variations in continental ice volume. The relationship between $\delta^{18}O$ of foraminifera, oxygen isotopic composition of the original water and temperature is clearly shown by the empirical equation of Craig (1965) given below

$$T = 16.9 - 4.2(\delta_C - \delta_W) + 0.13 (\delta_C - \delta_W)^2$$

T = calcification temperature of water in which organisms live

δ_C = is the per mil (‰) difference between the samples carbonate and PDB standard

δ_W = is the per mil (‰) difference between the $\delta\ ^{18}O$ of water in which the sample precipitated and the SMOW standard.

1.8.3 Mg/Ca Elemental Ratio:

The specific heat difference between the land and ocean influence the monsoon system in Northern Indian Ocean or we can say the temperature regulation between the land and ocean regulates the monsoon. Therefore, to have the better understanding of monsoon cycle or the climatic variation of past, we need to understand precise SST variations in the past. In fiftees after the pioneering work of Emiliani (1955) the In seventees and eightees the $\delta^{18}O$ values of mollusk shells were used to derive the paleotemperatures assuming that the fractionation of oxygen isotopes is a function of only temperature. Subsequently it was realized that the $\delta^{18}O$ composition of of calcite secreting organisms is not only temperature dependent but also the $\delta^{18}O$ composition of water in which the organism calcifies their tests. Therefore, $\delta^{18}O$ of foraminifera can not be used directly to refer the temperature change in the past.

Transfer functions and modern Analogue techniques were used to reconstruct the SST changes based on the planktonic foraminiferal species abundances in the sediment cores (Imbrie and Kipp 1971; Prell 1985). More recently Magnesium/Calcium ratios in palnktonic foraminifera have been used extensively to reconstruct the sea surface temperatures in the geologic past.

In addition, magnesium/calcium (Mg/Ca) ratios in foraminiferal calcite show temperature dependence due to the partitioning of Mg during calcification, therefore Mg/Ca ratios in planktonic foraminifera can used as a precise proxy to reconstruct SST. The Mg content of planktonic foraminifer shells is a proxy of past SST that has recently been validated in a number of oceanographic settings (Elderfield and Ganssen 2000). However, this proxy has few limitations, for example Mg/Ca ratios in larger benthic foraminifera (Raja *et al.*, 2007) and also in planktonic foraminifera

species which have photosynthesis respiration cycle of algal symbionts (Eggins *et al.*, 2004) do not provide reliable temperature estimations.

Mg/Ca paleothermometry has certain advantages over other proxies, the most important of which is that Mg/Ca is measured in foraminifer shells, which are by themselves a vital archive of past climate and the carrier phase of for oxygen isotopes. A paired measurement of both Mg/Ca and $\delta^{18}O$ in foraminifer shells from deep sea cores makes it possible to separate the magnitude and timing of SST and $\delta\ ^{18}O$ of water. Therefore, several researchers have been used the Mg/Ca thermometry to address the many paleoceanographic problems in the Pacific (Lea *et al.*, 2000, Stott *et al.*, 2004), Atlantic (Elderfield and Ganssen 2000) and Indian Ocean (Saraswat *et al.*, 2005). Mg/Ca ratios in benthic foraminifera were used to know the bottom water temperature (Russell *et al.*, 1994; Rosenthal *et al.*, 1997).

Several planktonic foraminifer species have been calibrated for Mg uptake using core tops and culturing (Mashiotta *et al.*, 1999; Nurnberg *et al.*, 1996b; Elderfield and Ganssen 2000). The absolute Mg/Ca of the shells at a given temperature appears to be species-specific which require an individual calibration of each species. Mg/Ca ratios of planktonic foraminifera in single and multiple species have been calibrated to temperatures in the Atlantic and Pacific (Nurnberg *et al.*, 1995, 1996a, 1996b; Mashiotta *et al.*, 1999; Lea *et al.*, 1999, 2000, 2002; Dekens *et al.*, 2002; Lear *et al.*, 2002; Anand *et al.*, 2003).

In this study Mg/Ca ratios in planktonic foraminifera species *Globigerinoides ruber* were used to reconstruct the SST at two cores from the Bay of Bengal and the Arabian Sea. SST derived from Mg/Ca data is used to quantify the influence of monsoon precipitation on the $\delta^{18}O$ of foraminifera.

1.8.4 Clay Minerals:

Over last four decades clay-minerals content in marine sediments have been used to characterize the sedimentary provinces of the world oceans (Biscaye 1965, Griffin *et al.*, 1968, Windom 1975). Earlier work on the clay mineralogy of the Arabian Sea sediments reveal that various sources such as runoff from India, dust contributions from Africa, Arabia, Pakistan and northern India, and in-situ weathering of basalts on mid-ocean ridges the supply of lithogenic material to the Arabian Sea (Sirocko and Lange 1991). Therefore, it would be difficult to assign specific source

areas and transport path ways. However, the large amounts of smectite off southern India are clearly derived from Indian rivers, and high palygorskite concentration off Arabia is specifically related to Aeolian transport from Arabia (Sirocko and Lange 1991). Having known the limitations of clay mineral applications in paleoceanographic and paleoclimatic studies, this proxy was used in this thesis to study the source of clay minerals in the Indus Fan sediments especially at the Ocean Drilling Program Site 720 A.

1.8.5 Geochemical Elements:

The Geochemical elements have been used as a tracer for productivity variations with the quantity of organic carbon on Interglacial-Glacial time scale in the Atlantic and Pacific (Pisias 1976; Lyle *et al.*, 1988). Sirocko *et al.*, (2000) have explored the uses of several geochemical elements to understand the source of dust to the Arabian Sea. The application of the geochemical multi-tracer approach indicates that the intensity of the southwest monsoon intensity was low during LGM (Sirocko *et al.*, 2000).

Aluminium (Al) and Titanium (Ti) content in the marine sediment mainly derive from continental origin supplied through eolian and fluvial pathways. Therefore, Al and Ti have been commonly used as geochemical indicators to discover the content of aluminosilicate detritus of continental origin (Pattan *et al.*, 2003). Similarly, Al concentration in the sediments off Somalia region represents the supply of dust as a result of continental aridity (Ivanochko *et al.*, 2005). It has been documented that Ti/Al and Cr/Al in the sediments of Arabian Sea exhibit strong precessional periodicity (cycles at 25 kyr) suggesting the SW monsoon and associated winds play a key role to transporting terrigenous material from the land (Shimmield and Mowbray 1991). In the present study also Al and Ti content at the ODP Site 720 was used as a proxy of terrigeneous material supply to the Indus Fan in the northwestern Arabian Sea.

1.8.6 Proxies of Paleoproductivity:

Numerous proxies have been used to determine paleoproductivity. Recent developments have focused on biogenic remnants such as organic carbon, carbonate, opal or biomarkers (specific organic compounds) which are preserved in deep sea marine sediments. In addition, barium, cadmium and copper or scavenged

radionuclides such as 230^{Th} were also used to trace the productivity. Another group of tracers such as stable isotope ratios of carbon in calcareous shells and of nitrogen $^{15}N/^{14}N$ in particulate organic matter (Ganeshram *et al.*, 2000) and Cadmium/Calcium ratios in foraminifera shells (Boyle 1988). Trophic proxies, namely species compositions of foraminifera, diatoms or any other such groups containing information about the trophic structure of the pelagic environment can also be used as paleoproductivity proxies. In the present study carbon isotopic ratios in planktonic foraminifera were used as a proxy of productivity.

1.8.6.1 Carbon Isotopes ($\delta^{13}C$):

There are a variety of naturally-occurring isotopes of carbon. These isotopes are characterized by differing atomic weights resulting from varying numbers of neutrons in the atomic nuclei. The relative abundances of these isotopes are given below:

$^{12}C = 98.89\%$, $^{13}C = 1.11\%$, ^{14}C = 1E-10%

^{12}C and ^{13}C are both stable isotopes and 14C radioactive isotope which undergoes radioactive decay.

Mostly in all Oceans, a linear correlation is observed between $\delta^{13}C_{\Sigma CO2}$ values and nutrient contents of deep and bottom water masses because the distributions of both are controlled by the interaction of biological uptake at the sea surface and decomposition in deeper water masses with the general circulation of the Ocean (Kroopnick 1980, Kroopnick 1985; Mackensen and Bickert 1999). The biological and chemical fractionation of carbon isotopes in the Ocean provide one of the most useful tracers or reconstructing past distributions of water masses and their properties (Curry *et al.*, 1988). The distribution of $\delta^{13}C$ in ocean is controlled principally by photosynthesis and remineralization of organic carbon, and by mixing between water masses of different isotopic composition. Photosynthesis in surface water preferentially extracts ^{12}C from seawater, causing the enrichment of the surface water $\sum CO_2$ in ^{13}C. The value of $\delta^{13}C$ in seawater, after primary producers have removed all nutrients, is controlled by the mean $\delta^{13}C$ and the mean nutrient concentration of the ocean (Broecker 1982; Broecker and Peng 1982).

1.8.6.2 Calcium Carbonate ($CaCO_3$):

Fifty percent of world's ocean bottom is covered by carbonate sediments (>30% calcium carbonate) (Lisitzen 1972). In nearshore environments and continental shelves benthic organisms such as mollusks, bryozoa, algae and echinoderms are the major source of carbonate accumulation. By contrast, carbonate production over continental slopes and in the abyssal plains is almost exclusively planktic, dominated by coccolithophores, foraminifera and to a minor extent pteropods and calcareous dinoflagellates. The distribution suspended calcium carbonate in surface waters resembles that of primary production.

Three factors controls the calcium carbonate content in the marine sediment; Productivity, dissolution and dilution by non-carbonate material (Damuth 1975). Thus, calcium carbonate content in the sediment can be used as proxy of productivity provided dissolution and dilution factors were ruled out in the selected region.

1.8.6.3 Organic Carbon:

Unicellular phytoplankton and zooplankton are the largest sources of organic carbon in the marine environment. Primary producers living in surface waters convert CO_2 into the organic matter. Part of this organic matter sinks to the deeper waters where it is oxidized, releasing initially fixed carbon back to water as CO_2 (Broecker and Peng 1993). The differences between $CaCO_3$ and organic carbon in different area are because of differential biological productivity in surface waters at the investigated area and/or differential preservations/dilution of $CaCO_3$ and organic carbon (Ortiz *et al.*, 2004). Indeed, these two mechanisms are not decoupled and higher organic carbon may cause enhanced $CaCO_3$ dissolution (Emerson and Bender 1981; Guptha *et al.*, 2005). Preservations of calcareous particles and organic matter follows different $CaCO_3$ saturation and oxygen concentration of subsurface to bottom water masses which follows the glacial/interglacial cycle (Ivanova *et al.*, 2003; Guptha *et al.*, 2005).

CHAPTER 2

Material and Analytical Methods

In this study, two sediment cores each from the Arabian Sea and Bay of Bengal were selected to address the proposed objectives (Fig. 2.1). Core length, water depth and position of the cores are listed in Table 2.1.

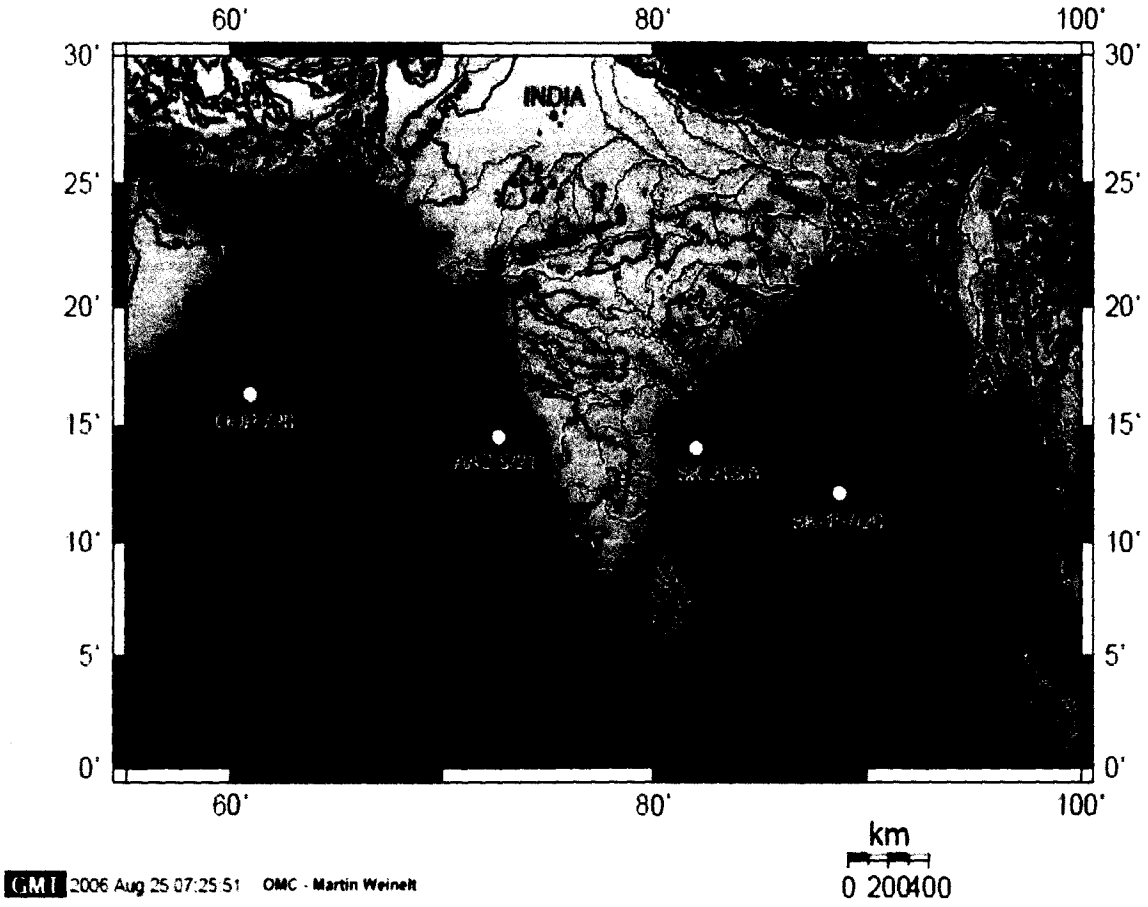

Figure 2.1 Core locations and physiographic features of the northern Indian Ocean.

2.1 Sediment Cores from Arabian Sea:

Two sediment cores were chosen from the Arabian Sea, Ocean Drilling Program (ODP) Site 720 is located in the Indus Fan. This site is mostly fed by the sediments supplied through Indus River. Therefore, this site provides necessary information about sediment supply to the Indus Fan and depositional history of Indus Fan during the Late Quaternary Period.

Table 2.1: Shows the core numbers, location, water depth and core length.

Cruise No.	Core No.	Latitude °N	Longitude °E	Water Depth (m)	Core Length (m)
ODP Leg 117	720A	16° 07.796'	60° 44.621'	4045	28.3
AAS 9	9/21	14° 30.539'	72° 39.118'	1807	4.4
SK 157	157/20	12° 08.808'	88° 42.159'	3171	4.58
SK 218	218/1	14° 02.1'	82° 00.12'	3307	8.26

Detailed and extensive paleoceanographic work has been carried out from the western Arabian Sea to reconstruct the monsoon variability based upwelling proxies (Prell *et al.*, 1992 and references their in) and very limited Paleoceanography data is available along the eastern Arabian Sea (Chodankar *et al.*, 2005). During SW monsoon period more precipitation and fresh water discharge through rivers occurs along the eastern Arabian Sea. Such signals can be easily traceable through the oxygen isotopic ratios in planktonic foraminifera. Therefore, it was decided to study a sediment core (AAS-9/21) from the eastern Arabian Sea to understand the SW monsoon variability by using Mg/Ca thermometry and oxygen isotope ratios in planktonic foraminifera.

2.2 Sediment Cores from the Bay of Bengal:

A robust indicator of monsoon rainfall is a key requirement in reconstructing Holocene monsoon variability. The summer monsoon rainfall over India is highest in the Indo-Gangetic Belt and the rainwater is funneled through the Ganges-Brahmaputra river system into the Bay of Bengal. The discharge from these globally important rivers causes a large drop in salinity in the order of 4 psu in the Northern the Bay of Bengal (Wyrtki 1973). In addition, the North-South salinity gradient in this region is also of similar magnitude. Therefore, the salinity changes in the Bay of Bengal track summer monsoon rainfall sensitively. Hence it is decided to study two cores SK-218/1 and SK-157/20 from Bay of Bengal in order to reconstruct salinity variations. These reconstructions will be used to recognize temporal and spatial (North-South gradient) patterns of changes in Sea Surface temperature (SST) and Sea Surface Salinity (SSS).

2.3 Field Methods:

Ocean Drilling Program (ODP) Site 720A samples were obtained from the ODP core repository at Texas A&M University, Texas, USA. Cores SK-218/1, SK-157/20 and AAS-9/21 were collected during *ORV Sagarkanya* cruises. SK-218/1 top 1m was subsampled at 1cm interval and from 1 to 8.26m at 4cm interval. Core SK-157/20 was subsamples at 2cm interval. ODP Site 720 samples were analyzed at 20 cm interval up to 28.3m length. Core AAS-9/21 was sub sampled at 3cm and 5cm intervals from 0-1m and 1 to 4.4m, respectively.

2.4 Processing of Samples for Foraminiferal Analysis:

A known quantity of sediment sample was dried keeping in an oven at 60^0C temperature. Dried sediment sample weighed and soaked in distilled water overnight. Next day the top part water decanted without disturbing the bottom settled sediment. To remove the lumps of the clay and to remove the organic matter, 10ml of 10% sodium hexa-meta-phosphate and 5ml of hydrogen peroxide was added, respectively and kept overnight. Subsequently these samples were wet sieved through a 150μm size sieve with enough care to prevent the breakage of foraminifer shells. Greater than 150μm fraction (coarse fraction) retained on the sieve was transferred in to 25 ml beaker and dried in the oven at 50-60^0C. The dried coarse fraction >150μm was used for census counts of planktonic foraminifera and selected planktonic foraminifer species were picked for oxygen and carbon isotopes and Magnesium/Calcium analyses.

2.5 Picking of Foraminifera:

The coarse fraction (>150μm) of each sample was splitted by splitter until to get minimum 300 planktonic foraminifer species and weighed this fraction and counted abundance of various species of planktonic foraminifera, total number of benthic foraminifera and foraminiferal fragments (broken shells which are >50% intact), by using Stereo Binolocular Microscope. Planktonic foraminifer species were identified by following the taxanomy of Be (1967); Hemleben and Spindler (1983).

2.6 Geochemical Analysis:

Major and minor elements analyses were carried out on the ODP Site 720A samples. For the analyses of elemental concentration the sample was finely powdered, powdered sample kept overnight oven-dried (at 105° ± 5°C). About 0.3gm of weighed sample transferred to PTFE beakers and added 20 ml of HF (removal of glass), 5ml of HNO_3 (removal of carbonate), 2ml of $HClO_4$ to the sample. Then PTFE beakers with sample kept on plate for evaporation. The incipiently dried digest was dissolved and brought to volume (50 ml) with 10 ml of HCL in 1:1 ratio and stored in 75ml plastic bottles. Repeated the digestion steps until clear solutions obtained to ensure complete digestion. The 50ml solutions of the standard (MAG-1) were also prepared by using similar steps described above. The 50ml of the solutions of the samples and (MAG-1) standard were analyzed for major and minor elements on a Perkin-Elmer® Plasma-400 sequential ICP-AES (Inductive Coupled Plasma-Atomic Emission Spectrometer) at the National Institute of Oceanography, Goa. The analyses were accurate and precise to, within ±5%.

Terrigenous matter was estimated by using Ti-based normative calculation (Murray and Leinen 1996) and assuming that the terrigenous matter of the sediment is almost similar to average Post-Archean Australian shale: Terrigenous matter (wt%) = $(Ti_{samp}/ Ti_{pass}) \times 100$.

2.7 Clay Mineralogy:

Clay mineral studies from a 2-μm fraction of the sediment, which was separated from the total sample based on settling velocity principle (stoke's Law) after removing the >63 μm fraction by wet sieving. The separated clay aliquots made free of carbonate and organic matter by treating the samples with 5ml of acetic acid and 10 ml of hydrogen peroxide, respectively. The aliquots were then washed several times with de-ionized water to remove the excess reagents and decanted. Oriented slides were then prepared by pipetting 1 ml of the concentrated clay suspensions on to glass slides following the procedures described in Rao and Rao (1995).

X-ray diffraction studies were then carried out on these slides from 3 to 35° 2θ at 0.05° 2θ/sec on a Philips X-ray diffractometer (1840 model) using nickel-filtered Cu Kα radiation. The instrument calibrated by running internal silica standards. The slides were then, exposed to ethylene glycol vapors at 100^0 C for 1 hr and rescanned

under the same instrumental settings. The peaks for major clay minerals such as kaolinite, smectite, chlorite and illite were identified. According to Biscaye (1965), smectite were multiplied by 1, illite by 4 and kaolinite and chlorite by 2. In order to differentiate the kaolinite and chlorite peaks, the slides were also scanned from 24 to 26° 2θ at 0.01^0 2θ /sec.

2.8 Analysis of $CaCO_3$:

The $CaCO_3$ % content was analyzed by using the gasometric technique, the analytical precision in this method is ± 1%.

2.9 Stable Isotope Ratio Analysis:

Planktonic foraminiferal species *Globigerinoides ruber* (white variety) was used for oxygen and carbon isotope analyses. 10-15 specimens of clean *G. ruber* in a size fraction of 250-355 μm were picked and crushed between two glass plates and were ultra sonically cleaned in ethanol for few seconds and transferred to stainless steel boats, loaded into an automated sample carousel for sequential acidification online. The CO_2 evolved in the reaction was transferred to the inlet of a gas ratio stable isotope mass spectrometer using cryogenically routine procedures and the sample gas was compared to an internal standard gas sequentially 10 times.

Figure 2.2 Apertural and Spiral view of *Globigerinoides ruber*

The difference in the $^{18}O/^{16}O$ of the sample and the internal standard is reported in the delta ($\delta^{18}O$) notation relative to the PDB standard. The Isotopic composition of the carbonate sample measured on the CO_2 gas evolved by the treatment of foraminiferal shells with orthophosphoric acid at a constant temperature. The standard gas was calibrated reference to the international carbonate standard Pee-Dee Belemnite (PDB) from rostrum of the belemnite *Belemnitella americana* from the cretaceous Pee Dee formation of South Carolina. Now for the calibrations NBS 19 and NBS 20 have been using, NBS 19 is a standard of marble and NBS 20 is a homogenized standard of Jurassic Solnhofen limestone from Southern Germany. The analytical precision based on replicate for $\delta^{18}O$ was better than ± 0.07‰ and for $\delta^{13}C$ was better than ± 0.04‰.

2.10 Magnesium/Calcium (Mg/Ca) Paleothermometry:

The calcareous skeletons of foraminifera does not consist pure $CaCO_3$; some of the Ca atoms are replaced by other bivalent cations such as Mg atoms. As incorporating atoms of aberrant size in a crystal lattice require extra energy, this occurs in warm environments due to ample availability of thermal energy. Therefore, ratio of Mg to Ca in a calcite shell serves as a measure of past sea water temperature. To reconstruct the paleotemperature through Late Quaternary Period Mg/Ca ratios have been used in the world oceans (Lea *et al.*, 2000; Elderfield and Ganssen 2000; Rosenthal *et al.*, 2000).

For determination of Mg/Ca, for each sample 30 to 40 individuals of *Globigerinoides ruber* (white variety) with a size range of 250 to 350μm were picked. The picked specimens were then cleaned using the elemental analysis technique (Barker *et al.*, 2003), applied to marine carbonate samples. Splits of the cleaned sample were then analyzed for Mg and Ca by inductively coupled plasma atomic mass spectrometry (ICP-MS) and the method followed described by Barker *et al.*, 2003. Study shows that the reproducibility of the method which will describe here obtained for *G. ruber* in a core-top sample from the Arabian Sea was ±1.8% (or 0.2^0C) for Mg/Ca and ±0.5% for Sr/Ca (Barker *et al.*, 2003). During the present study 40 replicate *G. ruber* samples were measured from site SK-218/1. However, the repeatability for Mg/Ca was routinely better than 0.1 mmol/mol. The analytical error

for the Mg and Ca concentrations was better than 0.7% relative standard deviation (RSD).

A multi step cleaning protocol was used following procedures described by Barker *et al.*, (2003). The cleaning protocol of Barker *et al.*, (2003) is reproduced below:

2.10.1 Crushing:

Foraminiferal tests are crushed using two clean glass plates. The aim here is to allow any chamber fill to escape during subsequent cleaning stages.

1. Place the text in a single layer on the lower glass slide. Keep the sample moist with excess water.
2. In a controlled manner, lower the second plate on to the sample and apply gentle pressure in order to open every shell chamber. Take care not to over-crush the sample; this will lead to excessive loss of sample during cleaning.
3. Remove the upper glass plate and transfer all particles to the lower plate.

   At this time, a piece of colored paper should be positioned beneath the sample while under a microscope. This will reveal the presence of any larger silicate grains that may not be removed during the following clay removal steps. It is not necessary to remove such grains at this stage but only to note their presence so that action may be taken later on.

   Steps 4 to 6 should be followed if the sample is intended for paired analyses of trace metals and stable isotopes or similar.
4. Add water to the sample in order to bring the shell particles into suspension.
5. Mix particles thoroughly with a brush with the aim of homogenizing the sample as far as possible.
6. Remove any excess water and divide in to the desired proportions.
7. Using a moistened brush, transfer the crushed sample to an acid cleaned 500 µl microcentrifuge tube or relevant sample tube.

2.10.2 Clay Removal:

During this stage, all samples should be treated individually in order to maximize cleaning effectiveness (batch treatment for ultrasonication is appropriate). It is important to use separate pipette tips for adding and removing reagents. Having

opened the test chambers during crushing, much of the test fill will be loosened and easily brought in to suspension.

1. Squirt 500µl of UHQ H_2O onto the crushed sample (trapped air bubbles may be freed by flicking the tube end with a fingernail).
2. Allow the sample to settle for 30 seconds or so.
3. Remove the overlying solution (supernatant) with a separate pipette. The size of a 500µl pipette tip is suitable for removing most of the overlying liquid from the tube without risk of sample loss.

At this stage, all tubes should still contain about 10-20 µl of H_2O.

1. Place the sample rack in an ultrasonic bath for 1-2 minutes. This will encourage separation of more tightly bound clays from the test surfaces.

Suspended clays will appear as a milky residue in the liquid just above the sample.

2. Squirt 500µl of UHQ H_2O onto each sample. This will agitate the sample and bring loose clays into suspension.
3. Briefly allow the sample to settle (minimal settling technique). Sufficient settling will only take a number of seconds (long enough for the distinct carbonate grains to reach the bottom). After this period the remaining settling material will mainly comprise unwanted silicate particles.
4. Remove the overlying solution.
5. Repeat steps 4 to 7 further 4 times. More repetitions may be necessary as long as clays are being visibly brought into suspension by ultrasonication.
6. After the water cleaning steps, methanol is used for further clay removal. The lower viscosity of this reagent should dislodge material still attached to the carbonate tests.
7. Squirt 250µl of Aristar methanol into each tube.
8. Ultrasonicate the tubes for 1-2 minutes.
9. Treating each tube individually, lift the methanol off the sample with a pipette and quirt straight back in to bring clays in to suspension.
10. Allow sample to settle for a few seconds and remove the methanol.
11. Repeat steps 9 to 12.
12. Repeat 5 to 7 in order to remove any remaining methanol (further ultrasonication may be applied if desired).

2.10.3 Removal of Organic Matter:

1. Add 250µl of alkali buffered 1% H_2O_2 solution to each tube and secure the rack with a lid to prevent tubes popping open while under pressure.
2. Place the sample rack in a boiling water bath for 10 minutes. At 2.5 and 7.5 minutes remove the rack momentarily and rap on the bench top to release any gaseous build-up. After 5 minutes place the rack in an ultrasonic bath for a few seconds and return to the water bath after rapping on the bench. The aim of these interim steps is to maintain contact between reagent and sample.
3. Remove the oxidizing reagent using a pipette.
4. Repeat steps 1 to 3.
5. Remove any remaining oxidizing reagent by filling the tube with UHQ H_2O and removing after settling. This step should be repeated 1-2 times.

2.10.4 Removal of Coarse-Grained Silicates:

This step is necessary if silicates were observed in the sample after crushing. It is a good idea to follow this step even if no larger particles were seen; any foreign body that has entered the sample during the proceeding steps might bias the desired measurement.

Particulate removal at this stage is less time consuming than straight after crushing as the clay treatment and oxidation steps will have broken down and removed some particles already.

A 100 µl pipette is used to transfer the sample into a 1ml glass micro-beaker.

1. Squirt 100 µl of UHQ H_2O into the sample and immediately transfer to a micro-beaker avoiding settling.
2. Repeat step (1) 3-4 times ensuring that the entire sample is transferred.
3. Remove excess H_2O leaving approximately 100 µl overlying the sample.
4. The sample is viewed under a microscope using a dark and light background in turn.
5. Remove any particles that are not apparently carbonate using a fine brush. Strongly discolored carbonate should also be removed.
6. Transfer the sample in to a clean microcentrifuge tube using the technique in step (1) and remove excess H_2O.

Note, if particles are not removed using the technique outlined above, it is nevertheless, good practice to transfer all samples to clean tubes before continuing. If

a transfer is not performed, thorough cleaning of the sample tube (including cap) with UHQ H_2O should be carried out to ensure that all oxidizing reagent is removed.

2.10.5 Weak Acid Leach:

A weak acid is used to remove any adsorbed contaminations from the test fragments.

1. Add 250 µl of 0.001 M HNO_3 to each sample.
2. Ultrasonicate all samples for 30 seconds.

Remove acid from each sample.

1. Squirt UHQ H_2O in to each tube.

It is important to replace the leach acid with H_2O as soon as possible for all samples in order to prevent excess dissolution.

1. Remove the overlying H_2O.
2. Repeat steps (4) and (5).
3. Using a 10 µl pipette, carefully remove any remaining solution from each sample.

2.10.6 Dissolution:

Dissolution should be performed with consideration given to any non-carbonate particles that may still be present in the sample. The following steps should act to reduce the risk of contamination from such phases.

1. Add 500 µl of 0.075M HNO_3 to each sample (for small samples 300 µl is adequate).
2. Place the sample rack in an ultrasonic bath to promote reaction.
3. Momentarily remove each tube in turn and flick with a fingernail to allow any build-up CO_2 cases in any sample tube remove that tube from the ultrasonic bath and leave the settle.
4. Once all samples are dissolved, they should be transferred to clean sample tubes.

Measured Mg/Ca ratio were converted to SST by using calibration equation of (Dekens *et al.*, 2002)

$$Mg/Ca = 0.38 \exp (0.09 (SST))$$

By using the SST derived from Mg/Ca, SST and substracting ice volume effect values adopted from (Shackleton 2000) from $\delta^{18}O$ of *G. ruber* $\delta^{18}O$ of sea water ($\delta^{18}O_{SW}$) were computed following equation of (Lea *et al.*, 2000):

$\delta^{18}Osw = 0.27 + ((T - 16.5 + 4.8 * \delta^{18}Ocalcite)/4.8)$

$\delta^{18}O_{SW}$ values were converted into salinity in the Arabian Sea by using Dahl and Oppo (2006) equation: $S = (\delta^{18}Osw + 20)/ 0.57$ and in the Bay of Bengal by using Rostek *et al.*, (1993) equation: $S = (\delta^{18}Osw + 15.2)/0.45$.

2.11 Artificial Neural Network:

Past annual, summer and winter season SSTs were estimated using artificial neural networks (ANNs). An ANN is an information-processing system inspired by the way the densely interconnected, parallel structure of the mammalian brain processes information. The ANN is composed of a great number of processing elements that are analogous to neurons and are tied together with weighted connections that are analogous to synapses. The most common type of ANNs is the multilayer perceptron, which is most often trained using the back propagation (BP) algorithm. The ANN is trained to reproduce the target variable(s) from the input variables by adaptively updating the synaptic weights that are associated with the strength of the connections. The optimum weights are determined iteratively by optimizing certain "energy" functions as training proceeds. Comprehensive descriptions of multilayer perceptron ANN can be found in Wasserman (1989), Webb (2002) and Malmgren and Nordlund (1996; 1997).

The objective behind the application of ANNs is thus to attempt at reproducing the output variable(s) from the input variables with a minimum error rate through a specific training process. ANNs have the ability to overcome problems of fuzzy and nonlinear relationships between the sets of input and output signals. In paleoceanographic applications the input variables are relative abundances of a number of species, for example, planktic foraminifers; the output most often consists of one single variable, such as SST. In this study the annual, summer and winter SSTs were analysed separately. Once trained on the basis of a reference set of modern microfossil and hydrographical data, the ANN can be employed for prognostication of past sea-surface conditions within some limits of precision using the same set of input signals.

The ANN training process involves subdivision of the initial data-set into two random portions, a training set, which is used for training the ANN, and a test set to which the trained network is applied for estimates of the error rate. The optimum measure of the error rate is the root-mean-square error of prediction (RMSEP), which is represented by the square root of the squared differences between the observed and estimated values divided by the number of observations in the test set. One such partition of the original data-set is not sufficient to estimate the RMSEP in the data-set; instead it is necessary to generate several such partitions to obtain an accurate estimate of the error rate.

We used the Neuro Genetic Optimizer (NGO, version 2.5) software © BioComp System, Inc) for the training of the ANNs. Planktic foraminiferal census counts of core tops are from the Brown University Foraminiferal Data Base (Prell *et al.*, 1999). In this application, the ANNs were trained on the planktic foraminiferal census of 361 core tops from the Indian Ocean. The species were used as input variables to the BP neural network. The training set consisted of 271 samples (75%) and the test set of the remaining 90 samples (25%). The training process was repeated ten times to obtain a reliable estimate of the precision of the predictions of the test-set observations. Annual SSTs can be predicted with an average precision of 0.92°C (range 0.72-1.14°C), and that the corresponding precision for the summer and winter seasons are 1.02 (range 0.82-1.19°C) and 1.05°C (range 0.77-1.40°C), respectively. Correlation coefficients for the relationship between observed and predicted SSTs are on the average 0.987 (range 0.981-0.991) for the annual SSTs, 0.980 (range 0.975-0.985) for the summer season and 0.984 (range 0.976-0.992) for the winter season. Subsequently, estimated annual and seasonal paleo-SSTs in core SK-157/20 are represented by the averages of the estimates of the ten ANNs.

2.12 Age Model:

Climatic reconstructions are meaningful only when placed in a time frame. Age models for marine records of glacial – interglacial time scales are generally constructed by either of two methods. Records not older than 40,000 years can be dated using ^{14}C dating. Chronology for older than 40,000 years are constructed by using oxygen isotope records. The chronology based on oxygen isotopes is essentially based on the assumption that the amount of continental ice is affected by changes in

the amount of or distribution of incoming solar radiation, and the timing of these changes is known (Berger 1978), a global $\delta^{18}O$ calibration curve, tuned to insolation, could be constructed. Ages, and the timing of these changes is known (Berger 1978), a global $\delta^{18}O$ calibration curve, tuned to insolation, could be constructed. Ages derived from carbon 14 dates are calibrated to calendar years. The glacial and interglacial stages are termed marine isotope stages (MIS) or oxygen isotopes stages (OIS), and have been assigned numbers. In general interglacials have odd number and glacials have even numbers.

To establish high-resolution chronology in this study cores SK-218/1, SK-157/20 and AAS-9/21 were dated by ^{14}C using Accelerator Mass Spectrometer (AMS) at Kiel University, Germany. About 10 mg of planktonic foraminifera consists of various species in the size range of (250-355μm) were used for AMS carbon dates. ^{14}C dates were calculated to calendar years by using the calibration program online CalPal version quickcal 2005 ver1.4 Weninger *et al.*, (2006).

CHAPTER 3

Quantification of paleo sea surface temperature and sea surface salinity in the Bay of Bengal: Implication on monsoon fluctuations

3.1 Introduction:

The Indian monsoon is an important component of global climate because monsoon transport heat and moisture from the warmest part of the tropical ocean across the equator and to higher latitudes. Seasonal reversal of monsoon winds and associated monsoon rainfall over Asia, have a direct effect on the socio-economic and agricultural development in the densely populated Asian region. The four major rivers Irrawaddy, Brahamaputra, Ganges and Godavari discharges annually approximately $1.5x10^{12}m^3$ of fresh water into the Bay of Bengal (Martin *et al.*, 1981). In addition, annual rainfall over the bay varies between 1 m off the east coast of India to more than 3 m in the Andaman (Baumgartner and Reichel 1975). The peak discharge of rivers and rainfall over the bay occurs during the SW monsoon season, which leads to a strongly stratified near-surface layer and a drop in salinity in the order of 4 psu in the northern Bay of Bengal (Wyrtki 1973). Thus, salinity variations are quite large in the Bay of Bengal as compared to other oceanic regions where surface water temperature variations are large than the surface water salinity changes. Hence, Bay of Bengal is a natural laboratory to study the past salinity variations which infer the monsoon precipitation in the Indian Subcontinent.

Previous monsoon reconstructions mainly from the Arabian Sea have shown that the strength of the Indian monsoon varied significantly over decades to ice ages, in some cases, for well-established reasons such as the precessionally forced variations in summer insolation. Though, Bay of Bengal is an ideal region to study monsoon variability not much work has been carried on these lines for unknown reasons. Therefore, an attempt has been made in this study to investigate the SST and $\delta^{18}O_{SW}$ changes of the Bay of Bengal at the millennial time scale for the last 33 kyr to determine: i) the past variability of the local salinity to infer changes in the monsoon precipitation ii) how variability of the fresh water flux and ocean dynamics of the Bay of Bengal was related to the high latitude climate changes which explore the teleconnection between monsoon activity and global climate on these time scales. This study will also bridge the gap between instrumental record showing (interannual

to decadal variability) and the existing paleoceanographic records (mainly glacial-interglacial to millennial time scales).

To reconstruct past changes of $\delta^{18}O_{SW}$ oxygen isotopic composition and Magnesium/Calcium (Mg/Ca) ratios were measured on the planktonic foraminiferal species *Globigerinoides ruber*. SSTs were reconstructed by using Mg/Ca thermometry, which has an uncertainty of $\pm 1°C$. By subtracting the Mg/Ca-derived temperature component from foraminiferal $\delta^{18}O$ we have computed the $\delta^{18}O_{SW}$. The chronology of the core is based on AMS ^{14}C dates calibrated to the calendar years by using the CalPal program (Weninger *et al.*, 2006) (for more details see sediment cores section 3.4). In order to differentiate the relative contribution of local SST and $\delta^{18}O$ composition of waters to the observed $\delta^{18}O$ of foraminifera at this site, we have reconstructed SST and δ^{18}Osw variability for last 30 kyr as the $\delta^{18}O$ of foraminifera (δ^{18}Oc) depends on the temperature and the δ^{18}Osw in which they calcify their shells. The δ^{18}Osw is linearly related to salinity, and the difference between δ^{18}Osw and δ^{18}Oc is controlled by temperature.

3.2 Hydrography:

3.2.1 Salinity:

The four major rivers Irrawaddy, Brahmaputra, Ganges and Godavari discharges annually approximately $1.5x10^{12}m^3$ of fresh water into the Bay of Bengal (Martin *et al.*, 1981). In addition annual rainfall over the bay varies between 1 m off the east coast of India to more than 3 m in the Andaman (Baumgartner and Reichel 1975). The peak discharge of rivers and rainfall over the bay occurs during the SW monsoon season, which leads to a strongly stratified near-surface layer. In the Bay of Bengal salinity varies from 22 to 34 psu during SW monsoon and 27 to 33 psu during NE monsoon (Fig. 3.1) (Wyrtki 1973; Varkey 1996).

3.2.2 Temperature:

In most oceanic areas variations in temperature are large compared to salinity, but in the Bay of Bengal temperature gradient throughout the year is very less as compared to salinity. Surface temperatures vary between 28^0C and 30^0C. In the northern coastal belt of Bay of Bengal temperature increase about 4^0C (26^0C to 30^0C)

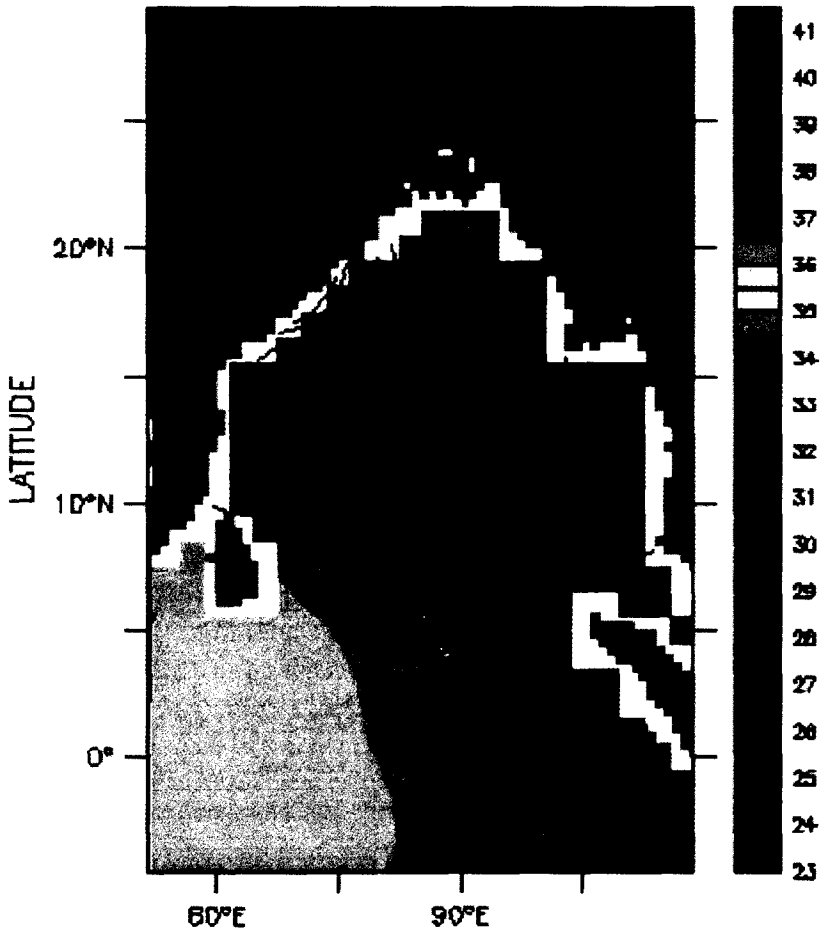

Figure 3.1 Average Sea surface salinity during SW monsoon in Bay of Bengal (Levitus *et al.*, 1994).

from winter to summer and interestingly, off Madras average temperature is 28^{0}C (Fig. 3.2). A north to south temperature gradient (about 1^{0}C) forms during winter, which is caused by the cold, dry northeasterly winds aiding latent heat flux (evaporative cooling) and sensible heat flux from the sea surface in northern Bay of Bengal. The latent heat flux variation (SST warming or cooling) in the BOB is highly controlled by atmospheric forcing largely driven by wind variability (Montegut *et al.*, 2007). Modern SST varies 28.4 to 29.6^{0}C at the location of SK-157/20.

3.3 Sediment Cores:

Core SK-218/1 was collected at a water depth of 3307 m from the Bay of Bengal (14°02'06" lat; 82°00'12" long) (Fig. 3.3), the location of this core shows

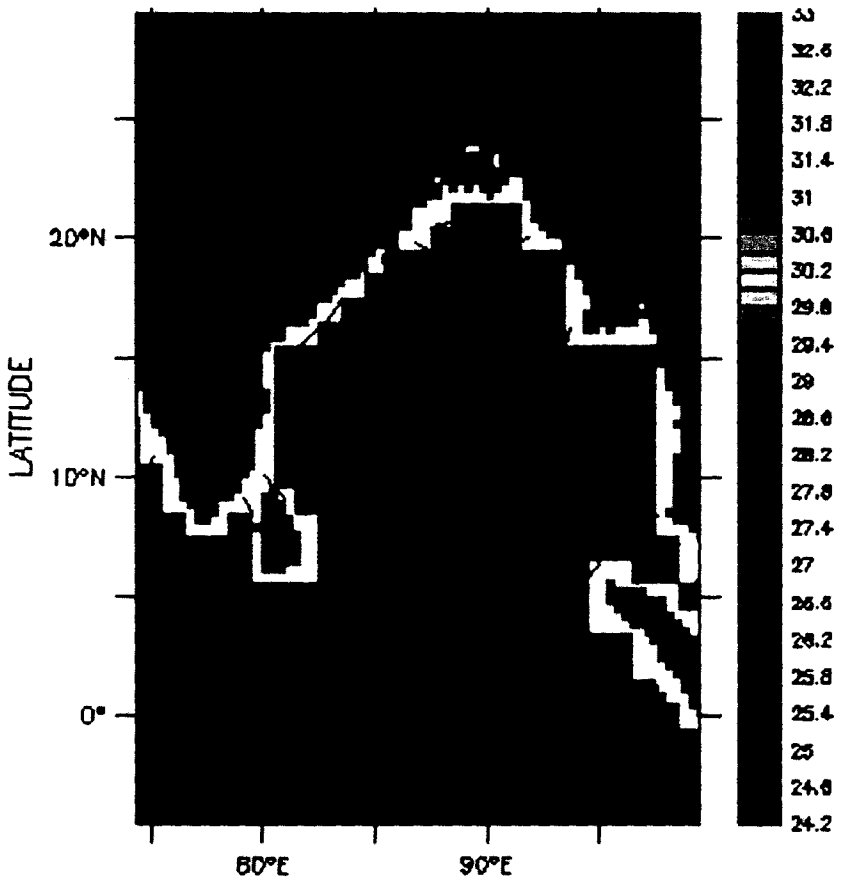

Figure 3.2 Average Sea surface temperature during SW monsoon in Bay of Bengal (Levitus and Boyer, 1994).

distinct salinity variations between the summer monsoon season and the rest of the year as a result of more than 2000 mm of rain that falls on the surface of the ocean at this location each year, primarily during the summer monsoon. Therefore, down core planktonic foraminiferal $\delta^{18}O$ should reflect changes of the surface water salinity and $\delta^{18}O_{SW}$ driven by the summer monsoon variability. Core SK-157/20 was collected at a water depth of 3171 from the central Bay of Bengal (Fig. 3.3). This core location is very ideal to look at the seasonal SST changes in the central Bay of Bengal.

Chronology of these two core were established based on AMS ^{14}C dates up to 30 kyr, further down chronology was established by correlating $\delta^{18}Oc$ record of this with low latitude $\delta^{18}Oc$ global isostack curve given by Martinson *et al.*, (1987). ^{14}C AMS dating were performed on monospecific samples of the planktonic foraminifera *Globigerinoides ruber* using Tandem Accelerator at Leibniz Labor fur Altersbestimmung und Isotopenforschung, Christian-Alberchts-Universitat, Kiel, Germany.

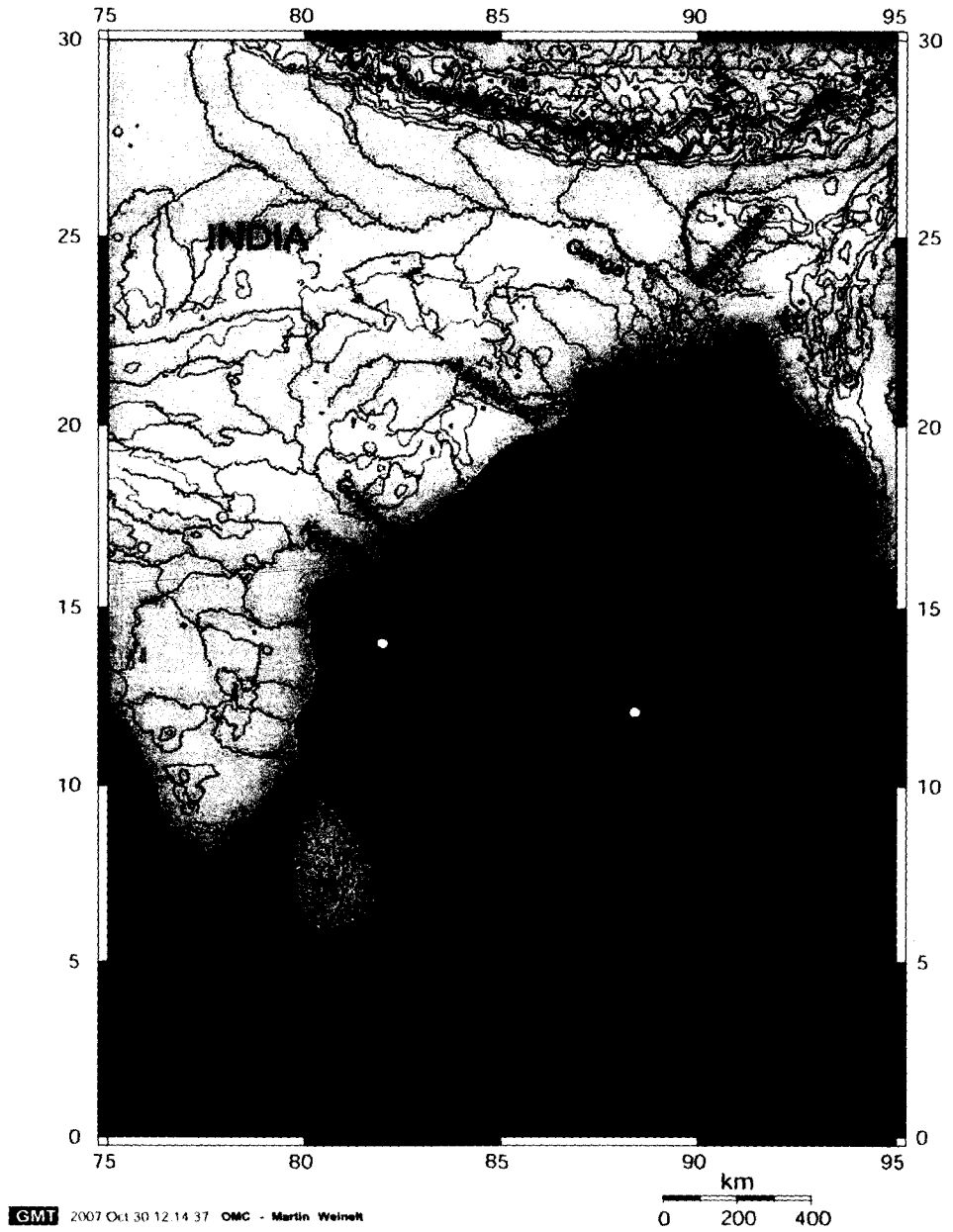

Figure 3.3 Sediment core SK-218/1 and SK-157/20 locations in Bay of Bengal.

The measured ^{14}C ages were converted to sediment ages using the online CalPal version quickcal 2005 ver1.4 (Weninger *et al.*, 2006). The radiocarbon dates were corrected for reservoir effect (400 years) before calibration. The ages calibrated by CalPal and compared with Calib 4.4 and it matches well. CALIB 4.4 software exceed up to 20,000 years.

The time scale was constructed assuming constant sedimentation rates between radiocarbon dates and isotope tie points presented in the (Fig. 3.4 a; b). The sediment accumulation rate varies from 5.9 to 18.2 cm/kyr over last 70 kyr. However,

it is required to mention here that 0 to 66cm sediment contains slumped material from the slope shows older age. Chronological evidences show that from 68cm downwards no reworked sediment is deposited at this site; therefore, we have used the age at 68 cm as core top age and constructed the chronology accordingly.

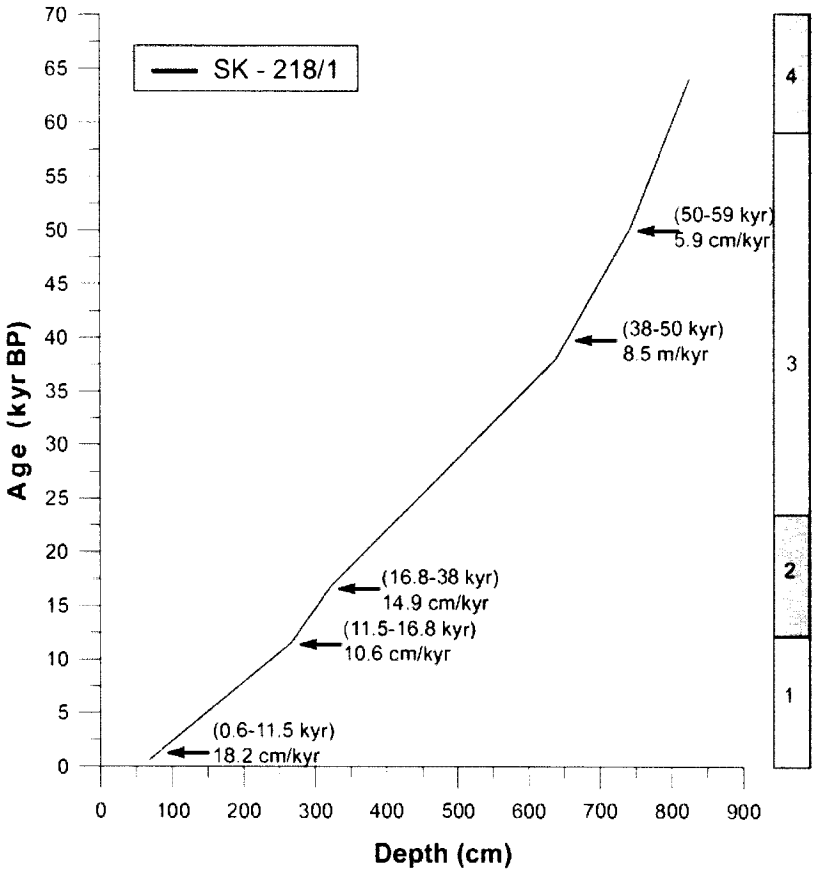

Figure 3.4 (a) Depth (cm) versus age (kyr BP) plot showing variations of sedimentation rate in core SK-218/1. Average sedimentation rates of different section of this core are shown. Marine Isotopes Stages (MIS) are listed on the right panel.

3.4 Results and Discussions:

3.4.1 Sea Surface Temperature (SST) Changes:

The inter-hemispheric heating contrasts between the land and ocean surface are the primary driving forces of monsoon in the Indian Ocean. Summer monsoon rainfall over the Indian region occurs in association with synoptic-scale convective systems generated over the warm seas surrounding the subcontinent that propagate onto the subcontinent (Gadgil 2003). Convection process in the Bay of Bengal and associated propagation from the Bay of Bengal significantly contributes to the summer monsoon

rainfall in the Indian Ocean. The convection processes are highly dependent on SST in the region. Therefore, a better understanding of the temporal variability and spatial redistribution of the upper ocean heat content is thus valuable to comprehend the monsoon dynamics. Therefore, to understand the heat budget of the Indian Ocean in the past it is essential to gain a better knowledge of past SST changes.

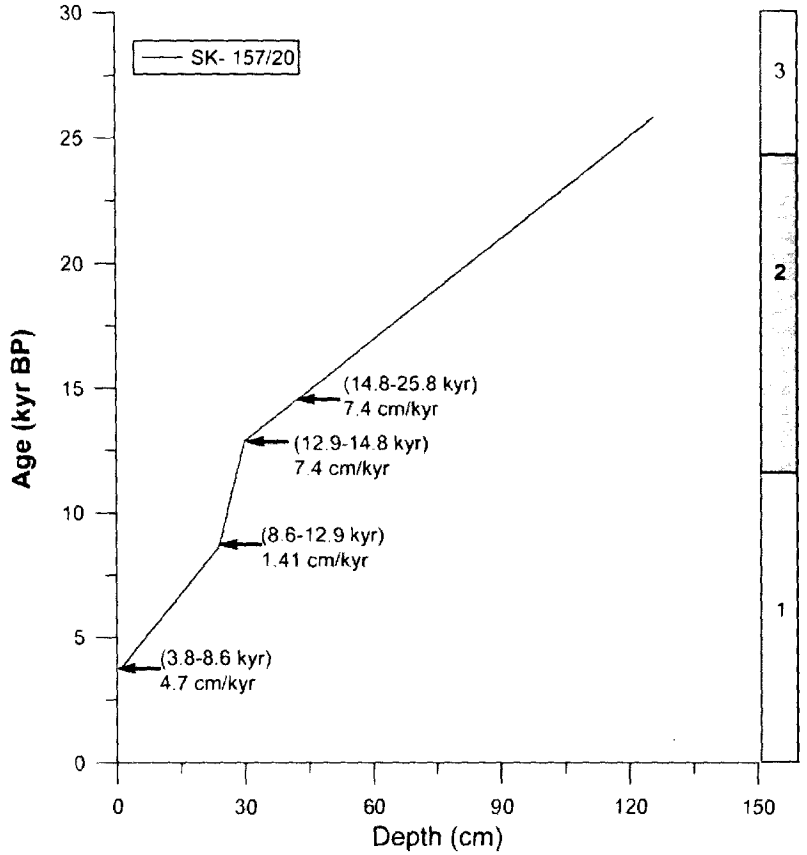

Figure 3.4 (b) Depth (cm) versus age (kyr BP) plot showing variations of sedimentation rate for sediment core SK-157/20. Average sedimentation rates of different parts of this core are shown. Marine Isotopes Stages (MIS) are listed on the right panel.

Statistically based SST estimates from Imbrie-Kipp transfer functions show that the LGM temperatures in the Indian Ocean in general and Arabian Sea in particular are about 1^0C less than Holocene (CLIMAP 1981). However, Kudrass *et al.*, (2001) made a first attempt to reconstruct SST record based on the alkenones from the Bay of Bengal, which document a shift of 2^0C from LGM to Holocene. In this context, for the first time high-resolution reconstructions of SSTs was carried out by

using two independent techniques. By using the magnesium/calcium ratios in planktonic foraminiferal species *G. ruber* a robust and precise SST estimates were derived at the core SK-218/1 from the western Bay of Bengal. Based on the Artificial Neural Networks (ANNs), the annual, summer and winter SSTs changes were estimated over last 22 kyr in the core SK-157/20 from the central Bay of Bengal.

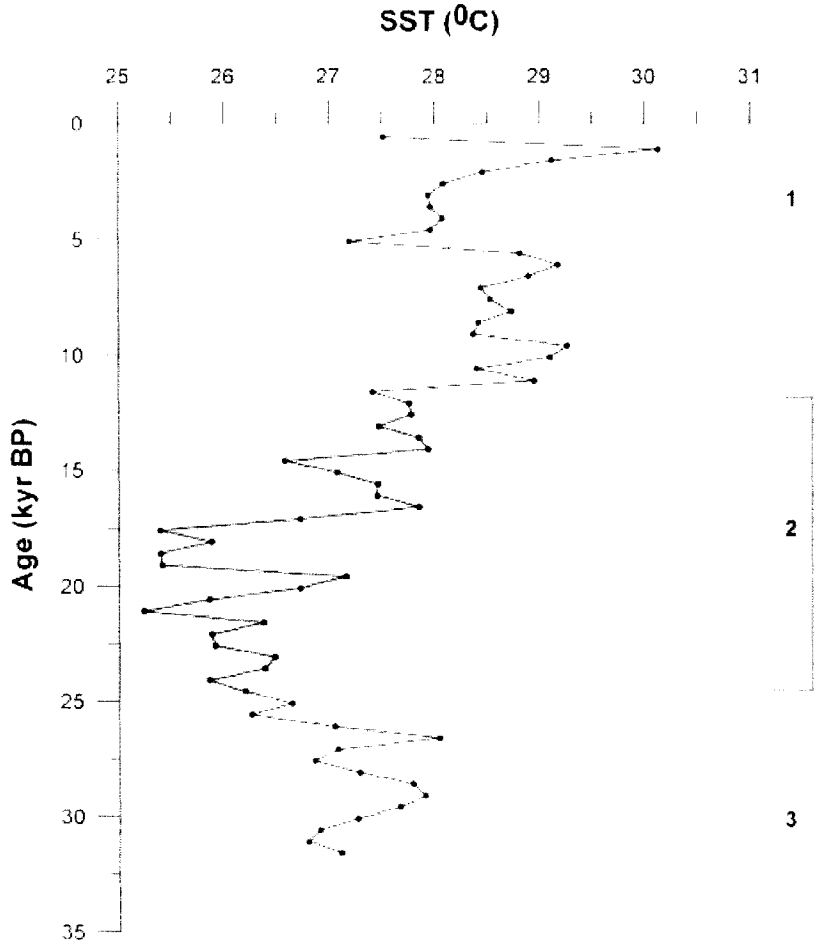

Figure 3.5 Mg/Ca derived Sea surface temperature at core SK – 218/1. Grey band shows the MIS 2 (glacial stage).

SST reconstructions show a temperature range of 30.1^{0}C to 25.2^{0}C over last 33 kyr in the western Bay of Bengal and from 25.5^{0}C to 29.4^{0}C from 25 to 3 kyr in the central Bay of Bengal (Fig. 3.5; 3.6). Although SST estimations from these two locations were estimated by different methods trend and absolute temperature changes are complimenting with each other. Both western and central Bay of Bengal was 3^{0}C colder during LGM than the modern Holocene. This supports the growing body of

evidence that the tropics SST were cooler than earlier SST estimates during LGM by CLIMAP (1981) based on transfer function techniques. SK-218/1 core contains well resolved temperature record than the SK-157/20 therefore based on the SK-218/1 record it is discussed the changes of SST within Marine Isotope Stages (MIS) 1, 2 and 3. A temperature range of 25.8^{0}C to 28^{0}C, 25.4^{0}C to 27.2^{0}C and 27.5^{0}C to 30.1^{0}C was noticed during MIS 3, 2 and 1 respectively. After the last glaciation initiation of warming in the Bay of Bengal started around 17.5 kyr with a SST shift of 2.4^{0}C (Fig. 3.5). This suggest that the effect of deglaciation on warming the tropics was felt first in the Indian Ocean, whereas deglaciation warming effect in the Pacific was noticed around 16 kyr (Lea *et al.*, 2003).

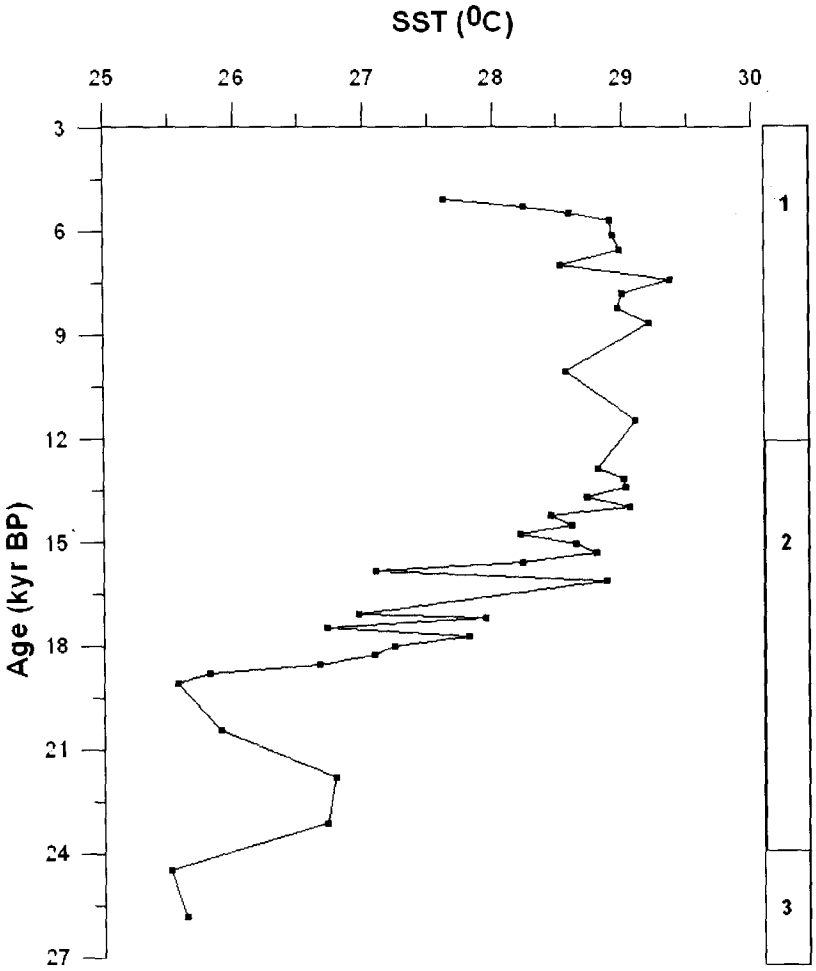

Figure 3.6 Sea surface temperature (SST) derived from Artificial Neural Network (ANN) method at core site SK–157/20. Grey band shows the MIS 2 (glacial stage).

These higher frequency fluctuations of SST in this region may be attributable to changes in cloud cover and water vapor and CO_2 content in the atmosphere. Further, SST of Bay of Bengal was consistently warmer during Holocene and LGM as compared to SST of the Arabian Sea during Holocene and LGM, which suggests that SST and convection process in Bay of Bengal had a major role in controlling the monsoon precipitation in the Indian subcontinent as it does in the modern days (Gadgil 2003).

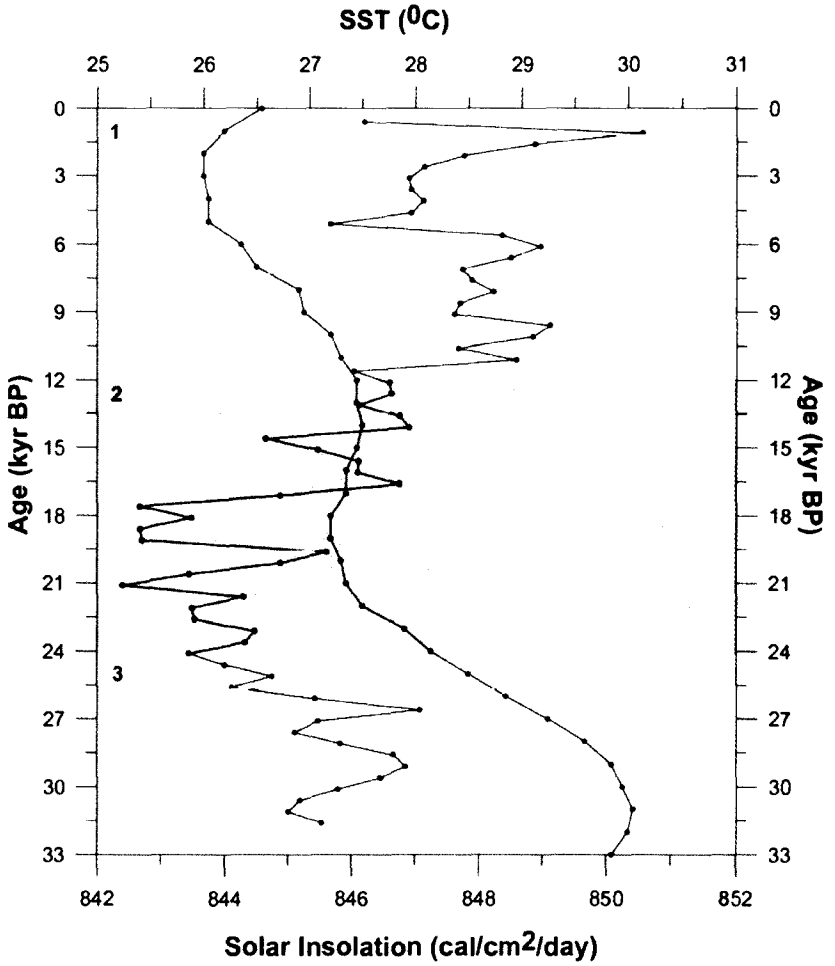

Figure 3.7 a) Profile of SST (blue color) changes in the core SK-218/1 and summer insolation (black color) at (10^0 N). Grey band shows the MIS 2 (glacial stage).

3.4.2 Teleconnections:

Here we use oxygen isotope and Mg/Ca data of foraminifera from a sediment core in the Bay of Bengal to reconstruct sea surface temperature (SST) and surface water oxygen isotopic values. We find that oxygen isotopic values (monsoon signal) and SST of the Bay of Bengal (BOB) lead the Dansgaard-Oeschger (D-O) events. We

therefore, suggest that the monsoon could kick the start of millennial scale abrupt climate changes through the shifts of the Intertropical Convergence Zone (ITCZ) and associated convection, water vapor supply to the tropical troposphere and latent heat penetration.

Monsoon proxies such as *Globigerina bulloides* abundances (Gupta *et al.*, 2003) total organic carbon records (Schulz *et al.*, 1998) from the Arabian Sea and oxygen isotopic ratios of speleothem deposits from Oman (Fleitman *et al.*, 2003) and China (Wang *et al.*, 2001) have demonstrated that abrupt changes in monsoon coincide with temperature changes indicated in the Greenland GISP2. Such kind of coherent changes between monsoon records and high latitude climate prompted to link the monsoon changes to the north Atlantic and or Greenland temperature changes (Schulz *et al.*, 1998; Kudrass *et al.*, 2001; Gupta *et al.*, 2003).

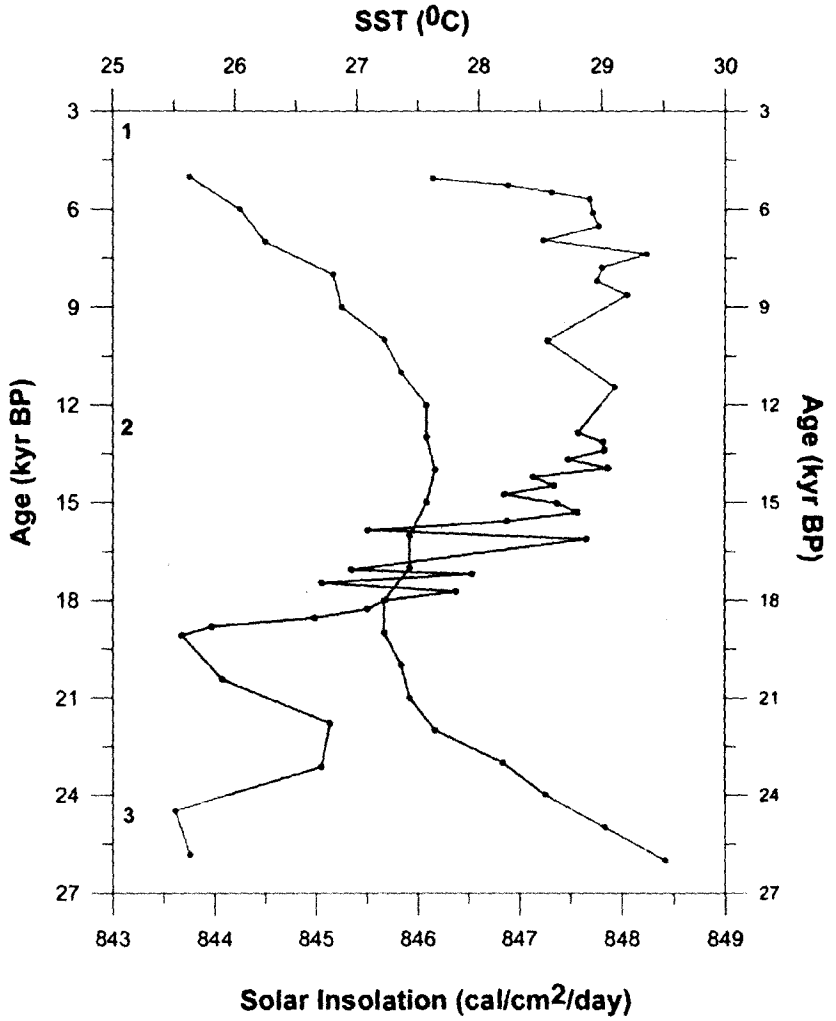

Figure 3.7 b) Profile of SST (blue color) changes in the core SK-157/20 and summer insolation (black color) at (10^0 N). Grey band shows the MIS 2 (glacial stage).

Similarly, synchronous occurrence of Dansgaard-Oeschger (D-O) events in the tropical Atlantic Ocean and South America (Jennerjahn *et al.*, 2004; Wang *et al.*, 2004) and in the equatorial Pacific (Kienast *et al.*, 2006) was documented. All these studies strongly support the hypotheses that temperature changes in the Arctic and Greenland steer the intensity of the Asian Monsoon (Schulz *et al.*, 1998; Kudrass *et al.*, 2001; Gupta *et al.*, 2003; Wang *et al.*, 2001). The puzzling synchronous changes in tropical and high latitude climates have drawn great attention of the paleoceanographic community over a decade. However, the physical link between the high latitude climate and monsoons are still elusive. The peak discharge of rivers and rainfall over the Bay of Bengal (BOB) occurs during the SW monsoon season, which leads to a strongly stratified near-surface layer. Salinity variation and oxygen isotopic values of surface water ($\delta^{18}O_{SW}$) of the Bay of Bengal on interannual and longer time scales are strongly controlled by SW monsoon rainfall. The δ^{18}Osw–salinity relationships of the BOB show 0.45 ‰ per psu (Rostek *et al.*, 1993) associated with strong dilution in the BOB. Greater precipitation and river run off to evaporation ratio in the BOB readily explains its dilution compared to the Arabian Sea. Further, $\delta^{18}O_{SW}$ and SST at this site show an insignificant relationship (r=-0.321), this also suggest dilution plays a major role in controlling the salinity variation. After the removal of global ice volume effect based the sea level changes (Shackleton 2000) from the δ^{18}O of *G. ruber* ($\delta^{18}O_C$), the fluctuation in δ^{18}Osw of the BOB essentially serves as a proxy of rainfall and river run off, both are strongly coupled to the summer monsoon, hence we will interpret changes in δ^{18}Osw in the BOB core solely as a monsoon signal.

Oxygen isotopic ratios of *G. ruber* (δ^{18}Oc) from the Bay of Bengal shows striking similarities with the GISP2 ice core δ^{18}O record which essentially represents changes of air temperature in the high latitudes of the northern hemisphere from 65 to 12 kyr (Dansgaard *et al.*, 1993). However, from 12 kyr to present day the BOB δ^{18}Oc record shows rapid fluctuations as compared to the GISP2 δ^{18}O record (Fig. 3.8). The δ^{18}Oc variations at this site exhibit synchronously depleted values corresponding to the Dansgaard-Oeschger (D-O) events of 1,3,5,6,7,8,9,10,12,14,15 and 16, suggesting that whenever the temperatures were warmer (Interstadials) in Greenland, the oxygen isotopic composition of foraminifera in the BOB are lighter (less saline) (Fig. 3.8). This observation is in line with several other studies from the Arabian Sea (Schulz *et*

al., 1998) and the Bay of Bengal (Kudrass *et al.*, 2001) and speleothem records from Hulu Cave, China (Wang *et al.*, 2001). However, two factors can contribute to the lighter $\delta^{18}O$ values in foraminifera; the warm calcification temperature can cause lighter $\delta^{18}O$ or fresher water supply and/or less evaporation (salinity component) would also lead to lighter $\delta^{18}Oc$. The SK-218/1 $\delta^{18}Oc$ record does exhibit a few differences compared to the GISP2 record: the D-O events 2 and 4 and the Younger Dryas event lead by 1 kyr. To isolate precipitation and river run off which are strongly associated with monsoon rainfall in this region (i.e. monsoon signal), we have compared $\delta^{18}Osw$ with the D-O events documented in the GISP2 record for the period where we have a good control on the chronology of the BOB core and GISP2 record (Fig. 3.9).

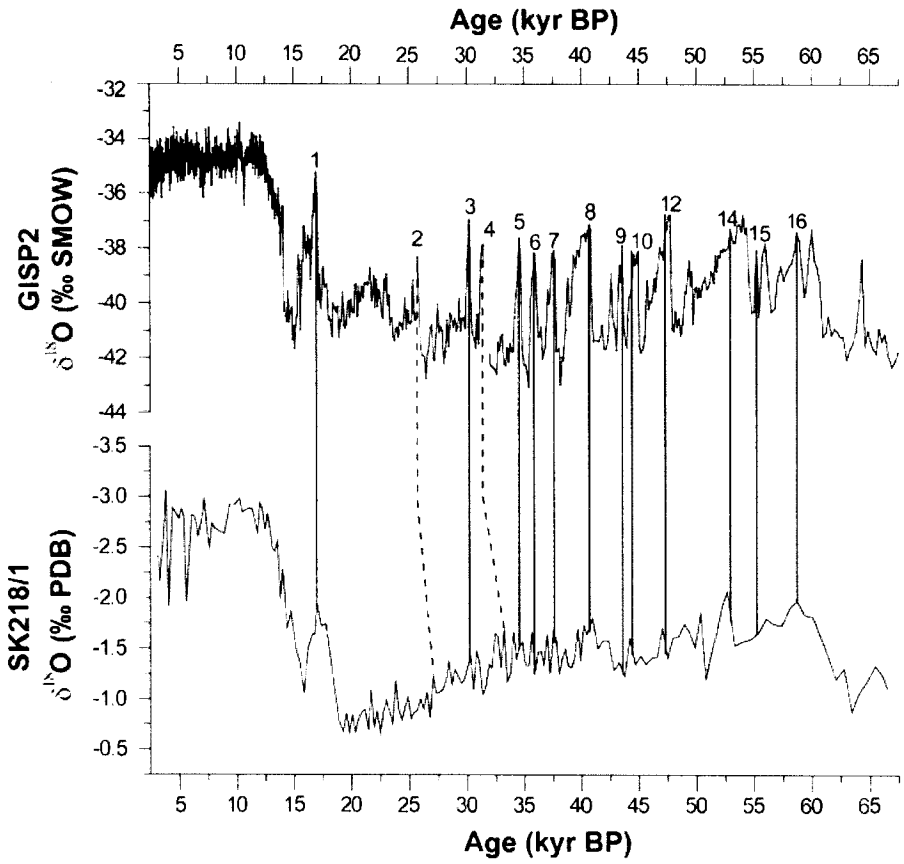

Figure 3.8 Correlation of oxygen isotopic values of *Globigerinoides ruber* ($\delta^{18}O_C$) from SK-218/1 sediment core from the Bay of Bengal and GISP2 Ice Core. The chronology of SK-218/1 and GISP2 are independent. The horizontal line (solid and broken) represents the occurrence of Dansgaard-Oeschger (D-O) events in both the records.

A mean $\delta^{18}Oc$ difference between the Holocene and last glacial maximum is about 2.1‰ after removing the global ice volume effect of 1.2‰. The remaining 0.86‰ reflect temperature and salinity changes. The 2^0C temperature change between LGM and Holocene (Fig. 3.8) accounts for 0.48‰, remaining 0.38‰ indicate that salinity was ~2 psu higher in the Bay of Bengal during the LGM, with more evaporation and less precipitation. Although the NE monsoon activity was stronger during the LGM (Duplessy 1982) this did not lower the salinity considerably in the BOB. However, one could see the difference in salinity gradient between Arabian Sea and BOB during LGM which is attributable to the cause of NE monsoon during LGM.

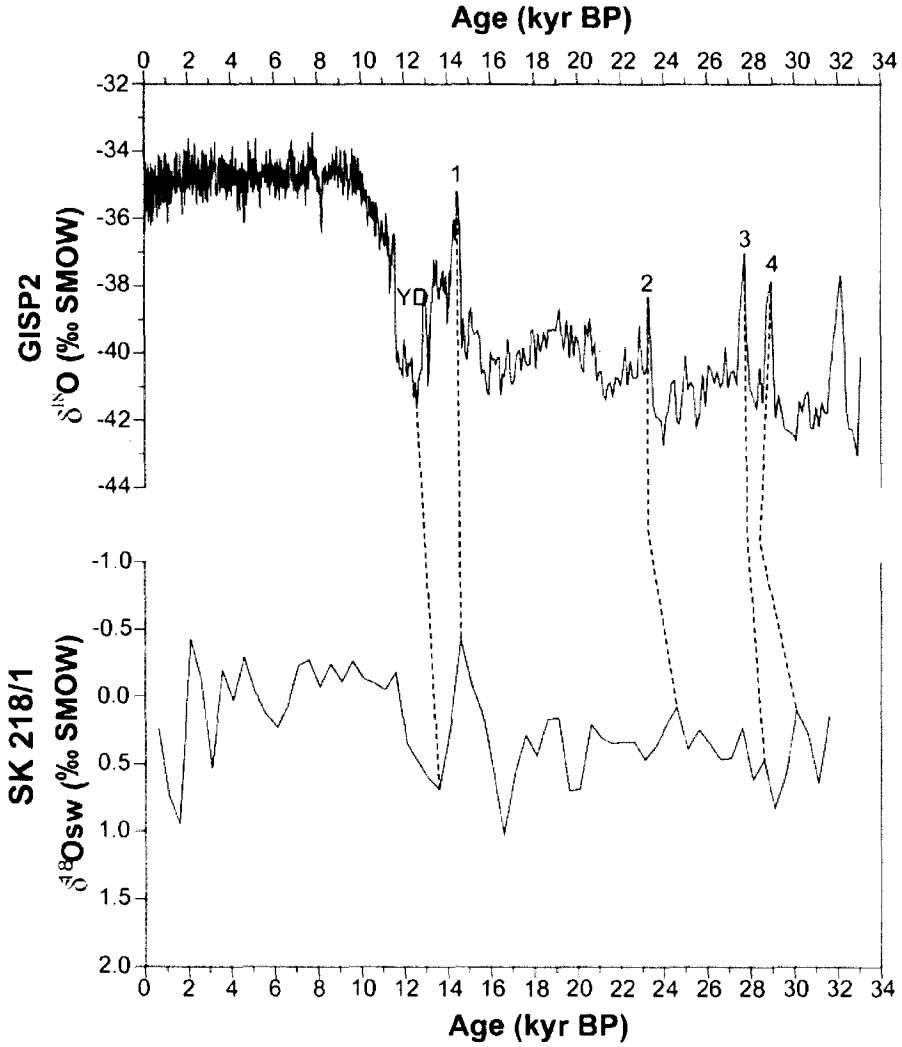

Figure 3.9 Correlation of oxygen isotopic values of sea waters ($\delta^{18}O_{SW}$) from the Bay of Bengal and oxygen isotopic values of GISP2 Ice Core. The abrupt changes in $\delta^{18}O_{SW}$ at YD, D-O event 1, 2, 3, 4 lead (horizontal broken lines) the similar changes in GISP2 Ice Core.

The δ^{18}Osw in the BOB shows D-O events 1, 2, 3 and 4 very prominently with a shift of 0.54‰, 0.31‰, 0.37‰ and 0.55‰ respectively, but the timing of $\delta^{18}O_{SW}$ shifts (events) differs as compared to the GISP2 data set, all four events in BOB record lead that of D-O events noticed in the GIPS2 core (Fig. 3.9). Similarly SST

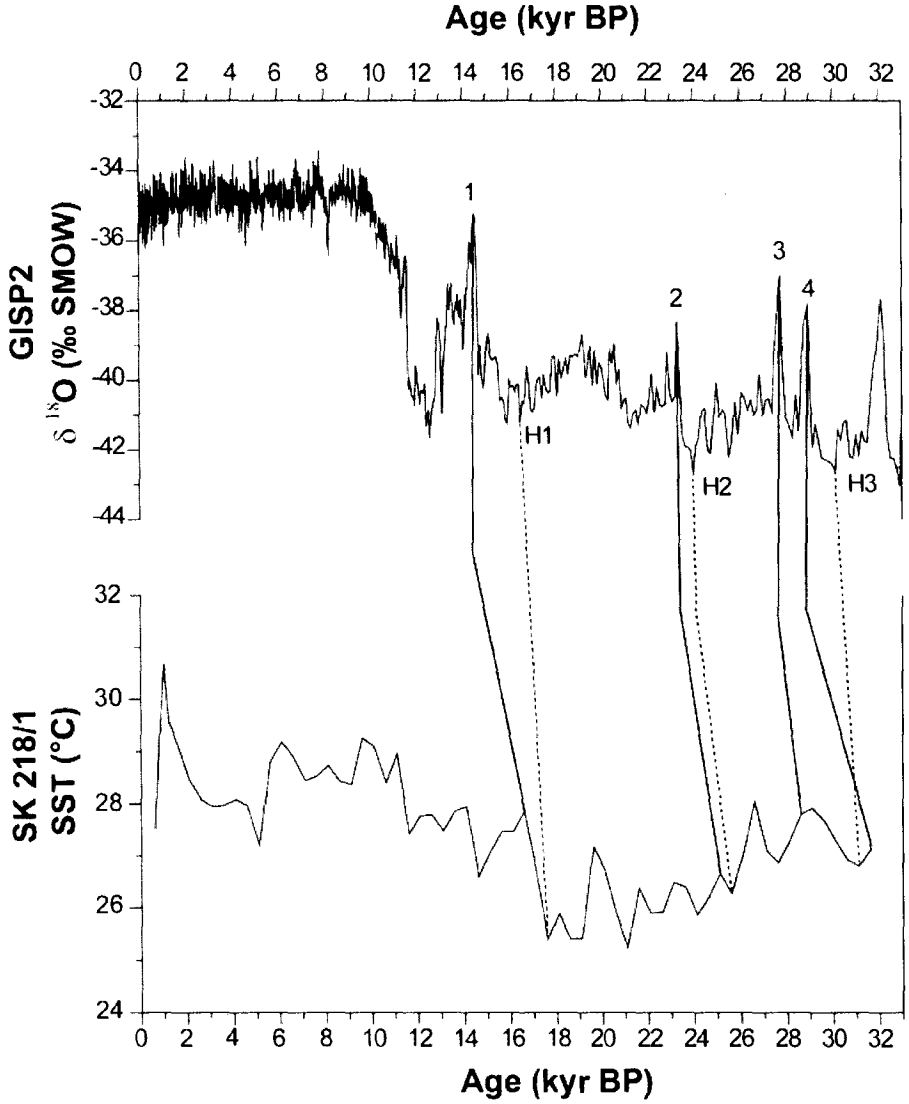

Figure 3.10 Correlation of sea surface temperatures (SST) variations in Bay of Bengal and oxygen isotopic variations of GISP2 Ice Core. Sea surface temperatures of Bay of Bengal lead the Greenland air temperatures. The horizontal lines (both solid and broken) represent the occurrence of Dansgaard-Oeschger (D-O) events in both the records.

changes in particular at Heinrich Events, during deglaciation and at D-O events 1, 2, 3 and 4 lead the $\delta^{18}O_{SW}$ record of GISP2 record (Fig. 3.10). More strikingly, the deglacial warming in the BOB started between 17 to 18 kyr (Fig. 3.10), leading the

warming of the high latitudes by 2-3 kyr. Similarly, other well dated cores from the Arabian Sea show an early deglacial warming (Sirocko *et al.*, 1993; Peeters *et al.*, 1999). We realized that the robustness of $\delta^{18}O_{SW}$, SST comparisons of BOB and GISP2 $\delta^{18}O$ record highly dependent on a meaningful synchronization of age scale. The age model does not have sub-millennial precision. In spite of this limitation SST and $\delta^{18}O_{SW}$ of the BOB do show a pronounced lead varying from 1000 to 600 years over the air temperature changes in Greenland. The observed lead is beyond the precision limits of age estimations; therefore, we believe that this is a robust and persisting feature in the monsoon records of BOB at least.

Our record of $\delta^{18}O_{SW}$ which is a more reliable proxy than the other marine proxies used so far in the northern Indian Ocean (Schulz *et al.*, 1998; Kudrass *et al.*, 2001) show an apparent lead over the D1, D2, D3 and D4 of GISP2 $\delta^{18}O$ record. Not only the $\delta^{18}O_{SW}$ but also the SST shows a clear lead over the GISP2 $\delta^{18}O$ record. Similarly, equatorial Pacific (Lea *et al.*, 2000), Sulu Sea (Rosenthal *et al.*, 2000) and equatorial Indian Ocean SST records (Saraswat *et al.*, 2005) also show a lead over the global ice volume curve. Accordingly, the temperature lead appears to be a robust feature of tropical Pacific and Indian Oceans. Therefore, we suggest that abrupt climate shifts such as the D-O events have first occurred in the monsoon-influenced regions and later in the northern hemisphere high latitudes.

Fresh water supply changes to the North Atlantic reveal a good agreement with past changes in the thermohaline circulation and North Atlantic climate, therefore, it was proposed that the thermohaline circulation changes of North Atlantic would cause abrupt climate shifts during the last glaciation (Clark *et al.*, 2001). Nevertheless, model simulations do not provide compelling proof to support the role of thermohaline circulation changes in governing the abrupt climate shifts on the global scale (Broecker 2003). Accordingly, the mechanism by which thermohaline circulation changes of the North Atlantic will propagate the abrupt climate changes to the tropics in general, and monsoon changes in particular are not clear yet. We therefore, invoke a role of the monsoon which could propagate the signal from tropics to high latitudes through tropical convection.

During Boreal Summer, the ITCZ migrates northward across the Indian Ocean and the Indian subcontinent, bringing with it summer monsoon rainfall (Gadgil 2003). The Asian monsoon plays a dominant role in the tropical climate because it transports

heat and moisture from the warmest part of the tropical ocean across the equator and to the high latitudes. The addition of water vapor to the atmosphere affects temperature both as a green house gas and as a mechanism of latent heat transport from the tropics to high latitudes. During Interstadials (D-O events 1, 2, 3 and 4) the ITCZ had moved to further north which increases the tropical convection, result an increase in overall tropical humidity and consequently an increase in the temperature of the tropics. As a consequence of air temperature rise in the Asian region ice melts in the Tibet Plateau, decreases the albedo in the region, developing greater pressure gradient between Indian Ocean and Tibet Plateau. This kind of set up accelerates monsoon circulation and precipitation over the Indian subcontinent. As the position of the ITCZ shifts away from the equator during the monsoon season the mass energy transport carried by the Hadley cell intensifies (Lindzen and Hou 1988). Such intensification enhances the water vapor supply to the tropical troposphere, which affects the mean tropical SST (Seager *et al.*, 1988). The tropics in general and the Indo-Pacific warm pool, in particular are the main regions from which water vapor is supplied to the atmosphere. As the water vapor is one of the main green house gases, its substantial variation in the atmosphere directly affect the SST in the region.

The global atmosphere is very sensitive to changes in tropical SST (Pierrehumbert 2000) and SST changes in the tropics must initiate feedbacks that alter the energy budget of the planet, which in turn affect climate over much of the globe through changes in the stationary wave pattern (Trenberth *et al.*, 1998). Further, tropical convection could reorganize in a way to shift the ITCZ, either through autonomous variability of the coupled atmosphere-ocean system or in response to orbital changes in the insolation pattern. The propensity for convection increase with SST, and there is a threshold value of SST of about 27.5°C for the Indian Ocean, above which propensity increases (Gadgil 2003). Thus, if the SST of the BOB exceeds 27.5 °C, as a result, the co-variation between SST and precipitation in the tropical Indian Ocean increases. A contraction and expansion of the tropical convection region can decrease and increase temperature, respectively in the tropics (Pierrehumbert 2000). Further, a decrease in Asian monsoon activity during stadials was related to less convectivity activity in the monsoon regions (Wang *et al.*, 2001), which supports the concept that tropical convection and monsoon strength are related. In this context it may mention here that the instrumental data of SST, cloudiness

(ITCZ), evaporation (latent heat) and rainfall were analyzed for the years from 1945 to 1985. It is found that during active monsoon years 1961, 1970, 1975, 1983 and 1988 a strong coupling among the ITCZ propagation and rate of evaporation and precipitation. Thus, high energy of the tropics and the associated hydrological cycle process of the monsoon system itself have a scope for reorganization that could lead to rapid climate transitions. Therefore, SST and $\delta^{18}O_{SW}$ changes in the BOB lead the D-O events in the high-latitude North Atlantic during the past 30 kyr.

It was pointed out earlier that the tropical Pacific is actively involved in forcing global climate change because the tropical Pacific serves as a heat engine for earth's climate and as a vapor source of its hydrological cycle (Lea 2001; Clement *et al.*, 1999; Visser *et al.*, 2003). On the other hand, it is evident that the Indian Ocean plays an active role in controlling the SST in other parts of tropics which includes the Pacific Ocean (Cobb and Charles 2001). Further, Indian Ocean SST anomalies peak 2-3 years prior to those in the Pacific and maximum Indian Ocean anomalies occur at a time when the external forcing from tropical Pacific SST is minimum (Cobb and Charles 2001). Thus, monsoonal processes in the Indian Ocean should exert considerable influence over the climate variability of both the tropical and mid latitudes.

A teleconnection mechanism through the Pacific El Niño system was invoked to explain synchronous changes between monsoon records from the Arabian Sea and northern hemisphere high latitude records (Sirocko *et al.*, 1996). However, linking the monsoon changes to El Niño is rather complex, because during the ENSO initiation phase (June-August), for example, Arabian Sea summer monsoon winds are weakened while those in the South China Sea are strengthened. In contrast, during the mature phase of ENSO (December-February) South China Sea winter monsoon winds are significantly weakened while Arabian Sea winter monsoon winds are only slightly weakened (Wang *et al.*, 2003).

Long-term rainfall variations in China (Wang *et al.*, 2005) and Oman (Neff *et al.*, 2001) appear to follow summer insolation changes. Similarly, temperature changes in the North Atlantic also show a similarity with solar insolation changes (Bond *et al.*, 2001). Such kind of synchronous shifts in high latitude climate and tropical monsoon, and their overall trends matching solar insolation changes suggest that the foot print of solar impact on climate extended from polar to tropical latitudes.

In the tropics the solar insolation is predominantly tied to the precession cycle of the Earth's orbit (Berger and Loutre 1991), the monsoon changes occurred in close association with the harmonic tones of Earth's precessional cycle (23 kyr) (Sirocko *et al.*, 1996). Hence, the precession cycle of variation in solar insolation, water vapor, convection, ITCZ movement in the tropics and the strong tropical ocean-atmosphere feedbacks (Wang *et al.*, 2001; Ivancho *et al.*, 2005) could initiate and enforce the millennial-scale abrupt climate changes on the global scale.

The primary implication of this study lies in monsoon and associated water vapor of the tropics has a strong bearing on the tropical SST and convection. Both monsoon changes and tropical convection can be forced by the solar insolation changes caused by the precession cycle, which would trigger the abrupt climate changes noticed in the northern hemisphere high latitudes. Hence, primary lead of monsoon signal over the northern hemisphere high latitude climate strongly supports the notion that the tropics are actively involved in forcing abrupt climate changes on the global scale, but such kind of tropical forcing mediated through monsoons.

3.4.3 Evaporation and Precipitation Changes in the Bay of Bengal:

Several researchers have studied the variability of SW monsoon mainly based on the upwelling indices (Prell 1984; Anderson and Prell 1993; Naidu and Malmgren 1996; Overpeck *et al.*, 1996) from the western Arabian Sea where the upwelling occurs during SW monsoon season. Attempts have also been made to reconstruct monsoon variability and/or precipitation by using the oxygen isotope ratios in foraminifera species from the western Arabian Sea (Sirocko *et al.*, 1993), eastern Arabian Sea (Sarkar *et al.*, 2000; Banakar *et al.*, 2005; Tiwari *et al.*, 2005), in Pakistan Margin (Schulz *et al.*, 1998) and in Bay of Bengal (Kudrass *et al.*, 2001). Monsoon reconstructions based on the $\delta^{18}O$ of foraminifera have assumed that SST changes within the Holocene were lower (0.5^0C). As discussed earlier (discussion on SST) in the Bay of Bengal as well as in the Arabian Sea a 2^0C shift has been documented within the Holocene, therefore earlier interpretations of monsoon variability based on the $\delta^{18}O$ needs to apply the SST corrections. Here we use a robust proxy of $\delta^{18}Osw$ which entirely depends on the regional changes in evaporation and precipitation was used to understand the monsoon variability.

$\delta^{18}Osw$ show high values (1.01 to 0.07‰) from 32 to 16.5 kyr suggesting the less precipitation and more evaporation due to weak SW monsoon (Fig. 3.11). A

conspicuous shift from more evaporative phase to high precipitation phase took place around 16.5 kyr refer here as strengthening of SW monsoon was initiated after the last glacial period (Fig. 3.11). From 12 to 3.5 kyr low δ^{18}Osw reflecting more precipitation caused by strong SW monsoon. Within the Holocene a weak phase of SW monsoon is recorded around 3.5 kyr and 1.31 kyr (Fig. 3.11). Overall, the monsoon variability reconstructed by the δ^{18}Osw corroborates well with the monsoon reconstructions based on upwelling indices in the western Arabian Sea.

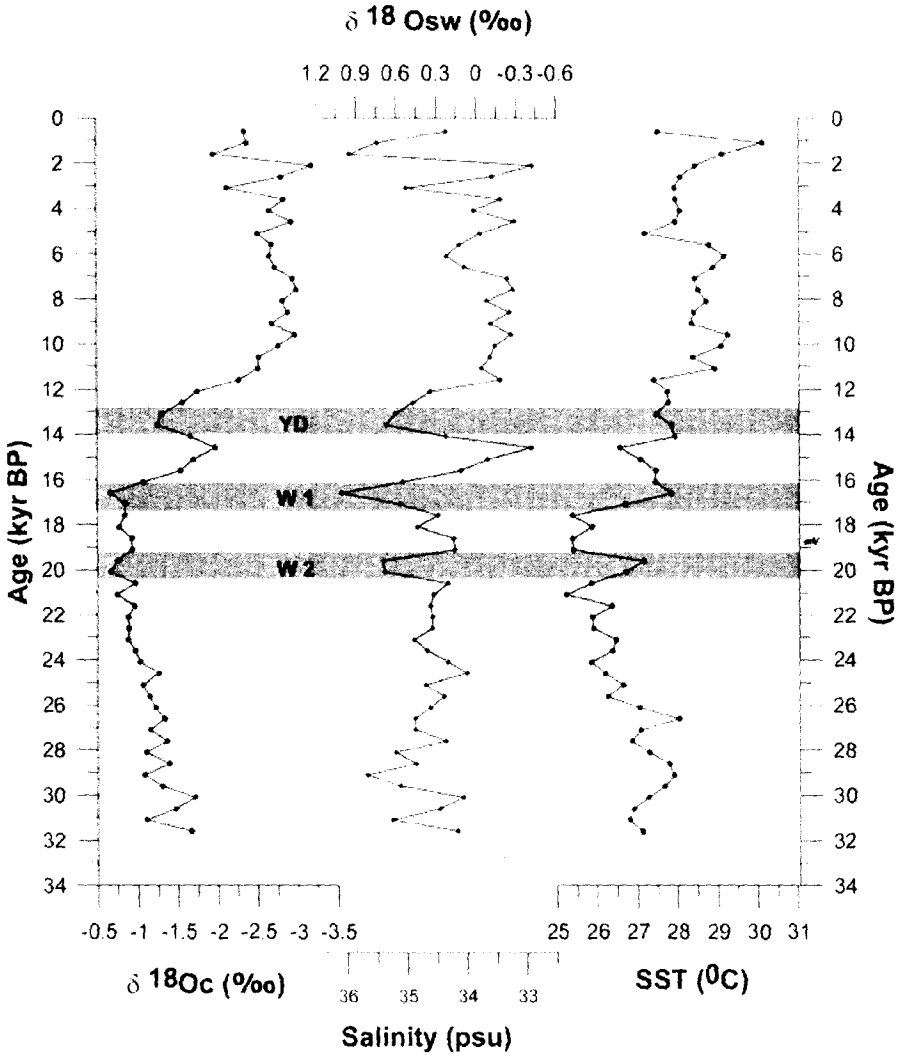

Figure 3.11 Changes of δ^{18}Oc, $\delta^{18}O_{SW}$, salinity and SST in SK-218/1 core. Note YD represent as Younger Dryas, W1 and W2 represents warming events in within the MIS 2. Grey band shows the MIS 2 (glacial stage).

Recently Saher *et al.*, (2007) have discovered two warm events in the Arabian Sea within MIS 2 and coined the event as Arabian Sea Warm Event 1 (ASW1) and

Arabian Sea Warm Event 2 (ASW2) based on the Mg/Ca thermometry. Our dataset of δ^{18}Osw and SST record of Bay of Bengal also register warming events (Fig. 3.11) exactly at same time which corresponds to ASW1 and ASW2 events of Arabian Sea. Saher *et al.*, (2007) have explained that ASW1 and ASW2 were driven by reduced upwelling in the Arabian Sea. Inspite, our core location in Bay of Bengal (Fig. 3.3) is not influenced by upwelling, but the warming events were well documented in our record. Presence of ASW1 and ASW2 in the Bay of Bengal core reveals that NE monsoon changes could trigger such kind of short span events in the Indian Ocean. Similar warming event was documented in the western Arabian Sea and in Bay of Bengal tempts to suggest that the flow of cold NE monsoon winds was reduced due to less pressure gradient between Tibetan Plateau and Indian Ocean would have caused the ASW1 and ASW2 warm events in both Arabian Sea and Bay of Bengal (see chapter 4).

Sea surface salinity has varied from 32.9 to 36.0 psu over last 32 kyr at the SK-218/1 core site, high values (34.1 to 36.0 psu) from 32 to 12 kyr, moderate values (32.8 to 35.9 psu) from 6 to 0.6 ky and low values from 11 to 6 kyr were noticed. δ^{18}Osw and sea surface salinity show similar changes throughout the record (Fig. 3.11). Higher sea surface salinity and enriched δ^{18}Osw were documented during ASW 1 and ASW 2 which points greater evaporation and less precipitation during these events which further supports our argument on weaker NE monsoon during these two warm episodes. δ^{18}Oc record exhibit Younger Dryas (YD) event at SK-218/1 (Fig.3.11), δ^{18}Oc of western Bay of Bengal core SK-218/1 shows a difference of 1.34‰ from modern to YD. However, there was no drop in SST during the YD at this site (Fig. 3.11), but δ^{18}Osw and Salinity show conspicuous increase during YD (Fig. 3.11). This suggest that monsoon rainfall and associated river discharge was reduced during the YD event.

3.4.4 Abrupt Climate Shifts during Holocene:

Holocene was considered as a period of stable climate conditions, however, the reconstruction of millennial and century time scale records reveals that Holocene climate variability is much larger and frequent than commonly understood. Examinations of ~50 globally distributed paleoclimate records revealed as many as six periods of significant rapid climate changes during the following time periods

9000-8000, 6000-5000, 4200-3800, 3500-2500, 1200-1000, and 600-150 cal yr B.P. (Mayewski *et al.*, 2004). Similarly, glacier fluctuations (Denton and Karlen 1973) and ice sheets drift in north Atlantic (Friedrich *et al.*, 1999, Bond *et al.*, 2001) were noticed more or less in the frequency of 1400 years during the Holocene.

The SW monsoon intensity was stronger in early Holocene (10-8 kyr) and arid phase starts at ~4 kyr (Overpeck *et al.*, 1996; Gupta *et al.*, 2003; Staubwasser *et al.*, 2003). These abrupt changes in SW monsoon cause changes in rainfall over India and affecting the fluvial systems and thus biota of the region (Nigam and khare 1990; Goodbred and Kuehl 2000; Hong *et al.*, 2003; Sharma *et al.*, 2004; Guptha *et al.*, 2005). Many researchers have suggested that solar activity was the primary cause in driving the abrupt climate shifts such as Bond Cycles in the North Atlantic (Bond *et al.*, 2001) and rainfall changes in Oman (Neff *et al.*, 2001). Results from the recent atmospheric general circulation (GCM) models support that a decrease in solar activity by 0.1% could produce a change in surface hydrography of the ocean and change in stratospheric ozone and temperature (Bond *et al.*, 2001).

3.5 Conclusion:

Reconstruction of sea surface temperatures (SST) based on Magnesium/Calcium thermometry and Artificial Neural Network (ANN) Technique reveals that both western and central Bay of Bengal was 3^0C colder during LGM than the modern Holocene. This provides evidence that the tropics were much cooler than it was believed earlier and CLIMAP (1981) reconstruction of sea surface temperature by using the transfer function technique of Imbrie and Kipp (1973) under estimated the LGM temperatures of the Indian Ocean. Furthermore within glacials (MIS 2 and 4) and interglacials (MIS1 and 2) about 1 to 2^0C SST change was noticed in the Bay of Bengal.

Oxygen isotopic values of *G. ruber* (δ^{18}Oc) from the Bay of Bengal shows striking similarities with the GISP2 ice core δ^{18}O record which essentially represents changes of air temperature in the high latitudes of the northern hemisphere from 65 to 12 kyr. Conspicuously, oxygen isotopic values of surface water (δ^{18}Osw) (monsoon signal) and SST changes at the SK-218/1 core site from the Bay of Bengal lead the Dansgaard-Oeschger (D-O) events. This suggests that the monsoon could kick the start of millennial scale abrupt climate changes through the shifts of the Intertropical

Convergence Zone (ITCZ) and associated convection, water vapor supply to the tropical troposphere and latent heat penetration. Thus monsoon and associated convection process in the tropics play an important role in driving the abrupt climate shifts on a global scale.

δ^{18}Osw variability demonstrates that the evaporation was higher than the precipitation from 32 to 16.5 during last glacial period and in the initial phase of MIS 3 representing weak SW monsoon. A striking shift from more evaporative phase to high precipitation phase took place around 16.5 kyr as strengthening of SW monsoon initiated around this time. During the Holocene descending strength of monsoon started around 3.5 kyr. Overall, the monsoon variability reconstructed by the δ^{18}Osw corroborates well with the monsoon reconstructions based on upwelling indices from the western Arabian Sea.

SST records of Bay of Bengal documents sharp warming events within last glacial period (MIS2) around 17 and 19 kyr which coincide with similar warm events in the Arabian Sea (ASW 1 and ASW 2) (Saher *et al.*, 2007). High δ^{18}Osw values were noticed during these warm events, which suggest a weak SW monsoon would lead to less fresh water discharge and monsoon precipitation in the Bay of Bengal.

CHAPTER 4

Quantification of paleo sea surface temperature and sea surface salinity over last 68,000 years in the Arabian Sea: Response of evaporation-precipitation budget

4.1 Introduction:

The southwest (SW) monsoon system in the Arabian Sea exerts a strong influence upon the climatic conditions in south and southeast Asia and the associated monsoon rainfall have great impact on the socio-economic and agricultural development in the densely populated south Asia. The interhemispheric heating contrasts between the land and the ocean surface are at the heart of the monsoon phenomenon in the Indian Ocean. The upper ocean heat supply feeds the necessary evaporation and atmospheric moisture transports during the summer monsoon season. Therefore, a strong link exists between ocean dynamics and the atmospheric heat and moisture transfer that are critical to the strength of the monsoons (Manghnani *et al.*, 2002; Naidu and Malmgren 2005) and also evaporation, precipitation and heat budget of the Arabian Sea is strongly coupled with SW monsoon intensity.

To track the evolution and variability of monsoon beyond the historical times one needs to depend on the monsoon proxy records which are preserved in the marine and terrestrial records. Long-term variations of monsoonal intensity tracers, especially the species diversity of calcareous nannofossil species, and the abundance of the planktonic foraminifera *Globigerina bulloides* and the radiolarian *Actinomma* spp. (upwelling indicators) show that the evolution of the monsoon started in the late Miocene, at about 9.5 Ma (million years ago). Between 9.5 and 5 Ma the monsoon increased noticeably in strength, with smaller fluctuations in monsoonal intensity from 5 to 2 Ma. Uplift of the Himalayas and the Tibetan Plateau occurred coeval with the increase in strength of the Asian Monsoon between 9.5 and 5 Ma (Niitsuma and Naidu 2001). Multi proxy based monsoon variability from the western Arabian Sea reveal that in general monsoons were stronger during interglacials and weaker during glacials (Clemens *et al.*, 1991).

Reconstruction of monsoon variability on glacial and interglacial time scales as well as on millennial time scale was carried out from western Arabian Sea because the strength of SW monsoon winds is linearly related with the intensity of upwelling.

Thus various upwelling proxies have been used to trace the SW monsoon intensity for last two decades (Prell 1984; Anderson and Prell 1993; Sirocko *et al.*, 1993; Naidu and Malmgren 1995; 1996; Overpack *et al.*, 1996; Altabet *et al.*, 2002; Gupta *et al.*, 2003; Naidu 2004). Attempts have also been made to trace the upwelling strength in western Arabian Sea based on the annual and seasonal SST differences between glacial and interglacial mainly derived from oxygen isotopes, alkenones and modern analog technique (Artificial Neural Network) respectively (Rostek *et al.*, 1993; 1997; Emeis *et al.*, 1995; Zahn and Pedersen 1991; Naidu and Malmgren 2005). These studies show that Last Glacial Maxima was 2^0C colder than modern Holocene (Naidu and Malmgren 2005). Although eastern Arabian Sea receives more amount of rainfall during SW monsoon as compared western Arabian Sea very limited studies were carried out to reconstruct the monsoon variability from the eastern Arabian Sea (Sarkar *et al.*, 1990; 2000; Chodankar *et al.*, 2005; Tiwari *et al.*, 2005). All these studies from eastern Arabian Sea have used the oxygen isotope ratios of foraminifera to understand the monsoon variability. Oxygen isotope ratios of foraminifera represent $\delta^{18}O$ of sea water (function of salinity) and sea surface temperature; hence with out SST data the interpretation of $\delta^{18}O$ data in terms of rainfall variability is highly subjected to assumption. However, these studies did not find any systematic correlation between SST changes and monsoon intensity on glacials and interglacials time scales because these authors did not dealt directly with measurement of SST and evaporation-precipitation proxies in eastern Arabian Sea. Therefore, in this study by using Magnesium/Calcium (Mg/Ca) thermometry and $\delta^{18}O$ of planktonic foraminifera *Globigerinoides ruber* estimates of $\delta^{18}O$seawater ($\delta^{18}O_{SW}$) were computed. The $\delta^{18}O_{SW}$ would be a more reliable proxy to address the monsoon variations because $\delta^{18}O_{SW}$ values are mainly controlled by evaporation and precipitation in the region.

4.2 Oceanographic Setting:

Seasonal reversal of the monsoon winds over the Arabian Sea influences surface circulation, productivity, biogenic and lithogenic fluxes, CO_2 uptake and heat budget in the region. The SW monsoon is accompanied by strong winds (~30 knots), cloudy skies and moist air. In addition, the ocean gains heat (an average of 89.5 Wm^{-2}), but SST decreases by 5.5^0C and the mixed layer deepens to almost 80 m in the central Arabian Sea and becomes shallow at the Oman Margin compared to the inter

monsoon seasons (Schott and McCreary 2001). The heat flux from the Arabian Sea to the atmosphere is higher during winter (November, December and January) as compared to other months (Hastenrath and Lamb 1979). During the SW monsoon the western Arabian Sea gains heat whereas the eastern Arabian Sea loses heat to the atmosphere.

The salinity in the upper water column during the SW monsoon is reasonably uniform, but decreases from about 36.5 to 36.0 psu during the course of the SW monsoon season (Fig. 4.1). The SW monsoon wind field causes upwelling along the Arabian coast, leading to persistent jets of cold upwelled water extending from the Oman coast and often advecting laterally about 600 km offshore (Brink *et al.*, 1998; Fischer *et al.*, 2002). Outside of the regions of coastal upwelling during the SW monsoon, SST's are generally high, varying from 27^0C to 29^0C (Fig. 4.2).

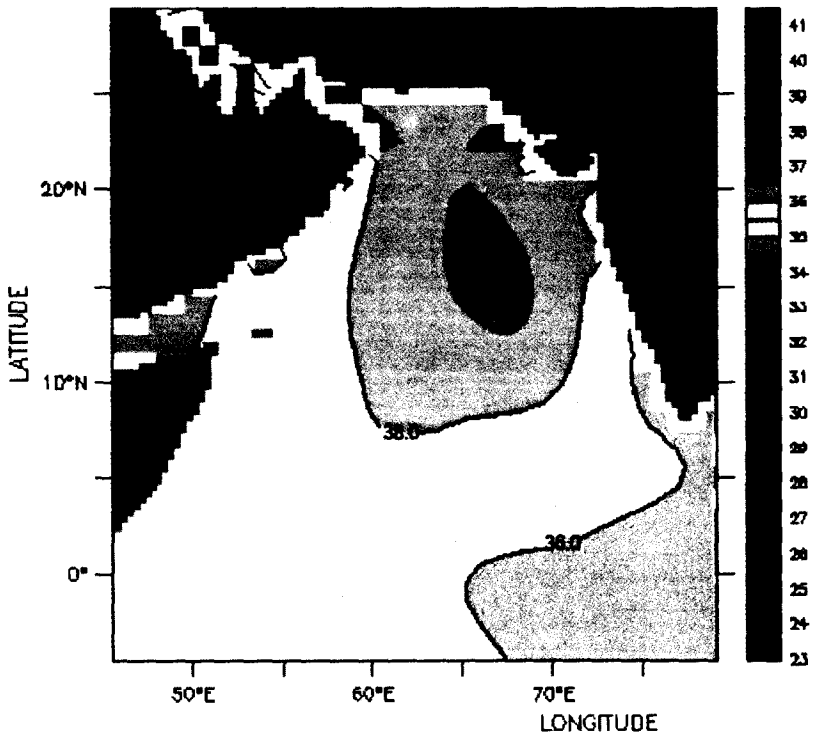

Figure 4.1 Average sea surface salinity during SW monsoon in Arabian Sea (Levitus et al., 1994).

The NE monsoon is characterized by moderate winds (~10 knots), clear skies and dry air. During the NE monsoon the ocean loses heat (an average of 19.7 Wm^{-2}) to the atmosphere with a 3^0C SST decrease (Weller *et al.*, 2002). The two intermonsoon seasons are substantially different from either of the monsoon seasons. These are

characterized by weak winds and strong sea-surface heating. The SW monsoon determines the climate of the northern Indian Ocean during the northern hemisphere summer and the NE monsoon the climate of the northern Indian Ocean during the northern hemisphere winter. The winds are generally weak during the intermonsoonal periods, with the Fall Intermonsoon being significantly shorter than the Spring Intermonsoon (Weller *et al.*, 2002).

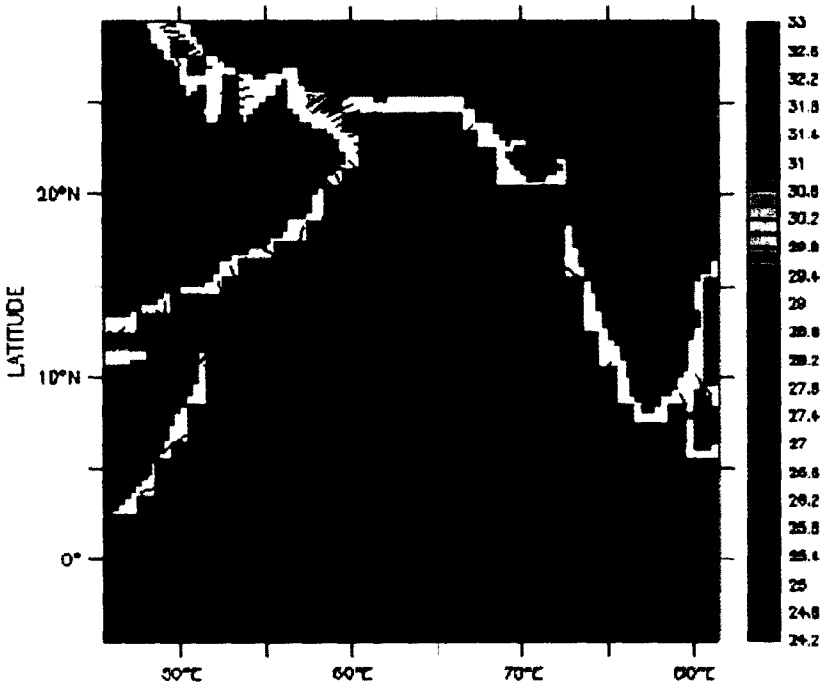

Figure 4.2 Average sea surface temperature during SW monsoon in Arabian Sea (Levitus and Boyre 994).

The general pattern of evaporation and precipitation in the eastern Arabian Sea is influenced by two major factors (Darbyshire 1967): 1) heavy rain fall above the Deccan Mountains (especially in western side) during SW monsoon and the fresh water drains in to the sea by seasonal rivers from coast of Kerala, south-west India, 2) the low salinity water tongue from western Bay of Bengal to the south of eastern Arabian Sea during NE monsoon (Wyrtki 1973). Sea surface salinity (SSS) in the Arabian Sea is relatively higher than in Bay of Bengal. It varies from 35.0 to 36.5 psu, reveals that high evaporation and intrusion of high saline water from Red Sea and Persian Gulf (Fig. 4.1).

4.3 Results:

The sediment core AAS-9/21 was collected at water depth of 1807m from eastern Arabian Sea (Fig. 4.3) and the chronology of this core was established based on six AMS ^{14}C dates up to 310 cm depth of the core, further down chronology was established by correlating $\delta^{18}O$ of *Globigerinoides ruber* ($\delta^{18}Oc$) record of this with low latitude $\delta^{18}Oc$ global isostack curve given by Martinson *et al.*, (1987). ^{14}C AMS dating were performed on monospecific samples of the planktonic foraminifera *Globigerinoides ruber* using Tandem Accelerator at Leibniz Labor fur Altersbestimmung und Isotopenforschung, Christian-Alberchts-Universitat, Kiel, Germany.

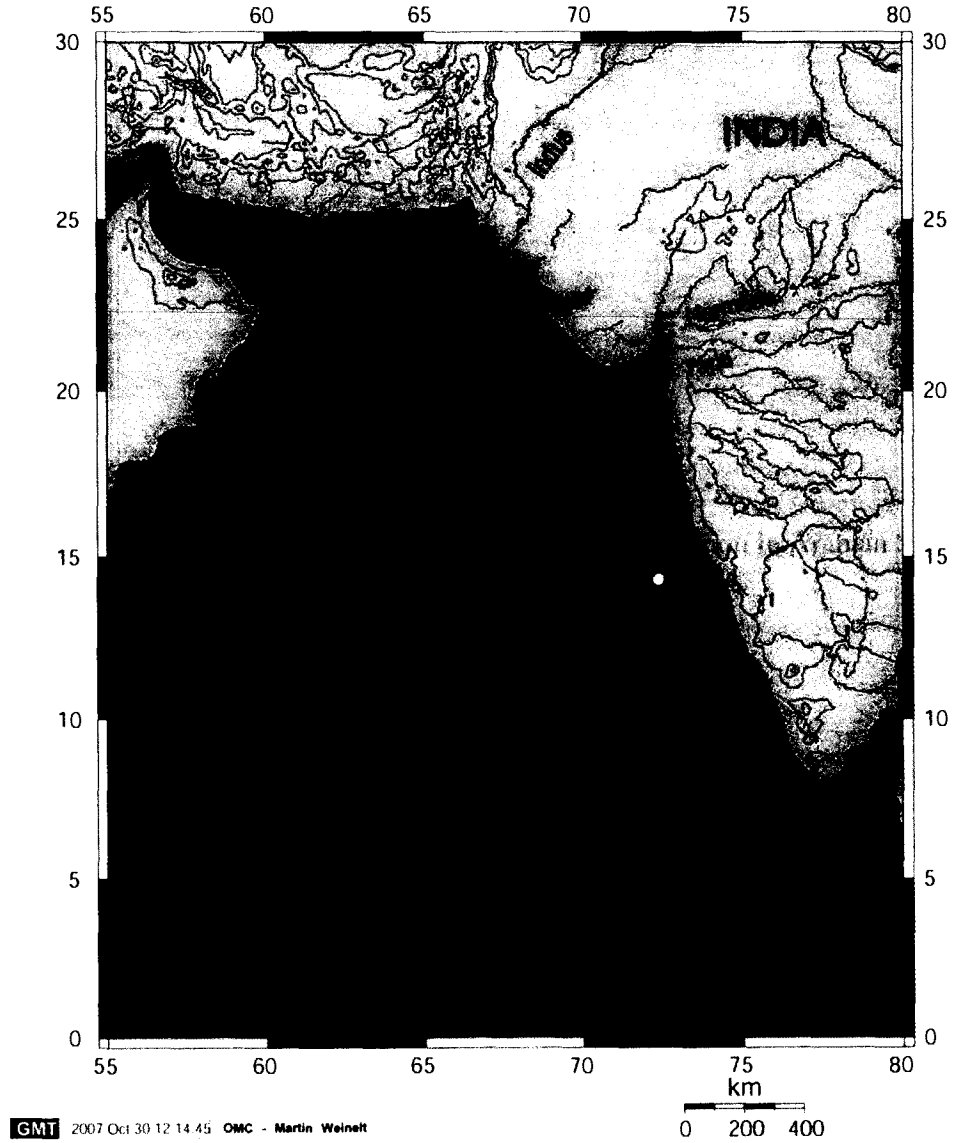

Figure 4.3 Location of core AAS-9/21 and physiography of Arabian Sea.

The measured ^{14}C ages were converted to sediment ages using the online CalPal version quickcal 2005 ver1.4 (Weninger *et al.*, 2006). The ages calibrated by CalPal and by Calib 4.4 were compared and matches well. CALIB 4.4 software exceed up to 20,000 years (As described in chapter 3). The depth and corresponding ages are shown in Fig. 4.4. The sedimentation rate at this location varies from 13 to 4 cm/kyr and time resolution between two data points corresponds to resolution between data points correspond to approximately 400 years.

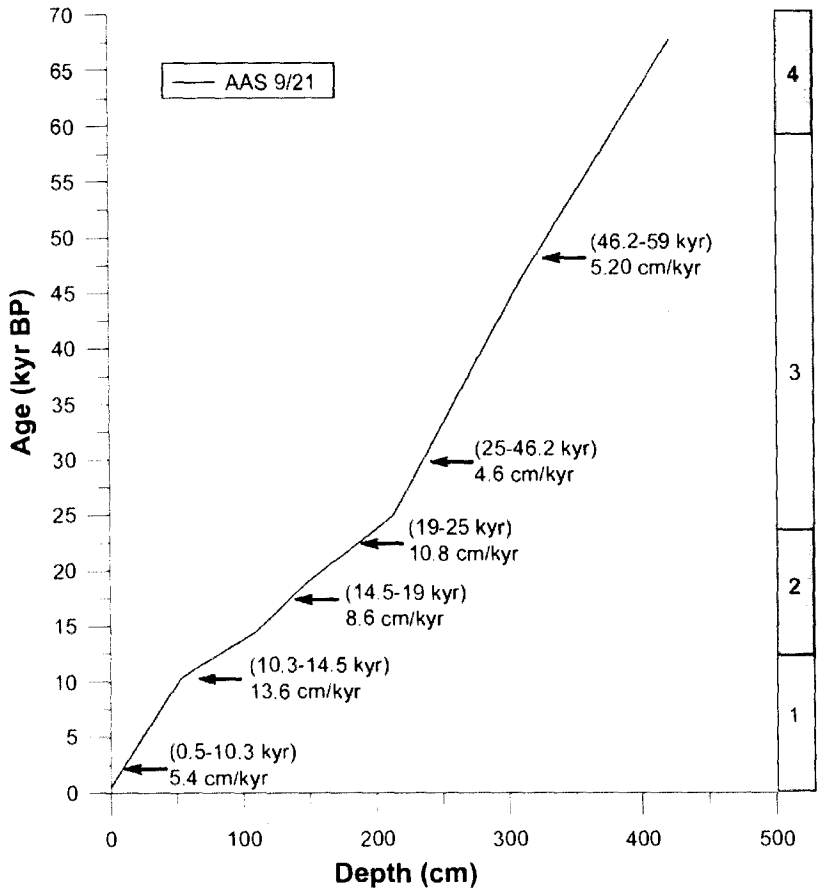

Figure 4.4 Depth (cm) versus age (kyr BP) plot showing variations of sedimentation rate in core AAS 9/21. Average sedimentation rates of different section of this core are also shown. Marine Isotope Stages (MIS) are marked on the right panel, glacial stages shows are shadowed.

4.3.1 Oxygen Isotopes:

The oxygen isotope of calcite shell ($\delta^{18}Oc$) record of core AAS-9/21 (Fig. 4.5) covers the time span of 68 kyr B.P. with a resolution of approximately 400 years. The $\delta^{18}Oc$ values ranges from 0.2‰ to -2.3‰. In Marine Isotope Stage (MIS) 4, $\delta^{18}Oc$ values vary from -0.92‰ to -0.55‰ with an average value of 0.76‰. In MIS 3, $\delta^{18}Oc$

values ranges from -1.40‰ to -0.37‰ with an average value of -1.11‰ (Fig. 4.5). The δ^{18}Oc values do not show any major shifts within MIS 3 and 4, whereas during MIS 2 an abrupt δ^{18}Oc shift of 1‰ is noticed (Fig. 4.5). δ^{18}Oc values show a gradually depleting trend from 19 kyr BP. δ^{18}Oc values at this site do not show Younger Dryas Event (Fig 4.5).

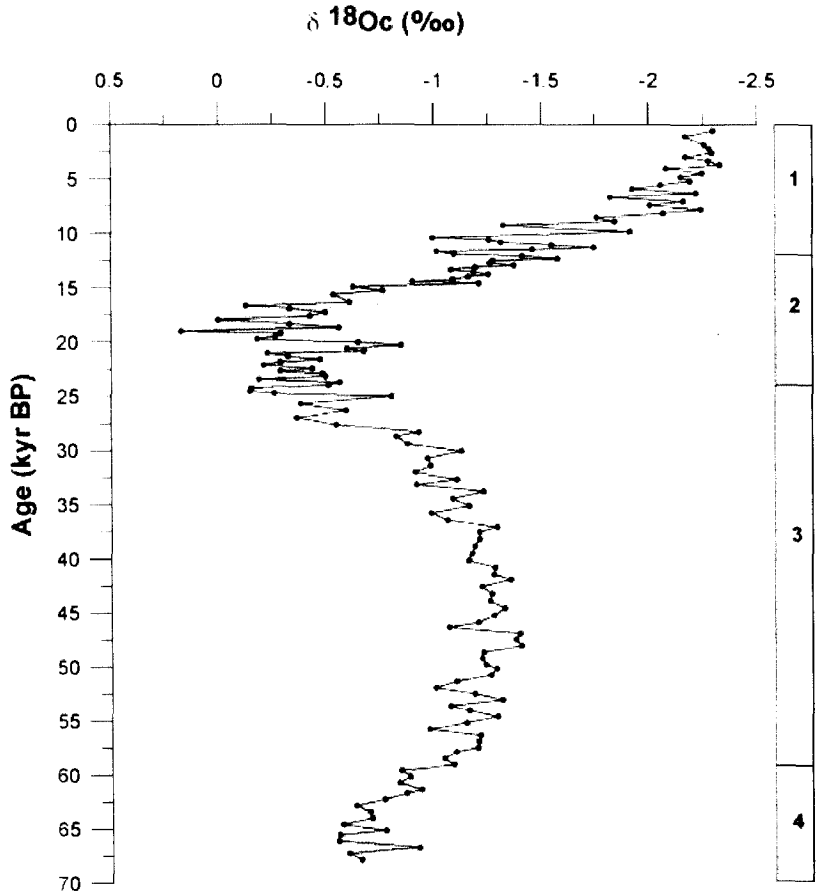

Figure 4.5 Oxygen isotope profile of core AAS-9/21 from the eastern Arabian Sea. Grey bands represent the MIS 2 and MIS 4 (Glacial Stage).

4.3.2 Mg/Ca Sea Surface Temperature Reconstruction:

The Mg/Ca based temperature record displays some interesting changes from MIS 4 to late Holocene period (Fig. 4.6). During MIS 4 the SST ranges from 28.1^{0}C to 26.6^{0}C reflecting a variation of 1.5^{0}C within in MIS 4, whereas in MIS 3 SST varied from 27.1^{0}C to 25.2^{0}C show variation of ~2^{0}C, which reveals that SST were warmer during MIS 4 compared to MIS 3. During MIS 2 SST varies from 27.3^{0}C to 24.5^{0}C with two warming brief warming events at 20 and 17 kyr BP. A steep SST rise (2.9^{0}C) was documented between 18.6 to 13.2 kyr BP. Within MIS 1, 2^{0}C SST

change has been recorded at this core location with highest SST of 29^{0}C at 0.5 kyr BP (Fig. 4.6).

4.3.3 Oxygen Isotope Ratios of Surface Waters (δ^{18}Osw):

δ^{18}Osw has been reconstructed after removing the temperature and global ice volume effect, which represent the direct influence of evaporation-precipitation at the core location, are presented in Fig. 4.6. During the MIS 4 δ^{18}Osw values range from 0.9‰ to 1.41‰, whereas 0.3 to 1.0‰ variation is documented in MIS3. Strikingly the δ^{18}Osw values were higher during MIS 4 as compared to MIS 1 (Holocene) (Fig. 4.6). Within MIS 2 δ^{18}Osw shows significant fluctuations in the order of 1‰ and these major excursions occurs in time coincidence with Arabian Sea Warm Event 1 and 2 (ASW1 and ASW2) (Saher *et al.*, 2007). At times, during MIS 2 the δ^{18}Osw were as

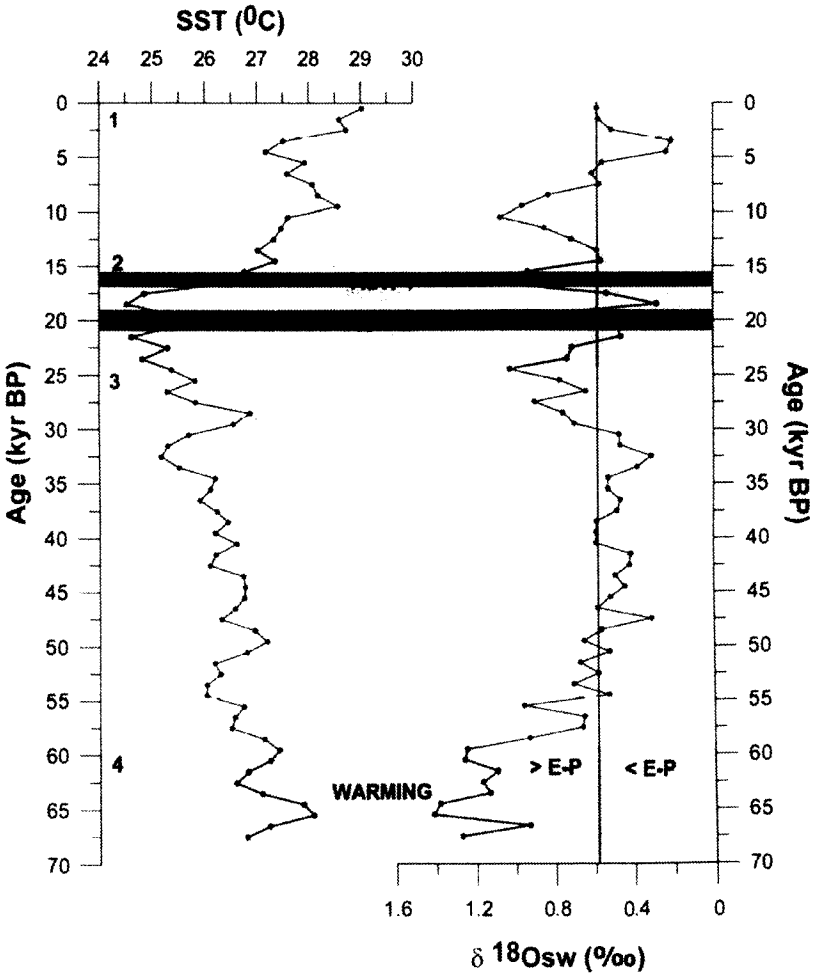

Figure 4.6 Profile of sea surface temperature (SST) and oxygen isotopic values c AAS-9/21 from the eastern Arabian Sea. Bands in red shows ASW1 and ASW2 MIS 2 shows early warming phase in eastern Arabian Sea.

high as modern values revealing rapid shift in the rainfall pattern in the region. During deglaciation also a steep decline in δ^{18}Osw from 1.14 to 0.54‰ was noticed. During MIS 1, δ^{18}Osw varies from 1.08‰ to 0.61‰ (Fig 4.6).

.

4.3.4 Sea Surface Salinity:

Sea surface salinity was estimated by using the salinity - δ^{18}Osw relationship obtained through JGOFS data set within the Arabian Sea (Dahl *et al.*, 2006). A 2.1 psu change in salinity is documented over last 68 kyr BP at this core location in the eastern Arabian Sea (Fig. 4.7). A major changes in sea surface salinity occurred during MIS 4 and MIS 2, further sea surface salinity was higher during MIS 4 than 2. The MIS 3 documents higher salinity values as compared to MIS 1 (Fig. 4.7).

4.4 Discussion:

Arabian Sea is an evaporative basin (Oberhuber 1988). Therefore, the δ^{18}Osw and salinity changes in the Arabian Sea are controlled by evaporation, precipitation and upwelling processes. Western Arabian Sea experiences the upwelling and brings the fresh water to the surface in summer, whereas eastern Arabian Sea receives more precipitation during SW monsoon.

4.4.1 Marine Isotope Stage 4:

MIS 4 (59-67 kyr BP) record higher SST (28.1^{0}C), more depleted δ^{18}Oc values, enriched δ^{18}Osw values and higher salinity as compared to MIS 2 (Fig 4.5; 4.6). This suggests that eastern Arabian Sea was more evaporative during MIS 4 than in MIS 2. Prevalence of higher SST during MIS 4 than the MIS 2 would result in more evaporation during MIS 4. Earlier it was reported that evaporation was higher during MIS 2 than in MIS 4 (Rostek *et al.*, 1993). The MD900963 core studied by Rostek *et al.*, (1993) was located further southward and is highly influenced by the low salinity water mass of Bay of Bengal. Therefore, low δ^{18}Osw during MIS 4 in MD900963 would reflect greater flow of low saline water into the core site. Furthermore, SST were higher in MIS4 as compared to MIS3 in both these cores provides another evidence that MD900963 core δ^{18}Osw were not only related to evaporation rather it was highly influenced by Bay of Bengal low saline water mass.

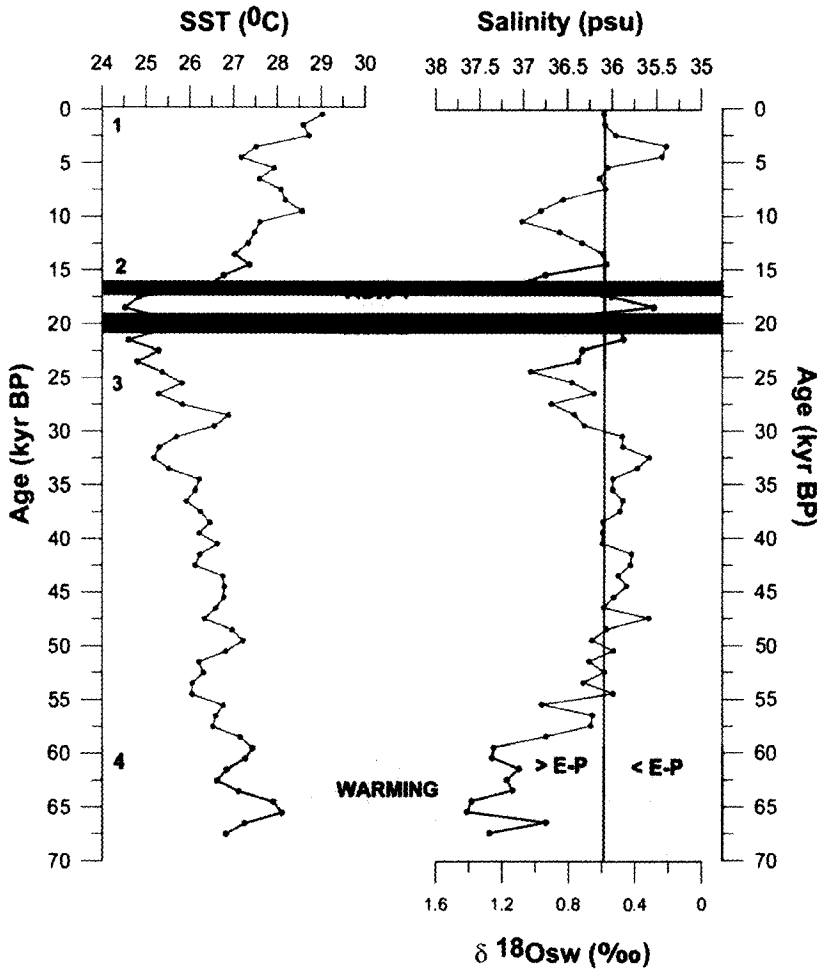

Figure 4.7 Profile of SST, SSS and δ ^{18}Osw at the core location AAS-9/21from the eastern Arabian Sea. Note during MIS 2 two warming events ASW1 and ASW2 shown by red bands. Vertical line shows the respective value of modern Holocene and E-P budget in the study area.

4.4.2 Marine Isotope Stage 3:

During transition from MIS 4 to MIS 3 a clear shift of high to lower δ^{18}Osw values representing change of more evaporation to more precipitation from the beginning of MIS 3 (Fig 4.6). In addition, major portion of MIS 3 show less temperature and more precipitation as compared to MIS 4 (Fig 4.6). Strong and weak SW monsoon during MIS 3 and MIS 4 respectively, would result corresponding changes in the δ^{18}Osw along the eastern Arabian Sea. MIS 3 record shows low δ^{18}Osw values and modern δ^{18}Osw values at this site reveal that SW monsoon precipitation during MIS 3 was as strong as the modern strength. Monsoon variability record based on the upwelling indices from the western Arabian Sea (Anderson and Prell 1993) and productivity records from the Pakistan Margin (Schulz *et al.*, 1998) also supports that

SW monsoon was more intense during MIS 3 compared to MIS 4. SST variability was minimum (<1^{0}C) during the MIS 3 and strikingly the SST values were lower than MIS 4, which points out that eastern Arabian Sea was cooler during MIS 3. However, from 32.5 to 24.5 kyr BP δ^{18}Osw values and SST increased, which reveals high evaporation phase started at the termination of MIS 3 and on set of weak phase of SW monsoon started around this time.

4.4.3 Marine Isotope Stage 2 (Last Glacial Maximum):

During MIS 2, SST has varied from 24.5 to 25.5^{0}C (1^{0}C change) and eastern Arabian Sea was 4^{0}C cooler during last glacial maximum than the Holocene (Fig 4.6). Earlier CLIMAP SST estimates based on Imbrie-Kipp transfer functions show that the average Ice Age zonal SST (the difference in SST between a single latitude point and the average temperature of the latitude band) for the entire Indian Ocean was 1.4^{0}C cooler during February and 1.5^{0}C cooler during August compared with the modern SST (Prell and Hutson 1979). SST estimations based on alkenone studies reveal that last glacial maximum (LGM) temperatures were about 2^{0}C cooler compared to modern values in the eastern Arabian Sea (Rostek *et al.*, 1993; 1997) and in the western Arabian (Emeis *et al.*, 1995). It is argued here that earlier SST estimates based on the statistical methods (Prell and Hutson 1979; Naidu and Mamlgren 2005) and alkenone based SST estimates (Emeis *et al.*, 1995) were from the western Arabian Sea where monsoon upwelling variability has greater role in controlling SST. Present studied core AAS-9/21 is from the eastern Arabian Sea where upwelling does not occur in any season. Therefore, this core location is expected to provide actual SST shift between LGM and Holocene. Alkenone based SST estimates of Rostek *et al.*, (1997) under estimates the SST shift between LGM and Holocene mainly due to saturation limitation of alkenone SST estimates above 27^{0}C. Present study reveals that eastern Arabian Sea was 4^{0}C cooler during the last glacial maximum than the modern day (Fig 4.6). Recently, Dahl and Oppo (2006) also documented greater amount of cooling (3.5^{0}C) across the Arabian Sea than the earlier CLIMAP estimates (CLIMAP 1981).

Various studies have demonstrated that SW monsoon was weaker during LGM (Prell 1984; Naidu and Malmgren 1995; Overpeck *et al.*, 1996; Naidu 1998 and references therein). On the other hand it was suggested that, NE monsoons were

stronger during LGM than in Holocene (Duplessy 1982). During NE monsoon an average of 6 Sv of low salinity Bay of Bengal water enter into the eastern Arabian Sea (Shetye *et al.*, 1991), the flow of Bay of Bengal low saline water into the Arabian Sea depends on the strength of winter circulation. It was reported earlier that the transport of low salinity water from the Bay of Bengal to the Arabian Sea was higher during LGM (Sarkar *et al.*, 1990). Subsequently, it was found that NE monsoon was strengthened during early deglaciation period which correspond to 18 kyr BP ago (Tiwari *et al.*, 2005). In the present study low δ^{18}Osw and salinity values were noticed from 19 to 18 kyr suggest that flow of low saline Bay of Bengal water into the Arabian Sea occurred after the LGM, therefore the present study confirms early deglacial strengthening of NE monsoon shown by Tiwari *et al.*, (2005).

Overall, MIS 2 documented higher salinity and δ^{18}Osw values (except a brief excursion low saline and δ^{18}Osw between 19 to 18 kyr BP) compared to MIS 3 suggests that MIS 2 of the eastern Arabian experienced greater evaporation. The cold and dry NE winds would cause the more evaporation during MIS 2.

4.4.4 Early Deglacial Warming:

The last deglaciation was not a smooth transition from one climate state to another, but occurred in a series of steps. It is well documented that δ^{18}O record of the world oceans exhibit a two step deglaciation model that included two phases of rapid ice melting separated by a brief period of climate stability (Peeters *et al.*, 2003). Two step deglaciation i.e. termination 1A and termination 1B has occurred around 12.5 kyr and 9.5 kyr respectively (Duplessy *et al.*, 1981) and sea level also rose during this time due to huge amount of melt water flux caused due to warming (Fairbanks 1989). It is generally believed that the timing of the transition from the Oldest Dryas to Bolling/Allerod at 14.7 kyr B.P. in Greenland snow accumulation record (Alley *et al.*, 1993). SST record of AAS- 9/21 from the eastern Arabian Sea show early deglaciation at 18 kyr BP (Fig 4.6), similarly δ^{18}Oc values also show depleting trend from 18 kyr BP (Fig 4.5). Both these records from the eastern Arabian Sea and δ^{18}Oc record from the western Arabian Sea (Peeters *et al.*, 2003) provides a strong evidence that in the Arabian Sea deglaciation was initiated around 18 kyr B.P. Evidences exist that tropical SST leads over high latitude SST during deglaciation (Bard *et al.*, 1997; Schnieder *et al.*, 1999; Lea *et al.*, 2000; Herbert *et al.*, 2001; Seltzer *et al.*, 2002;

Visser *et al.*, 2003). Two theories has been proposed to explain lead role of tropics: 1) internal processes of tropics can generate changes within the tropics which then propagate to the region corresponding to the Northern Hemisphere ice sheets through atmosphere (Cane 1998; Bush and Philander 1998; Clement *et al.*, 1999) and 2) changes in high-latitudes Southern Hemisphere insolation that trigger a Southern Ocean change (Toggweiler *et al.*, 1999; Sigman and Boyle 2000), which then propagates to the high latitude Northern Hemisphere, possibly through the control of CO_2.

During MIS 2 two warm excursions were noticed at this site (Fig 4.6), similar warm events were noticed along the western Arabian Sea (ASW 1 and ASW 2) (Saher *et al.*, 2007). At ASW 1 and ASW 2, the δ^{18}Osw and salinity show higher values than in the LGM (Fig 4.7). Two alternative mechanisms have been suggested to explain the warming events in the Arabian Sea: 1) reduced in upwelling intensity may cause to increase in SST in western Arabian Sea in these two warming events (ASW 1 and ASW 2) (Saher *et al.*, 2007). 2) The South Equatorial Current (SEC) flows westward towards Madagascar (Schott *et al.*, 2002) and splits in to two branches such as northern and southern. The northern branch, the Northeast Madagascar Current (NEMC), merges with the East African Coast Current, bringing warm water in to the Arabian Sea. An increase in the flux, possibly related to influence the trade wind strength, would have caused the SST rises in Arabian Sea.

The abrupt warming events ASW 1 and ASW 2 occurred not only in the western Arabian but also documented in the eastern Arabian Sea and Bay of Bengal (see chapter 3), where upwelling does not occur. The ASW 1 and ASW 2 occurred during the weak and strong phase of SW and NE monsoons respectively; therefore the changes of NE monsoon intensity during the LGM could trigger these warming events. It has been shown earlier that the NE monsoon intensity in glacial period exerts the larger influence on Arabian Sea SST than during interglacial time periods (Duplessy 1982; Fontugne and Duplessy 1986; Prell and Campo 1986). Therefore, variation in NE monsoon intensity during glacial time period may have caused changes in the SST on larger amplitude compare to present condition in both western and eastern Arabian Sea, however magnitude of NE monsoon effect must higher in the eastern Arabian Sea and Bay of Bengal. Further reduction of NE monsoon and associated warming event (ASW 1) coincides with the cooling episode in the

Greenland i.e Heinrich event 1 (da Garidel-Thoron *et al.*, 2001; Ivanova 1999; Schulz 2002).

4.4.5 Marine Isotope Stage 1 (Holocene):

Within the MIS 1 about 2^0C change of SST is documented along the eastern Arabian Sea (Fig 4.8) Earlier SST estimates based on alkenone show similar SST all through in MIS 1 (Rostek *et al.*, 1993). Decreasing trend of salinity and δ ^{18}Osw started around 10.5 kyr BP indicates more precipitation due to on set of strong SW monsoon, increasing strength of SW monsoon continued up to 3.5 kyr BP as evidenced from the low salinity and δ ^{18}Osw values (Fig 4.8). From 3.5 kyr BP increasing trend of salinity and δ^{18}Osw is noticed (Fig 4.8) and increase in SST was noticed.

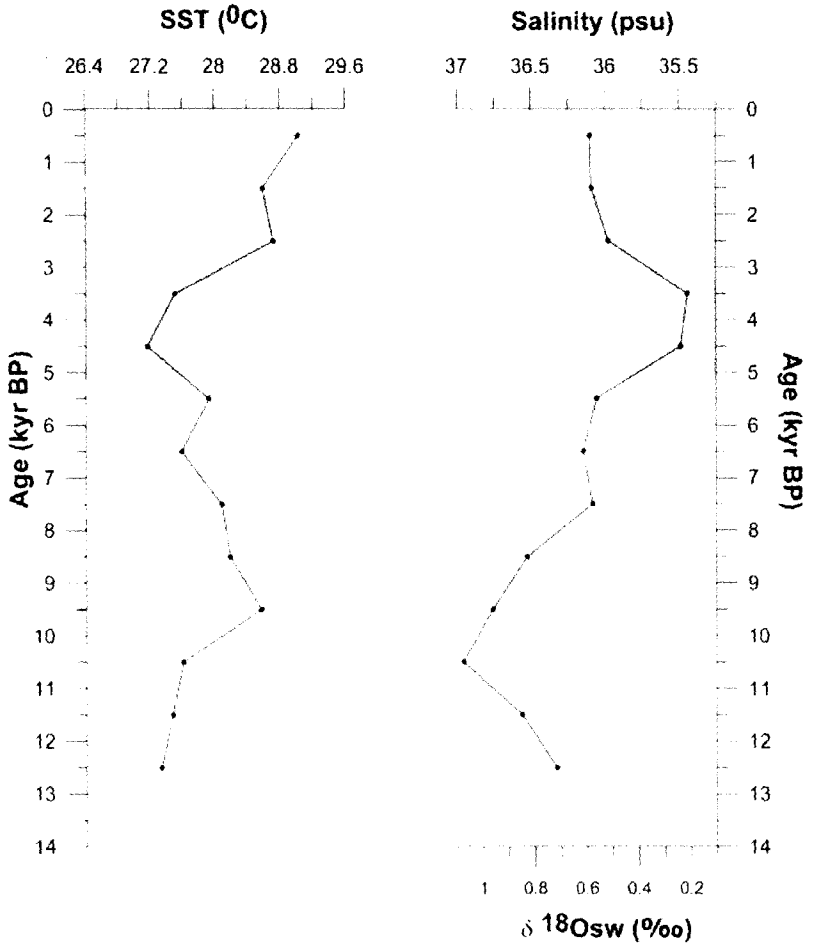

Figure 4.8 Profile of SST, SSS and δ ^{18}Osw shows variation in Holocene. Grey band shows decrease SST and precipitation during ~5 to ~3 kyr BP.

This increase in salinity and δ^{18}Osw is attributable to the onset of weak phase of SW monsoon around 3.5 kyr BP. Monsoon variability derived by δ^{18}Osw from AAS-9/21 in the eastern Arabian Sea (present study) is in agreement with the monsoon changes derived from upwelling indices from the western Arabian Sea (Overpeck *et al.*, 1996; Naidu and Malmgren 1996).

Based on 50 globally distributed paleoclimate records it was pointed out a brief cold episodes during 9000-8000, 6000-5000, 4200-3800, 3500-2500, 1200-1000 and 600-150 cal yr BP (Mayewski *et al.*, 2004). These episodes were characterized by polar cooling, tropical aridity and major atmospheric circulations changes. Similar cold events were documented in glacier fluctuations records (Denton and Karlen 1973), marine sediments (Bond *et al.*, 1997; 1999) and ice core records (O'Brien *et al.*, 1995). Some of these events for example drop in SST ~9 kyr BP and 4.5 kyr BP were documented in the eastern Arabian Sea SST record (Fig 4.8). Several records such as alpine glacier advances (Denton and Kerlen 1973), increase in ice rafting drifts (Bond *et al.*, 1997), strengthened westerlies over the North Atlantic and Siberia (Meeker and Mayewski 2002). Aridification record of Africa (Gasse 2000; 2001) show a change in climate during Late Holocene and this change in climate was attributed as a main cause to collapse the ancient civilizations such as, Maya and Indus Civilizations.

4.5 Conclusions:

Marine Isotope Stage 4 had documented higher SST (28.1^{0}C), more depleted δ^{18}Oc values, enriched δ^{18}Osw values and higher salinity as compared to MIS 2. This suggests that eastern Arabian Sea was more evaporative during MIS 4 than in MIS 2. Prevalence of higher SST during MIS 4 than in the MIS 2 would result in more evaporation during MIS 4 along the eastern Arabian Sea.

Transition of MIS 4 to MIS 3 was marked with a conspicuous shift from higher to lower δ^{18}Osw values, which reflects that a changeover from more evaporative phase to more precipitation phase was initiated during the MIS 3 in the eastern Arabian Sea. Eastern Arabian Sea document more or less similar δ^{18}Osw values during MIS 3 and in core top revealing that that SW monsoon precipitation during MIS 3 was as strong as the modern precipitation.

In the eastern Arabian Sea SST has varied from 24.5 to 25.5^{0}C (1^{0}C change) during MIS 2 and this region was 4^{0}C cooler during last glacial maximum (LGM) than in the Holocene. A 4^{0}C cooling during the LGM in the Arabian Sea as well as in the other parts tropics might have driven synchronous climate shifts between high and low latitudes. Earlier studies mostly from the upwelling influenced region of western Arabian Sea have under estimated the SST shift from LGM to Holocene (CLIMAP 1981), Naidu and Malmgren (2005) because these studies could not isolate the SST changes related to upwelling and cooling associated with the LGM. Present studied core AAS-9/21 is from the eastern Arabian Sea where upwelling does not occur in any season, therefore this core location is expected to provide actual SST shift between LGM and Holocene. Therefore, it is concluded that Arabian Sea was 4^{0}C cooler during LGM than in Holocene.

With in the last glacial period (MIS 2) two warm excursions around 17 and 19 kyr were noticed at this site, similar warm events were reported from western Arabian Sea (ASW 1 and ASW 2) (Saher *et al.*, 2007), these two warm events were probably caused due to the reduction of NE monsoon winds within the last glacial period.

It is generally believed that the timing of the transition from the Oldest Dryas to Bolling/Allerod at 14.7 kyr B.P. in Greenland snow accumulation record (Alley *et al.*, 1993). SST record of AAS-9/21 from the eastern Arabian Sea show early deglaciation at 18 kyr BP, similarly δ^{18}Oc values also show depleting trend from 18 kyr BP. Both these records from the eastern Arabian Sea and δ^{18}Oc record from the western Arabian Sea (Peeters *et al.*, 2003) provides a strong evidence that in the Arabian Sea deglaciation was initiated around 18 kyr B.P.

Overall, reconstruction of monsoon variability based on the δ^{18}Osw values from the present study is in agreement with the monsoon reconstructions based on the upwelling indices from the western Arabian Sea. This reconfirms that the SW monsoon wind driven upwelling along the western Arabian Sea and precipitation in the Indian subcontinent and river discharge to the Arabian Sea were related at centennial time scale.

CHAPTER 5

Productivity Changes in the Arabian Sea and Bay of Bengal over last 70 kyr

5.1 Introduction:

Oceans hold about 60 times more carbon than the atmosphere; a small change in the chemistry of oceans can produce a marked change in atmospheric reservoir. There are number of ways in which the ocean can change its ability to hold carbon dioxide, among several other factors ocean productivity helps to control the partitioning of carbon between large ocean reservoir and the relatively small atmospheric reservoir (Berger *et al.*, 1989). Therefore, productivity changes play an important role in providing feedback to climatic changes. A strong linkage between glacial and interglacial climatic change and atmospheric CO_2 changes were reported (Barnola *et al.*, 1987) which spurred the interest of biologists to understand the role played by biological pump. A central problem to understand is to understand the working of biological pump, which pulls carbon out of surface waters and sequesters it at depth and within sediments.

The Pleistocene record in sediments of the continental slope have shown large fluctuation in the burial rates of organic carbon, which are interpreted as productivity fluctuations. Such fluctuations appear to be in phase with changes in atmospheric carbon dioxide content (Emerson and Hedges 1988).

In the northern Indian Ocean monsoon plays a dominant role in controlling the biological productivity and particulate flux supply to the sediment. Sediment trap experiments have demonstrated that the biological productivity and terrigenous supply in the Arabian Sea is strongly linked to the intensity of monsoon (Nair et al., 1989). Detailed studies have been carried out in the Arabian Sea to understand the monsoon influence on the biological productivity and terrigenous supply during the Late Quaternary (Sirocko and Sarnthein 1989; Shimmield *et al.*, 1990; Clemens *et al.*, 1991; Murray and Prell 1992; Naidu 1991; Naidu *et al.*, 1993; Naidu and Shankar 1999; Bhusan *et al.*, 2001). It is generally understood that the summer monsoon was stronger during interglacials than glacials (Prell *et al.*, 1992 and references there in).

Various proxies have been used to determine paleoproductivity in different regions of the Oceans. For example within each group of planktonic foraminifera

some species occur preferentially in high productivity regions while other species can not compete in bloom situations. Thus, the relative abundances of certain species should contain clues to the intensity of production at the time of sedimentation. A number planktonic foraminiferal species have been identified as indicators of productivity (Prell and Curry 1981; Vincent and Berger 1981). Similarly, the fluxes of organic matter, opal, calcium carbonate and benthic foraminifera have been used extensively to study the paleoproductivity of the ocean basins (Shimmield *et al.*, 1990).

Nevertheless, productivity proxies behave differently in different regions of the Arabian Sea, leading to contradictory conclusions on the relationship between productivity and monsoon strength (Clemens *et al.*, 1991; Naidu and Shankar 1999; Agnihotri *et al.*, 2003). This chapter is aimed to address the productivity changes over last 70 kyr BP in both the Arabian Sea and the Bay of Bengal.

5.2 Sediment Cores:

Core SK-218/1 was collected at a water depth of 3000 m from the Bay of Bengal (14°02'06" lat; 82°00'12" long) and core AAS-9/21 was collected from 1807 m from eastern Arabian Sea (14° 30.539' Lat; 72° 39.118') (Fig. 5.1).

5.3 Results:

In the Bay of Bengal Core (SK-218/1) $\delta^{13}C$ values ranges from 0.0 to 1.5 ‰ over last 65 kyr BP. $\delta^{13}C$ values show an increasing trend (0.1 to 1.2 ‰) from 60 to 17 kyr BP and strikingly depleted values between 17 and 10 kyr BP and from 10 kyr BP onwards enriched $\delta^{13}C$ (>1.1 ‰) was noticed (Fig 5.2).Overall trend of $\delta^{13}C$ in the Bay of Bengal show an enriched $\delta^{13}C$ values during Holocene as compared to MIS 2 and 3 and most depleted values during were noticed during MIS 4.

$\delta^{13}C$ values of the Arabian Sea Core (AAS-9/21) vary from 0.5 to 1.65 ‰. A gradually enriched $\delta^{13}C$ values were noticed from 60 to 17 kyr BP and depleted $\delta^{13}C$ values between 17 and 10 kyr BP and enriched $\delta^{13}C$ values from 10 kyr BP onwards were noticed (Fig. 5.3). Overall alike in the Bay of Bengal in the Arabian Sea enriched $\delta^{13}C$ values during Holocene as compared to the MIS 2 and 3 and the lowest $\delta^{13}C$ values during the MIS 4 were noticed.

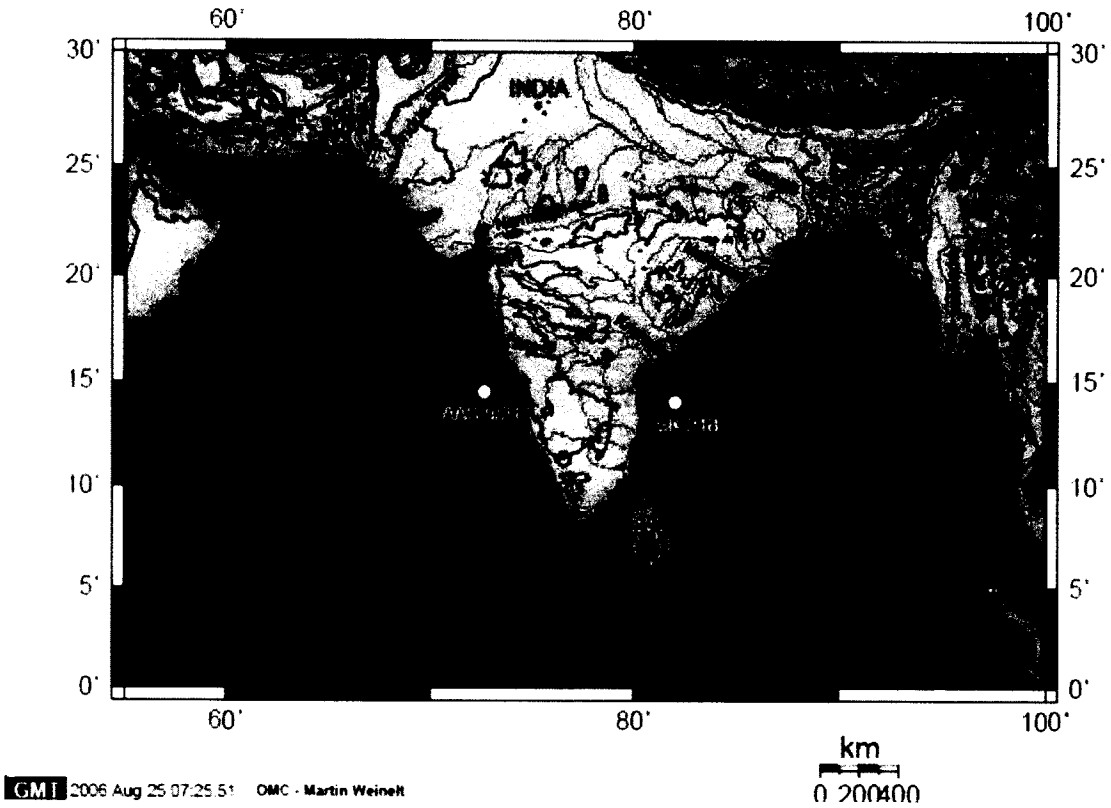

Figure 5.1 Core locations and physiographic features of the northern Indian Ocean.

5.4 Discussion:

The classical marker for the fertility of surface waters is the carbon isotope ratio of carbonate secreting organisms, $^{13}C/^{12}C$, expressed as $\delta^{13}C$. Within the water, this ratio is set by competing processes of CO_2 exchange with the air, removal of carbon in solids by export production, and resupply of dissolved carbon from subsurface waters (Wefer *et al.*, 1999). As a result of these fluxes and associated fractionation, the surface water will generally be enriched in ^{13}C except in areas of strong mixing with deeper waters. Surface waters are generally enriched in ^{13}C, compared to the deeper subsurface water due to photosynthesis uses ^{12}C preferentially in the formation of organic matter. Thus the export flux is enriched in ^{12}C and ^{13}C tends to be left behind. This process of enrichment depends on carbon fixation into organic matter and is limited by the supply of nitrate and phosphate, which also get incorporated into the organic matter. In deep waters organic matter is remineralized, lowering the $\delta^{13}C$ of the total dissolved CO_2. Along with this decrease in ^{13}C, nutrient concentrations increase and oxygen concentration decrease. Thus, the $^{13}C/^{12}C$ ration in the ocean is inversely correlated to the nutrient concentration, since planktonic

foraminifera calcifies in the surface waters which incorporates the carbon isotopic ratios of waters in their tests. Therefore, planktonic foraminifera are primary tool for the reconstruction of the paleo-carbon isotopic composition of surface waters.

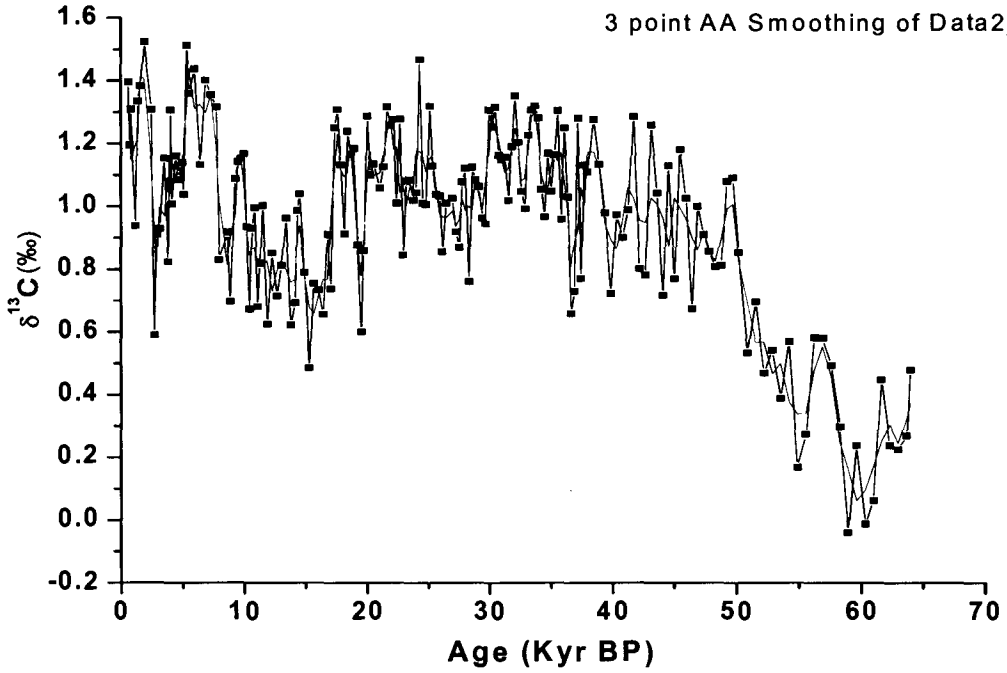

Figure 5.2 Profile of the carbon isotopic ratio ($\delta^{13}C$) from core SK-218/1. 3 point smoothing of data shown by solid red line.

Shackleton (1977) was the first to use the $\delta^{13}C$ composition of benthic foraminifera and demonstrated that glacial oceans contain low $\delta^{13}C$ ratios than the Holocene. Lower carbon isotope values during glacials were observed in all three oceans and also in shallow dwelling planktonic foraminifer species. Lower $\delta^{13}C$ changes during glacials were caused due to transfer of organic carbon depleted in ^{13}C from the terrestrial biosphere to oceanic dissolved organic carbon pool (Shackleton 1977). However, subsequent studies revealed that the changes in benthic $\delta^{13}C$ can also be ascribed to other factors such as shifts in the abyssal circulation (Boyle and Keigwin 1982; Curry and Lohaman 1982; Shackleton *et al.*, 1983), air sea exchange (Charles *et al.*, 1993) and physiological and/or environmental artifacts (McCorkle *et al.*, 1990; Mackensen *et al.*, 1993). Hence the combined influence of all these factors highly complicates the interpretation of $\delta^{13}C$ records.

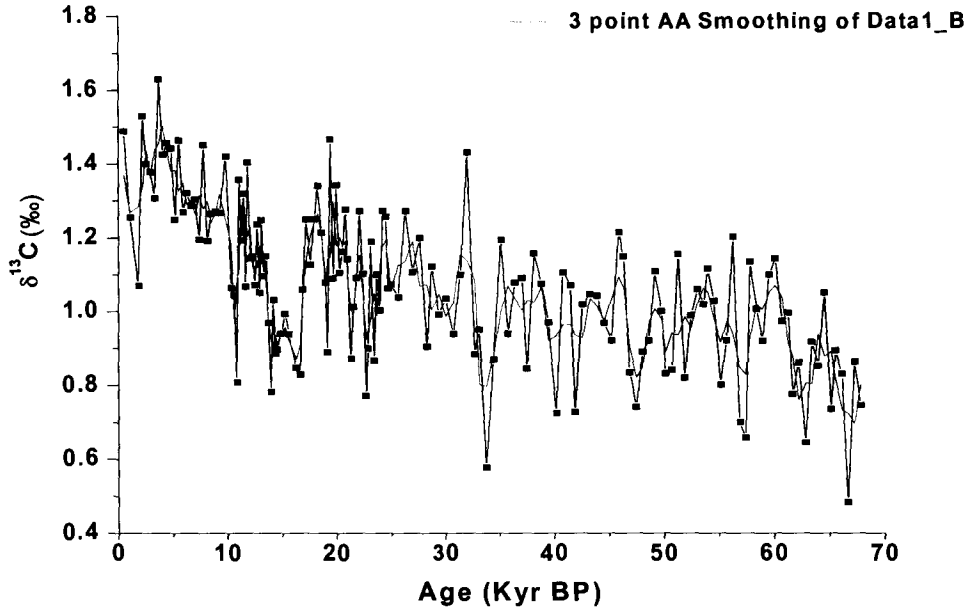

Figure 5.3 Profile of the carbon isotopic ratio ($\delta^{13}C$) from core AAS-9/21. 3 point smoothing of data shown by solid red line.

Inspite of planktonic foraminiferal $\delta^{13}C$ records are complicated by isotopic offsets between species, variations in $\delta^{13}C$ with shell size, and the disequilibrium effects attributable to the presence of symbiotic algae (Spero and Williams 1988; Spero and Lea 1996), still planktonic foraminifera $\delta^{13}C$ record is only the source from which one can derive the partitioning of ^{12}C and ^{13}C through the photosynthesis. Here $\delta^{13}C$ of *Globigerinoides ruber* was used to address the paleoproductivity mainly because both cores sites were devoid of upwelling hence the supply of ^{12}C rich water through upwelling would not affect the record and it was shown that *G. ruber* calcifies with the isotopic equilibrium of the ambient waters (Spero and Lea 1996).

Enriched $\delta^{13}C$ values during MIS 1 and 3 and depleted values in MIS 2 and 4 in the eastern Arabian Sea and Bay of Bengal (Fig. 5.3) suggests that higher productivity during interglacials (MIS 1 and 3) and lower productivity during glacials (MIS 2 and 4) (glacials) in both Arabian Sea and Bay of Bengal. Earlier findings from the eastern Arabian Sea (Ganeshram *et al.*, 2000; Pattan *et al.*, 2003) and from the western Arabian Sea (Murray and Prell 1993; Naidu and Malmgren 1996) also revealed high productivity during interglacials as a result of strong SW monsoon and low productivity during glacials due to weak SW monsoon. However, based on the accumulation rates of organic carbon and alkenones it was suggested high

productivity during LGM than in the Holocene (Rostek *et al.*, 1997; Banakar *et al.*, 2005) in the eastern Arabian Sea. In the eastern Arabian Sea the TOC and alkenone maxima are in phase with maximum ice volume indicating an additional influence of stronger and prolonged NE monsoon winds associated with cold climates as proposed by Rostek *et al.*, (1997). Therefore, in the eastern Arabian Sea paleoproductivity is predominantly linked to variations in the NE monsoon winds, which are probably related to maximum processionals ice volume (Budziak *et al.*, 2000). It is argued here that if strong NE monsoon had influenced the productivity changes along the eastern Arabian Sea, one would expect high productivity in the Bay of Bengal because NE monsoon activity was much stronger in the Bay of Bengal than in the eastern Arabian Sea. Therefore, in both Arabian Sea and Bay of Bengal the productivity was higher during the interglacials than in glacials, documented high productivity in AAS-9/21 and SK-218/1 was driven by SW monsoon strength rather than the NE monsoon. Furthermore, the most depleted $\delta^{13}C$ during MIS 4 and MIS 2 (during 17 to12 kyr BP) (Fig. 5.2; 5.3) show a perfect match with weakest phase of SW monsoon (Anderson and Prell 1993; Naidu and Malmgren 1996) advocate that productivity changes over last 70 kyr BP in the Arabian Sea and Bay of Bengal were driven by the strength of SW monsoon.

5.4.1 Relationship between monsoon and productivity in the Arabian Sea and Bay of Bengal:

Numerous paleoclimatic studies have shown that summer monsoon was stronger during interglacials than in glacials from the western Arabian Sea (Prell and Kutzbach 1987; Clemens *et al.*, 1991; Anderson and Prell 1993 and references their in) as well as in the eastern Arabian Sea (Rostek *et al.*, 1993; Naidu and Shankar 1999). The sediment traps data from western, central and eastern Arabian Sea show that lithogenic, carbonate, carbon and foraminiferal flux supply are tightly coupled to monsoon intensity. A distinct bi-modal distribution is observed representing higher fluxes during summer and winter monsoons and minimum flux during inter monsoon (Nair *et al.*, 1989; Curry *et al.*, 1992; Rixen *et al.*, 1996). This implies that across the Arabian Sea (from west to east) the biological productivity is higher during monsoons and lowest during inter monsoons.

It was suggested that there is a strong link between the precessional component of the Earth's orbital parameter and productivity in the Arabian Sea (Prell

1984; Rostek *et al.*, 1997; Budziak *et al.*, 2000) and intensity of summer monsoon winds over the Arabian Sea (Clemens *et al.*, 1991). Further, insolation changes associated with the precession cycle play a dominant role in forcing the SW monsoon strength than the glacial and interglacial boundary conditions (Clemens *et al.*, 1991). There is a strong evidence suggesting that productivity and boreal summer insolation show significant coherency but exhibit a time lag of 6 to 9 ka between the two (Clemens *et al.*, 1991; Altabet *et al.*, 1995). The spectrum of the SW monsoon indicates that the amount of variance in the obliquity band (26%) is slightly greater than that in the precession band (18%) and an additional 22% of the total variance resides in peaks at the 16 and 66 kyr BP, these periods possibly representing heterodynes associated with heating of obliquity and precession (Clemens and Prell 2003), where as the radiation spectrum is dominated by precession band. Thus more monsoon variation resides in the obliquity band than in the precession band. The existing time lag between insolation changes of precession and productivity records may provide a good reasoning for not showing any systematic relationship between productivity records and glacial and interglacial cycles.

5.4.2 Glacial to Holocene Shift in $\delta^{13}C$:

Low latitude planktic $\delta^{13}C$ records of glacial sections are 0.2 ‰ negative than the Holocene sections, further low latitude planktic records are characterized by the most negative $\delta^{13}C$ values occurring on the glacial terminations rather than during the LGM (Lea *et al.*, 1999). Recent compilation of mean ocean $\delta^{13}C$ was 0.32 ‰ more negative during last glacial maximum (LGM) (Curry *et al.*, 1988; Boyle 1992), in the Arabian Sea (Core AAS-9/21) and Bay of Bengal (SK-218/1) most depleted values were noticed after initiation of deglaciation around 17 kyr BP, which shows a 0.7 ‰ shift in Bay of Bengal and 0.6 ‰ shift in the Arabian Sea.

5.4.3 Comparison of $\delta^{13}C$ changes between Eastern Arabian Sea and Western Arabian Sea:

$\delta^{13}C$ values of eastern Arabian Sea show enriched values as compared to western Arabian Sea, upwelling occurs during the SW monsoon along western Arabian Sea, which brings $\delta^{13}C$ depleted water to the surface therefore $\delta^{13}C$ of the western and eastern Arabian were higher during intense upwelling periods and lower during weak upwelling period.

5.4.4 Comparison between Bay of Bengal and Eastern Arabian Sea Productivity Signals:

The Bay of Bengal core (SK-218/1) and the eastern Arabian Sea core (AAS-9/21) show nearly similar values over last 45 kyr BP suggesting similar productivity levels, provided if the influence of other factors on $\delta^{13}C$ remains same between these two regions. A conspicuously, low $\delta^{13}C$ values from 65 to 45 kyr BP was noticed in the Bay of Bengal as compared to the eastern Arabian Sea, this change in $\delta^{13}C$ could be due to two factors: 1) influence of terrestrial carbon supply to the core site in the Bay of Bengal and/or 2) a drop in productivity at the beginning of MIS 3 in the Bay of Bengal.

5.5 Conclusions:

Carbon isotopic ratios ($\delta^{13}C$) were used to reconstruct the productivity changes associated with SW and NE monsoons in the eastern Arabian Sea and Bay of Bengal over last 70 kyr BP. The $\delta^{13}C$ variations of eastern Arabian Sea Core (AAS-9/21) and Bay of Bengal Core (SK-218/1) show enriched $\delta^{13}C$ values during MIS 1 and MIS 3 (interglacials) and depleted $\delta^{13}C$ during MIS2 and 4 (glacials).

It was shown earlier that enhanced productivity during glacials along the eastern Arabian Sea as a result of strong NE monsoon. By contrast in both eastern Arabian Sea and Bay of Bengal the enriched and depleted values of $\delta^{13}C$ corresponding very well the strong and weak phase of SW monsoon respectively, therefore it has been suggested here the productivity changes of Eastern Arabian Sea and Bay of Bengal controlled by the SW monsoon. Strong SW monsoon during interglacial resulted high productivity and weak SW monsoon caused low productivity during glacials.

CHAPTER 6

Changes of depositional environment in the Indus Fan during Late Quaternary

6.1 Introduction:

The initiation of Indus Fan deposition is thought to have begun in Oligocene to early Miocene times, when the Indian and Arabian plates collided and caused major uplift of the Himalayas and the cause of Fan sedimentary sequences have been deposited because of Himalayan uplifts and sea level lowering (Koumes and Kolla 1982).

The primary source of sediments to the Indus Fan is derived from the Indus River, which drains the arid to semi-arid western Himalaya Mountains, with headwaters at elevations greater than 4000 m and a catchment area of c. $1 * 10^6$ km^2 and discharge of about $400 * 10^6$ metric tons of sediment per year (Wells and Coleman 1982). Peak discharge occurs during the summer months as a result of seasonal glacier melting and the increased runoff generated by the summer monsoon (Milliman *et al.*, 1984).

Indus Fan is one of the largest deep-sea fans in the world, totaling c.$5 * 10^6$ km^2. Terrigenous input from the Indus River dominates sediments in the northern Arabian Sea. Sediments are characterized by coarse size, low calcium carbonate content and an abundance of quartz and feldspar (Naini and Kolla 1982). The sediment discharge of the Indus River varied from 675 to 435 million tons before 1950 (Holeman 1968). After construction of dams at several places, the sediment discharge was reduced to 50 million tons (Milliman *et al.*, 1984). These sediments supplied by the Indus River to the northern Arabian Sea may be distributed on the inner shelf as well as in the offshore. However, much of the coarse sediment is carried directly offshore to the Indus Fan through the Indus Submarine Canyon (Islam 1959). A strong relationship between weathering /erosion and climate has been established by previous studies (Colin *et al.*, 1999; 2001). It has been suggested that during glacial events, the intense Himalayan aridity leads to weak SW monsoons with scanty rainfall, and very intense NE monsoons (Sarkar *et al.*, 1990 and references therein). Thus the monsoon precipitation during glacial and interglacial was well correlated with Indus River discharge in to the Arabian Sea.

The lithostratigraphy of the Ocean Drilling Program (ODP) core 720 A shows two units: unit I, from 0 to 18 mbsf (meters below seafloor) is composed of pelagic nannofossil ooze, with a non-carbonate component of primarily consisting of quartz and clay minerals. Unit II, from 18 mbsf to the bottom of the hole is dominated by turbidite facies, comprising interbedded silty clays, silty sands, and sands which commonly occur in fining-upward sequences on scales of <2 to >50 cm (Prell and Niitsuma 1989).

It has been identified a major turbidite sequence of late Quaternary between 18 to 28 mbsf at the ODP site 720A (Govil *et al.*, 2004). In the present study, detailed studies were carried out on oxygen isotopes of planktic foraminifera, grain size and clay mineralogy to address the depositional history of the Indus Fan over the last 525 ka BP in order to identify sediment sources and potential factors controlling sediment supply to the Indus Fan.

6.2 Physiography of the Region:

The Indus Fan, which is 1,500 km long and has a maximum width of 960 km, is the most extensive physiographic feature in the Arabian Sea. The Fan is bounded by the Indian continental margin-Chagos-Laccadive Ridge in the east, the Owen-Murray Ridge in the west, and the Mid-Indian Ridge (Carlsberg Ridge) in the south (Fig. 6.1).

The Oman (part of the Gulf of Oman) and the Owen basins are the main physiographic features in the westernmost Arabian Sea (Kolla *et al.*, 1981). Indus River is the largest source of sediments in the Arabian Sea.

6.3 Results:

Oxygen isotope analysis were carried out up to 18 mbsf, the reconstructed chronology being based on the isotope stage boundaries up to 11 described in Bassinot *et al.* (1994). Oxygen isotopic analyses were not carried out below 18 mbsf, due to insufficient number of foraminifera specimens. Therefore, by using the linear sedimentation rate within isotope stage 11, it has been extrapolated the ages further down at this site. A discrepancy was observed when comparing the oxygen isotope chronology with an earlier chronology based on nannofossil datums (Govil *et al.*, 2004). Since the chronology based on the oxygen isotope boundaries is better constrained than the chronology derived from biostratigraphy, therefore, in the present

study the identification were based on the oxygen isotope chronology (Fig. 6.2). The Calcium Carbonate ($CaCO_3$) content varied from 4.5 to 74.4%. Higher $CaCO_3$ values (>30%) occur from 0 to 375 ka BP, whereas strikingly low $CaCO_3$ values (<10%) mark the period from 375 to 525 ka BP (Fig. 6.3). $CaCO_3$ fluctuations at this site were evidently controlled by terrigenous dilution. High terrigenous material supply (mostly sand and silt) between 375 and 525 ka BP has reduced the overall $CaCO_3$ content.

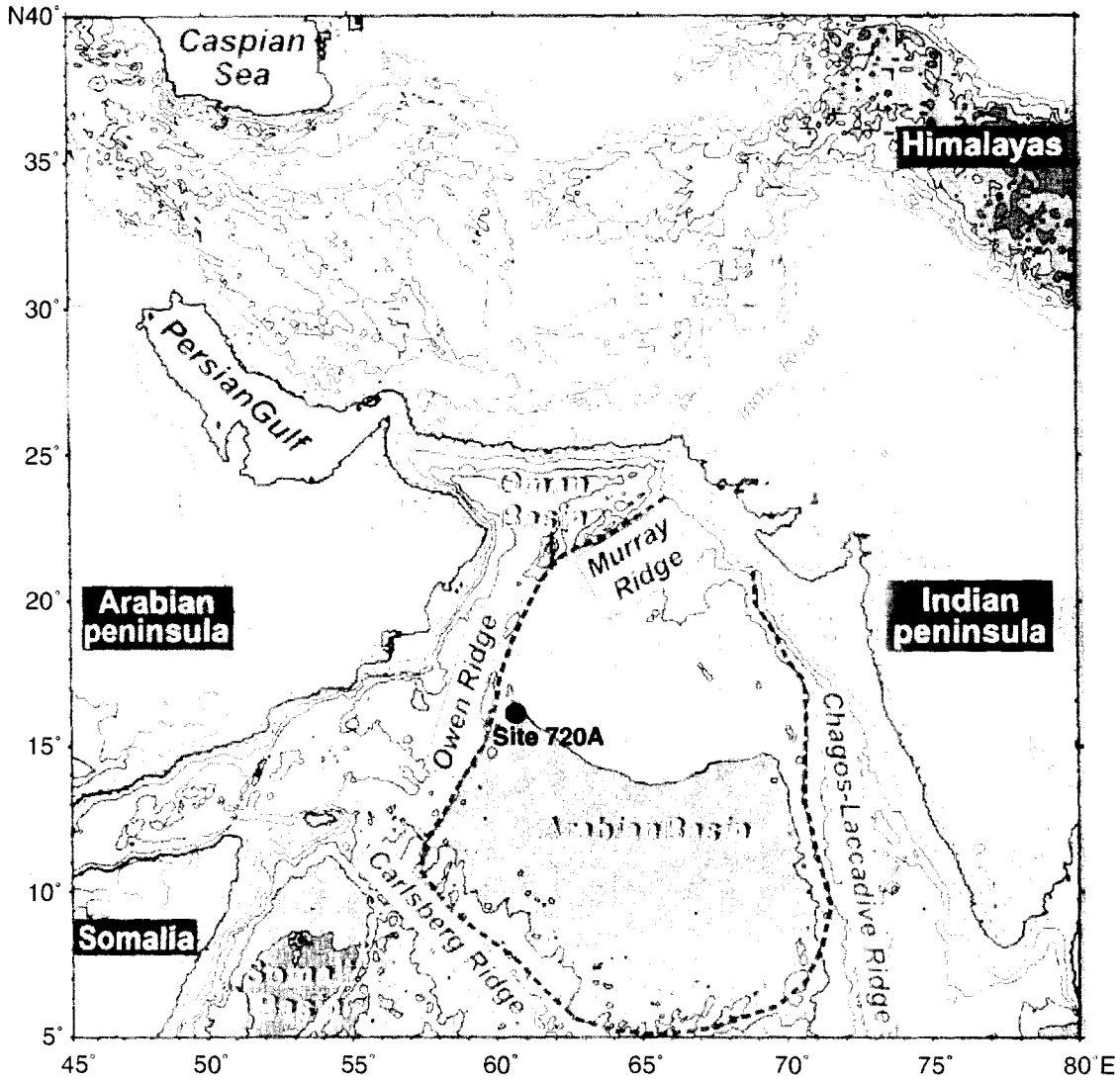

Figure 6.1 Bathymetry and Physiography of Indus Fan and location of ODP Site 720A (modified from Prins *et al.*, 2000).

The Aluminium (Al), Titanium (Ti), and terrigenous matter contents vary from 1.4 to 7.8%, 0.03 to 0.4% and 5.5 to 66.67% respectively (Fig. 6.4). Low Al, Ti and terrigenous matter contents between 0 and 375 ka BP (Fig. 6.4) coincide with high

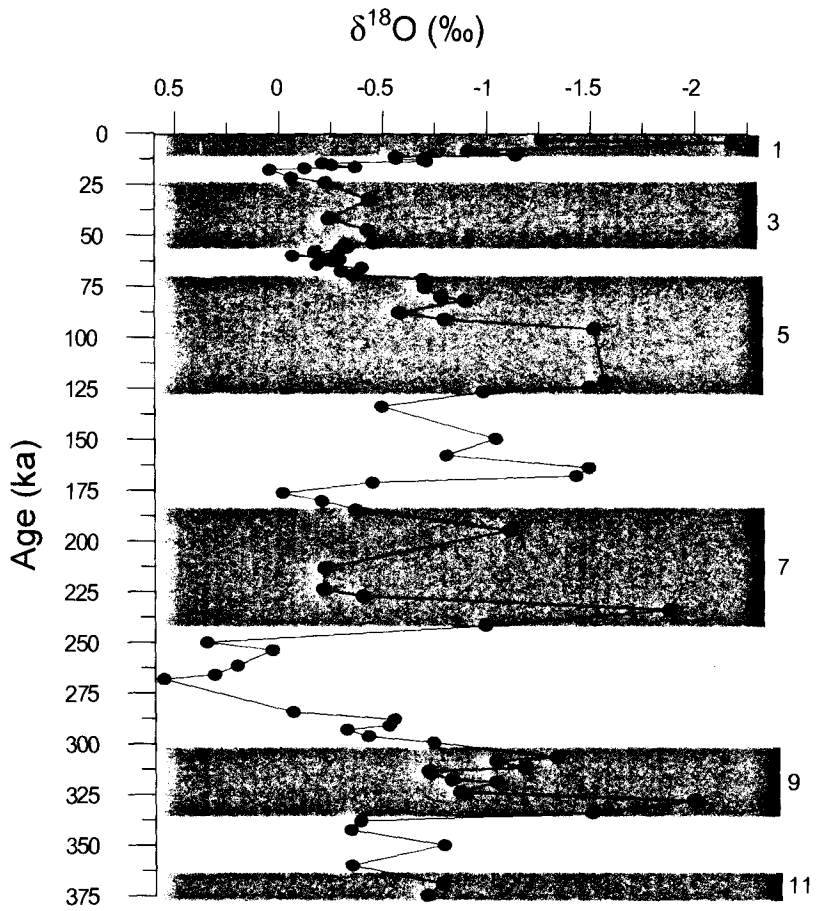

Figure 6.2 Chronology of ODP site core based on $\delta^{18}O$ stratigraphy. Interglacial isotope stages are highlighted by *dark shades* and are *lebelled.*

$CaCO_3$ contents (Fig. 6.3), whereas high Al, Ti and terrigenous matter contents 375 to 525 ka BP (Fig. 6.4) correspond to low $CaCO_3$ contents between 375 and 525 ka BP (Fig. 6.3) suggesting that terrigenous material supply from the Indus Fan between was considerably higher from 375 and 525 ka BP. The higher terrigenous material supply to the Indus Fan during 375 and 525 ka BP was the result of the increased turbidity flow.

From 375 ka onwards a predominantly pelagic sequence was deposited. Evidently, two distinct types of sedimentary sequences characterize the western part of the Indus Fan over the last 525 ka. From 525 to 375 ka, a turbidite sequence occurs, which is dominated by sand and coarser silt (Fig. 6.5). By contrast, the younger pelagic sequence consisting of finer silt and clay (Fig. 6.5). The mean grain

size of sediment also documents large variations between the turbidite and pelagic sequences at the study site. The turbidite sequence shows mean grain sizes varying strongly from 86 to 107 μm whereas the mean grain sizes of the pelagic sequence are more uniform at <13.3 μm (Fig. 6.6). Four clay minerals were recorded at the site. Of these, illite (60-77 wt %) is the dominant, followed by kaolinite (10-25 wt %), chlorite (3-16 wt %) and smectite (trace to 7 wt %) at this site (Fig. 6.7). The distribution patterns of clay minerals in the pelagic and the turbidity sequences are very similar (Fig. 6.7).

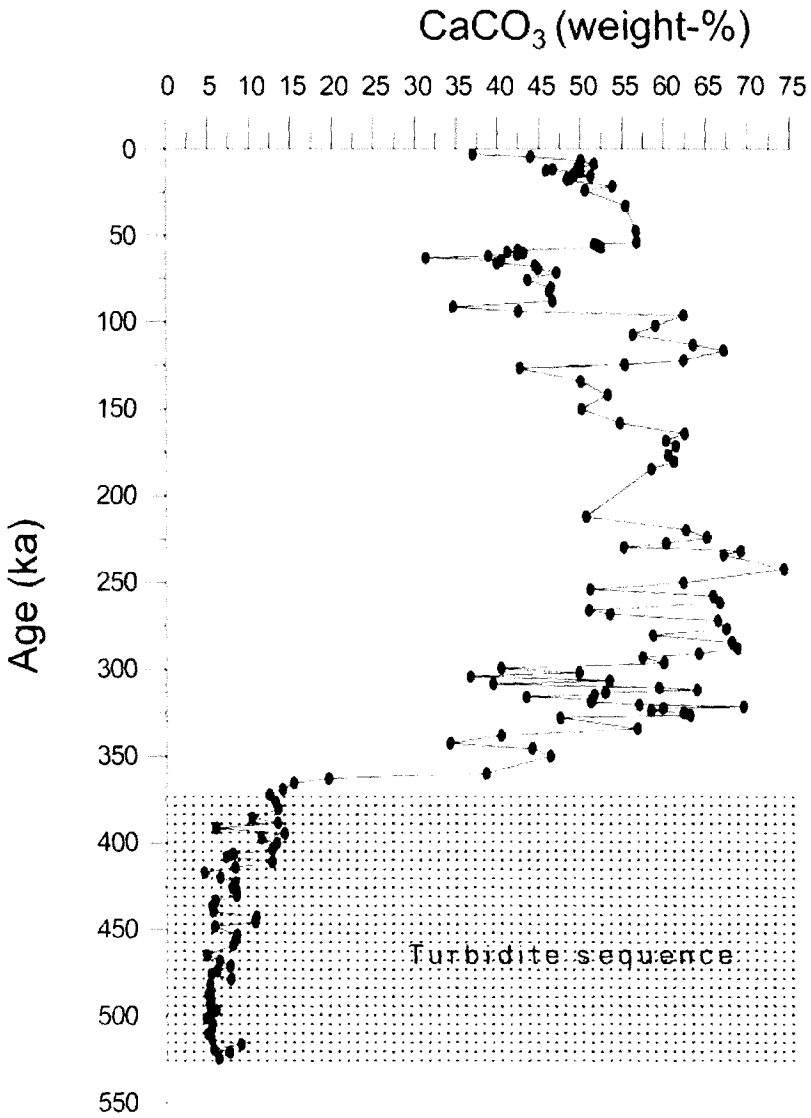

Figure 6.3 Calcium carbonate fluctuations at ODP Site 720A during the late Quaternary. Note the strong reduction in calcium carbonate from 375 ka onwards.

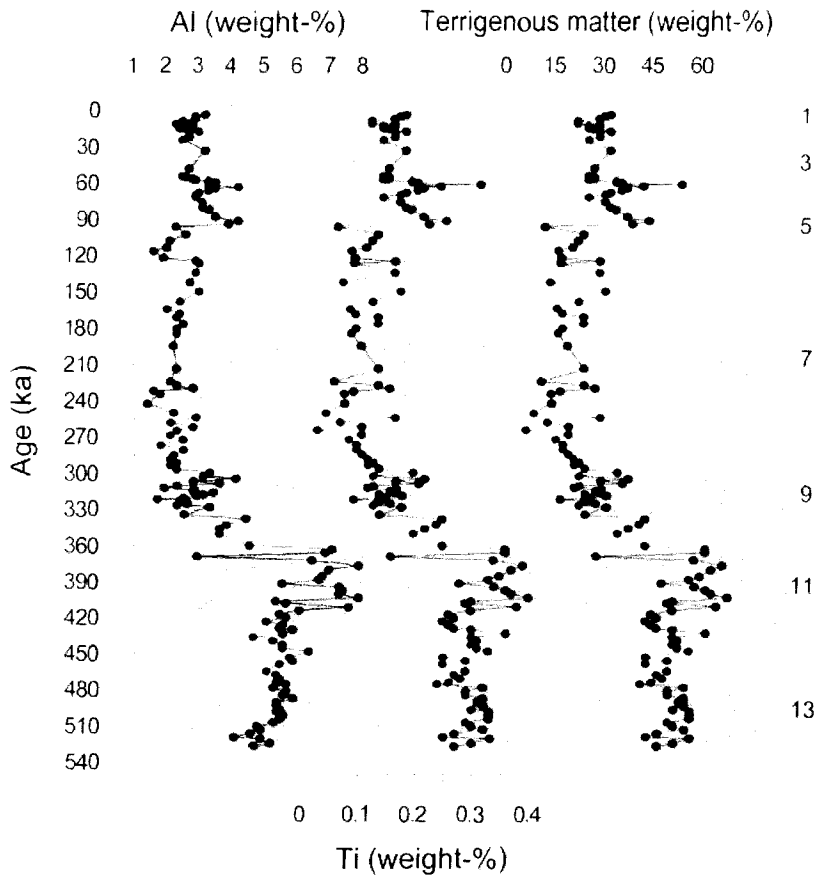

Figure 6.4 Al, Ti and terrigenous matter from ODP site 720. The higher concentration of Al, Ti and terrigenous matter corresponds to 375 to 525kyr. Interglacial isotope stages are highlighted by *dark shades* and are *labelled*.

6.4 Discussion:

The accumulation of calcium carbonate on the sea floor is mainly controlled by the surface water biological production, rate of dissolution during its journey through the water column as well as on the sea floor and dilution by the non-carbonate fraction and terrigenous matter (Damuth 1975). The ODP Site 720A was drilled in the water depth of 4045 m (Fig. 6.1) which is above the calcium carbonate compensation depth (CCD) in this region (Cullen and Prell 1984), therefore dissolution of calcium carbonate factor can be ruled out. Further, the foraminiferal fragments data also confirms that calcium carbonate dissolution was insignificant. No evidences were exit that four fold change in productivity in the Arabian Sea over last 400 kyr (Prell and Kutzbach 1992). Since both productivity and dissolution seems not played a major role in shaping the carbonate fluctuations at this site. Therefore, we

suggest that calcium carbonate changes were controlled by the terrigenous dilution (Govil *et al.*, 2004).

6.4.1 Turbidity Sequence:

Al and Ti content in the marine sediment mainly derive from continental origin supplied through eolian and fluvial pathways. Therefore, Al and Ti have been commonly used as geochemical indicators to discover the content of aluminosilicate detritus of continental origin (Pattan *et al.*, 2003). Coarse fraction that above 18mbsf samples content foraminiferal oozes and terrigenous material but below 18 mbsf to 28 mbsf samples mainly shows terrigenous material. In addition, lowest $CaCO_3$ content with high Al, Ti and terrigenous matter coincides with dominated sand and high mean grain size values between ~525 and ~375 kyr regimes suggest massive turbidity flows to the Indus Fan (Figs. 6.4, 6.5, 6.6, 6.7).

Examination of coarse fraction show that above 18 mbsf corresponding to ~375 kyr interval samples mostly contain foraminifer ooze and terrigenous material (Fig. 6.8a), however below 18 mbsf interval samples show only turbidity silts and sands (Fig. 6.8b). This observation also supports that massive turbidity flows below ~375 kyr. The present data do not show any major turbidity flows from ~375 kyr to the Holocene. However, it is admitted that present study cannot rule out minor turbidite sedimentation of few centimeter thicknesses within the main feeder channel and Indus Canyon. Such kind of turbidite sedimentation was noticed on the eastern part of Indus Fan during last glacial maximum when sea level was low (Prins *et al.*, 2000). A sharp decrease in turbidity frequency during the late Holocene is observed on the upper continental slope, the deep slope basin and the abyssal plain (Prins *et al.*, 2000).

The depositional history at site 720 has been dominated by turbidite deposition with brief interbeds that are characterized by an increase in pelagic components. Pelagic beds occurrence at site 720 results from a major late Pleistocene eastward shift of active channel deposition on the Indus Fan (Kolla and Coumes 1987). The magnetic susceptibility data also reveals that turbidite facies dominate the sediments between 18-30 mbsf, pelagic facies dominate the upper 18mbsf (Prell and Niitsuma 1989).

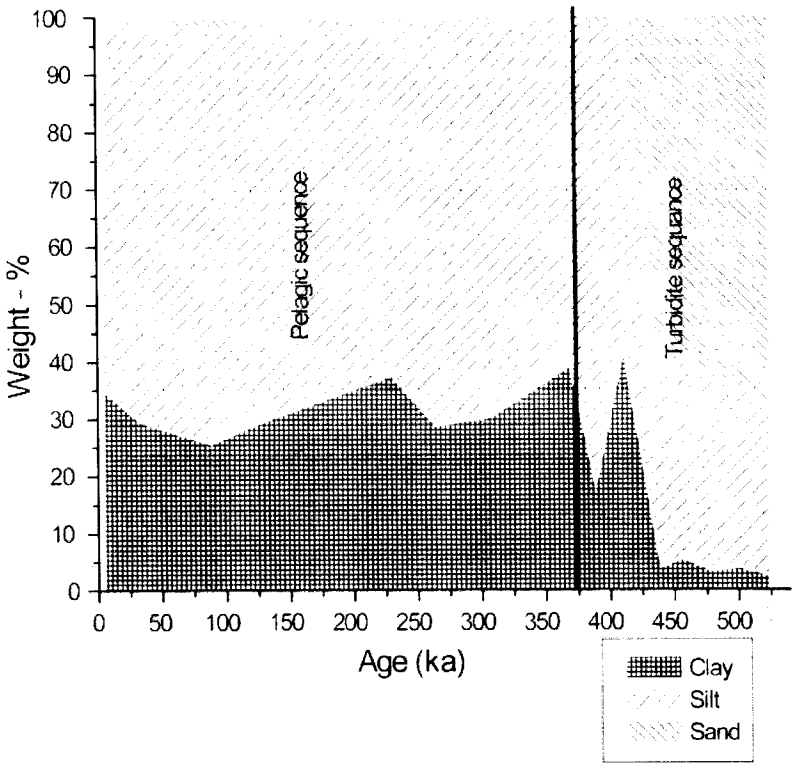

Figure 6.5 Down core fluctuations in sand, silt and clay at ODP site 720A. The turbidity sequence is generally dominated by sand and coarser silt, the pelagic sequence by clay and finer silt.

6.4.2 Depositional History of the Indus Fan:

Turbidity currents are the major process to let the sediment in to the deep sea fan system. The intensity and frequency of the turbidity currents varied in response to the sea-level changes. The turbidity currents are the dominant controlling process, along with the pelagic sedimentation and mass wasting deposition, in the formation of the Indus Fan. Growth of submarine fans is generally believed to occur during low sea-level stands. Therefore, sea-level fall activates the Fan due to an increase of sediment transport from the river and shelf toward the deeper parts of the basin (Prins and Postma 2000) and canyon forms in continental shelf. Then, the sediment can easily be transported to the deep sea fan by channels. In contrast, during the sea-level rise, sediment trapped in to the near offshore region; prevent the sediment transport to the deep-sea basin (Stow 1985; Mutti and Normark 1987).

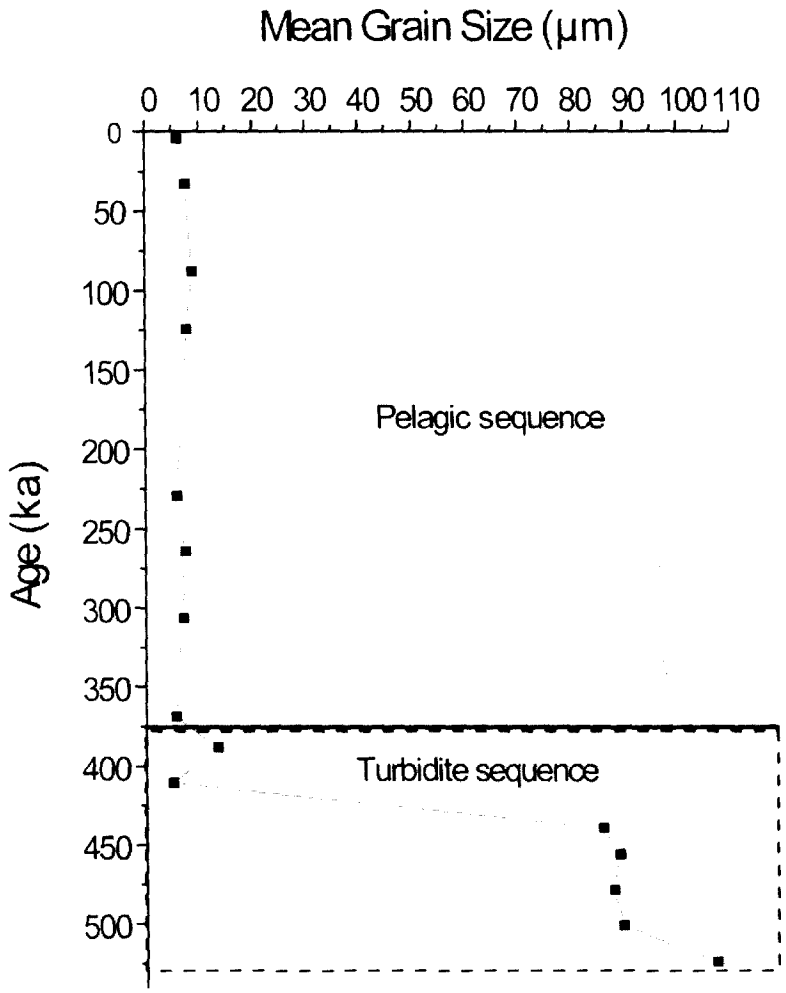

Figure 6.6 Variation in Mean Grain Size (µm) at ODP Site 720A.

However, understanding of turbidite sedimentation and terrigenous sediment in the fan systems and in deep sea is controlled by tectonic activity, climate changes and sea level changes (Prins *et al.*, 2000). In addition, to controlling factors, autocyclic mechanism includes cannel plugging and sediment builds-ups within the channels (Prins *et al.*, 2000). It has been shown that, despite a variety of controlling factors, in recent time scale large deep sea fans system like Amazon Fan, Mississippi Fan and the Indus Fan turbidite sedimentation influenced by the changes in sea level (Manely and Flood 1988; Prins *et al.*, 2000; Bouma *et al.*, 1989; Feely *et al.*, 1990; Weimer 1990). The deposition of the pelagic sequence on the Indus Fan clearly reflects a decrease in clastic influx may have been caused by local mechanisms. For example, a sea-level high stand would have reduced the clastic flux to the Indus Fan.

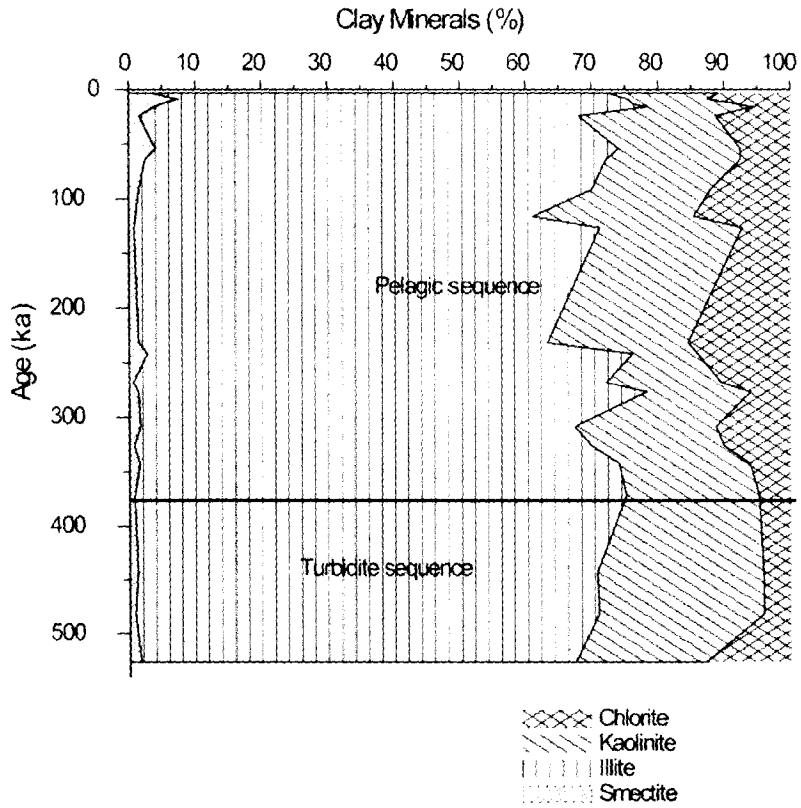

Figure 6.7 Variation in clay mineral content at ODP site 720A. The distribution patterns of clay minerals in the turbidite and pelagic sequences are very similar.

This pattern is observed in the Holocene sediments of Indus Fan, which consist of foraminiferal marls and oozes (Kolla and Coumes 1987). Similarly higher terrigenous inputs to the Arabian Sea during glacials were attributed to the low sea levels (Gupta *et al.*, 2005). However, the sea level rise and fall may not explain the reduction of terrigenous material to the Indus Fan from 375 kyr onwards, because the terrigenous proxies such as Al and Ti do not show any systematic variation corresponding to glacial and interglacials at this site. Therefore, we invoke the other local mechanism, which would facilitate the deposition of pelagic sequence from ~375 kyr onwards. The abandonment of active channels or buried of active channels results by ~375 kyr could produce predominantly pelagic deposits on the elevated levee deposits. This mechanism would be local in extent and would allow pelagic sediments to accumulate over the sea level cycles. Therefore, we attribute that from ~375 kyr onwards channel switching and abandonment of active channels are buried by ~375 kyr, therefore, the terrigenous material supply through channel system was

reduced from ~375 kyr to present day is probably related to switching of the distributary channel away from the site rather than to a general decrease in turbidite deposition on the Indus Fan.

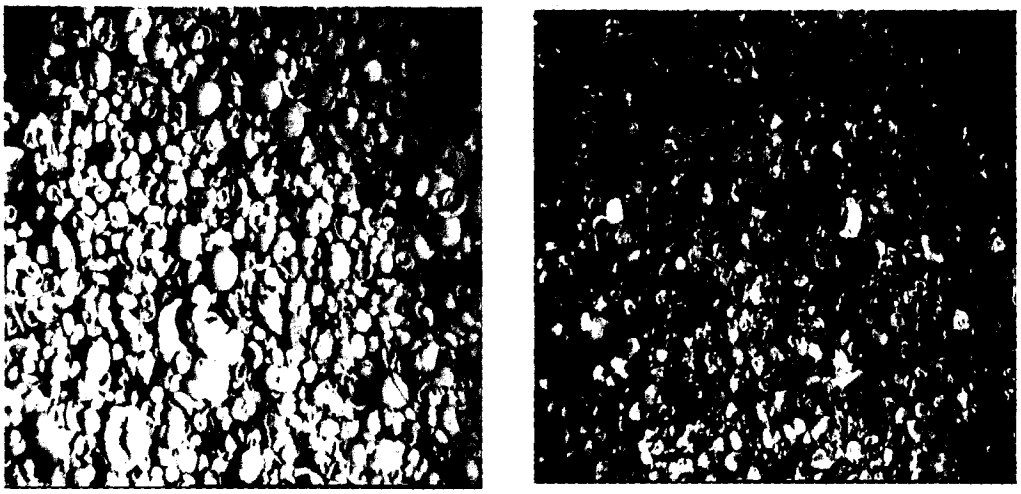

a) b)

Figure 6.8. Photograph depicting (a) carbonate-rich coarse fraction from 0 to 375kyr intervals (0-18mbsf depth) and (b) terrigenous detritus material rich fraction from 375 to 525kyr (18-28mbsf depth).

A major eastward shift of active channel deposition during late Pleistocene was noticed in the Indus Fan (Kolla and Coumes 1987). In general the turbidite deposition rates are twice higher in the Indus Fan as compared to the distal Ganges Fan. These high accumulation rates are consistent with accelerated uplift and erosion in the Indus source area (Prell and Niitsuma 1989).

6.4.3 Source of Clay Minerals in the Indus Fan:

Clay-mineral content values have been used to characterize the sediment provinces of the world oceans (Biscay, 1965; Windom 1975). Several studies have demonstrated the influence of climatic variation on production and supply of clays. The clay minerals in sediments of the Arabian Sea are derived from various sources, e.g river run-off from India, dust contributed from Africa, Arabia, Pakistan and northern India as well as from basalts on the mid-ocean ridges (Kolla *et al.*, 1981; Naidu *et al.*, 1985). Unfortunately, most of the clay minerals in the Arabian Sea can not be related to any specific source areas and transport pathways. High percentages of illite and chlorite are usually associated with cold climates and are physical and mechanical weathering products (Kolla *et al.*, 1976). Illite characterizes the oceanic

areas tributary either to high altitude cold climate regions like the Himalayan region (Kolla *et al.*, 1976). In contrast, kaolinite is influenced by the warm and humid climate and strongly controlled by the intensity of continental hydrolysis (Griffin *et al.*, 1968). Therefore, the sediments transport from other region may be a cause of >10% kaolinite to the site location. Through out the entire Arabian Sea concentration values of kaolinite show little variation, thus the mineral must occur at more or less uniform concentration in all the major sediment source areas (Sirocko and Lange 1991). As chlorite is a high latitude clay mineral, chlorite is produced by weathering under arid, cold climate conditions (Weaver 1989). Since chlorite forms under intense arid climate, a higher supply of chlorite or reduced content of illite will reflect a drier, arid climate and result in enhanced chlorite/illite (C/I) ratio. Similarly, a high kaolinite/chlorite (K/C) ratio should signify a humid climate (Chauhan 1999).

In contrast, the supply of chlorite (3-16%) is likely from the Indus river input (Fig. 6.7), which drains the Himalayan region, and not from the Penisular India. Smectite is the weathering product of basalts and penisular India, which is high in inner shelf of Saurastra, from the suspended and bed load from Tapti and Narmada River in eastern Arabian Sea (Naidu *et al.*, 1985). Smectite (trace to 7%) is deficient at this core site (Fig. 6.7), which appear to be influenced by Indus River supply, shows the climatic significance of glacial Himalayan region. Therefore, illite (>60%) and chlorite (>10%) represents the Himalaya as a source region and same source in both pelagic and turbidite sequence. The Persian Gulf and Red Sea are not considered important sources of sediment to the Indus shelf, but significant contributions may be derived from the dust bearing winds blowing off Africa in summer and northern India in winter (Sirocko and Sarnthein 1989). Studies have demonstrated, influence of climatic variation on production and supply of clays, like kaolinite, chlorite, and smectite–poor hemipelagic muds prior to ca. 11,500 ^{14}C yr B.P., indicated a dominant supply from Indus River in Arabian Basin (Prins and Postma 2000).

The distribution pattern of clay minerals in both the pelagic and the turbidity sequence is very similar (Fig. 6.7). This suggests that the main source of the clay minerals on the Indus Fan is the Himalayas, the material being supplied by the Indus River. However, in addition to the Indus a very minor amount of clay minerals may also have been derived from an aeolian source located on the Arabian Peninsula.

6.5 Conclusion:

The calcium carbonate content at the study site was controlled by terrigenous material dilution. In the pelagic sequence, the calcium carbonate was diluted by clays, whereas in the turbidite sequence it was diluted by sand and silt. Al, Ti and terrigenous material not show any consistent responses to glacial and interglacial climatic conditions. The terrigenous material supply to the site is therefore not linearly related to the sea-level changes.

Calcium carbonate and elemental contents (Al and Ti) as well as grain-size analysis data reveal a turbidite sequence from 525 to 375 ka which is overlain by a pelagic sequence from 375 to the present day. Most of the channels were buried by 375 ka BP, which caused the distributary channel to switch away from the site. This in turn resulted in a general decrease in turbidite deposition at the study site rather than indicating a decrease in terrigenous supply to the Indus Fan.

The high abundance of Indus-derived clay minerals originating from the Himalayas (illite and chlorite) in both the turbidite sequence as well as the pelagic sequence suggests that the source and supply of clay minerals to the Indus Fan remained constant over last 525ka.

CHAPTER 7

Summary

The Indian monsoon is an important component of global climate because monsoon transport heat and moisture from the warmest part of the tropical ocean across the equator and to higher latitudes. In India summer monsoon precipitation accounts for a large part of the annual total precipitation and significantly affects the annual gross national product, an important index to measure the economic growth of the country. Therefore, understanding the forcing mechanism of the monsoon is very important because it has wide impact on the socio-economic development in the country. The monsoon fluctuates with large amplitudes on various timescales such as inter annual, decadal and centennial, millennial time scales. Multi proxy based monsoon variability from the western Arabian Sea reveal that in general monsoons were stronger during interglacials (warm periods) and weaker during glacial period (cold periods).

Scientific consensus exist that most of the monsoon variability during glacial and interglacial were caused due to Earth's orbital parameter changes. However, high-resolution studies on monsoon variability questions the linear linkages between monsoon and insolation changes caused due to Earth's orbital changes and proposed that air temperature changes in the Arctic and Greenland play an important role in controlling the monsoon variability. Reconstruction of monsoon variability on glacial and interglacial time scales as well as on millennial time scale was carried out from western Arabian Sea because the strength of SW monsoon winds is linearly related with the intensity of upwelling. Thus various upwelling proxies have been used to trace the SW monsoon intensity for last two decades.

Although Bay of Bengal and Eastern Arabian Sea receives more amount of rainfall during SW monsoon as compared to western Arabian Sea, very limited studies were carried out to reconstruct the monsoon variability from these regions. Therefore, here an attempt has been made to reconstruct the sea surface temperature, sea surface salinity by using the Magnesium/Calcium and oxygen isotopic ratios in planktonic foraminifer species *G. ruber* in sediment cores from the Bay of Bengal and eastern Arabian Sea, in order to understand the variability of monsoon at centennial time scale.

Reconstruction of sea surface temperatures (SST) based on Magnesium/Calcium thermometry and Atificial Neural Network Technique (ANN) reveals that both western and central Bay of Bengal was 3^0C colder during LGM than the modern Holocene. This provides an evidence that the tropics were much cooler than it was believed earlier and CLIMAP (1981) reconstruction of sea surface temperature by using the transfer function technique of Imbrie and Kipp (1973)_under estimated the LGM temperatures of the Indian Ocean. Furthermore within glacials (MIS 2 and 4) and interglacials (MIS1 and 3) about 1 to 2^0C SST change was noticed in the Bay of Bengal.

Oxygen isotopic values of *G. ruber* (δ^{18}Oc) from the Bay of Bengal shows striking similarities with the GISP2 ice core δ^{18}O record which essentially represents changes of air temperature in the high latitudes of the northern hemisphere from 65 to 12 kyr. Conspicuously, oxygen isotopic values of surface water (δ^{18}Osw) (monsoon signal) and SST changes at the SK-218/1 core site from the Bay of Bengal lead the Dansgaard-Oeschger (D-O) events. Therefore, it is suggested here that the monsoon could initiate the start of millennial scale abrupt climate changes through the shifts of the Intertropical Convergence Zone (ITCZ) and associated convection, water vapor supply to the tropical troposphere and latent heat penetration. Thus, monsoons and associated convection process in the tropics play an important role in driving the abrupt climate shifts on a global scale.

δ^{18}Osw variability demonstrates that the evaporation was higher than the precipitation from 32 to 16.5 during last glacial period and in the initial phase of MIS 3 representing weak SW monsoon. A striking shift from more evaporative phase to high precipitation phase took place around 16.5 kyr as strengthening of SW monsoon initiated around this time. During the Holocene descending strength of monsoon started around 3.5 kyr. Overall, the monsoon variability reconstructed by the δ^{18}Osw corroborates well with the monsoon reconstructions based on upwelling indices from the western Arabian Sea.

In the eastern Arabian Sea SST has varied from 24.5 to 25.5^0C (1^0C change) during MIS 2 and this region was 4^0C cooler during last glacial maximum (LGM) than in the Holocene. A 4^0C cooling during the LGM in the Arabian Sea as well as in the other parts tropics might have driven synchronous climate shifts between high and low latitudes. Earlier studies mostly from the upwelling influenced region of western

Arabian Sea have under estimated the SST shift from LGM to Holocene (CLIMAP 1981; Naidu and Malmgren 2005) because these studies could not isolate the SST changes related to upwelling and cooling associated with the LGM. Present studied core AAS-9/21 is from the eastern Arabian Sea where upwelling does not occur in any season, therefore this core location is expected to provide actual SST shift between LGM and Holocene. Therefore, it is concluded that Arabian Sea was 4^0C cooler during LGM than in the Holocene.

Transition of MIS 4 to MIS 3 was marked with a conspicuous shift from higher to lower δ^{18}Osw values, which reflects that a changeover from more evaporative phase to more precipitation phase was initiated during the MIS 3 in the eastern Arabian Sea. Eastern Arabian Sea document more or less similar δ^{18}Osw values during MIS 3 and in core top revealing that SW monsoon precipitation during MIS 3 was as strong as the modern precipitation.

In both eastern Arabian Sea and Bay of Bengal during last glacial period (MIS 2) two warm excursions were noticed at 17 and 19 kyr. These warm excursions were associated with enriched δ^{18}Osw. Similar warm events (ASW 1 and ASW 2) were reported earlier from the western Arabian Sea (Saher *et al.*, 2007). This appears to suggest that these two warm events have a large spatial variability in the Northern Indian Ocean. SW monsoon strength was relatively weaker than the NE monsoon during last glacial period (Duplessy *et al.*, 1982). Therefore, the reduction of cold NE winds from continent to ocean could result these two warm events during the last glacial period.

Overall, reconstruction of monsoon variability based on the δ^{18}Osw values from the present study is in agreement with the monsoon reconstructions based on the upwelling indices from the western Arabian Sea. This reconfirms that the SW monsoon wind driven upwelling along the western Arabian Sea and precipitation in the Indian subcontinent and river discharge to the Arabian Sea were related at centennial time scale.

Marine Isotope Stage 4 had documented higher SST (28.1^0C), more depleted δ^{18}Oc values, enriched δ^{18}Osw values and higher salinity as compared to MIS 2. This suggests that eastern Arabian Sea was more evaporative during MIS 4 than in MIS 2. Prevalence of higher SST during MIS 4 than in the MIS 2 would result in more evaporation during MIS 4 along the eastern Arabian Sea. .

The last deglaciation was not a smooth transition from one climate state to another, but occurred in a series of steps. It is well documented that $\delta^{18}O$ record of the world oceans exhibit a two step deglaciation model that included two phases of rapid ice melting separated by a brief period of climate stability. Two step deglaciation i.e. termination 1A and termination 1B has occurred around 12.5 kyr and 9.5 kyr respectively (Duplessy *et al.*, 1981) and sea level also rose during this time due to huge amount of melt water flux caused due to warming (Fairbanks 1989). It is generally believed that the timing of the transition from the Oldest Dryas to Bolling/Allerod at 14.7 kyr BP in Greenland snow accumulation record (Alley *et al.*, 1993). SST records from eastern Arabian Sea (Core AAS-9/21) and Bay of Bengal (Core SK-218/1) show early deglaciation at 18 kyr BP. Similarly $\delta^{18}Oc$ values of these two cores also show depleting trend from 18 kyr BP. This provides strong evidence that in the northern Indian Ocean (Arabian Sea and Bay of Bengal) deglaciation was initiated around 18 kyr B.P.

Earlier SST estimates based on alkenone unsaturation ratios document no significant change in SST with in the Holocene in the Arabian Sea. By contrast, the present study based on Mg/Ca thermometry provide an evidence that ~2^0C SST change during the Holocene.

The strength of monsoon, biological productivity and lithogenic particulate supply to the sediment in the northern Indian Ocean are strongly coupled in the modern day (Nair *et al.*, 1989). It has been debated about the linkages between productivity and monsoon strength (Gupta *et al.*, 2005). However, it is not clear yet whether productivity changes in the northern Indian Ocean are linearly related to the strength of monsoon in the geological past or not. Enriched $\delta^{13}C$ values during MIS 1 and 3 and depleted values in MIS 2 and 4 in the eastern Arabian Sea and Bay of Bengal were noticed. This suggests that higher productivity during interglacials (MIS 1 and 3) and lower productivity during glacials (MIS 2 and 4) in both Arabian Sea and Bay of Bengal. Earlier findings from the eastern Arabian Sea (Ganeshram *et al.*, Pattan *et al.*, 2003) and from the western Arabian Sea (Murray and Prell 1993; Naidu and Malmgren 1996) also revealed high productivity during interglacials as a result of strong SW monsoon and low productivity during glacials due to weak SW monsoon. Therefore, it is suggested here that the productivity changes of eastern Arabian Sea and Bay of Bengal are controlled by the SW monsoon strength.

Indus Fan is one of the largest deep-sea fans in the world, totaling c.5 * 10^6 km^2. Terrigenous input from the Indus River dominates sediments in the northern Arabian Sea. The primary source of sediments to the Indus Fan is derived from the Indus River, which drains the arid to semi-arid western Himalaya Mountains. Peak discharge occurs during the summer months as a result of seasonal glacier melting and the increased runoff generated by the summer monsoon. Thus, the sediment discharge from the Indus River also depends on the rainfall during SW monsoon. Detailed studies on ODP Site 720A from Indus Fan revealed two distinct sediment sequences in the Indus Fan during late Quaternary: i) Turbidite sequence from 525 to 375 ka and ii) Pelagic sequence from 375 to the present day. It is suggested here that most of the channels were buried by 375 ka BP, which caused the distributary channel to switch away from the site. This in turn result in a general decrease in turbidite deposition at the study site rather than indicating a decrease in terrigenous supply to the Indus Fan. The calcium carbonate content at the study site was controlled by terrigenous material dilution. In the pelagic sequence, the calcium carbonate was diluted by clays, whereas in the turbidite sequence it was diluted by sand and silt. Al, Ti and terrigenous material not show any consistent responses to glacial and interglacial climatic conditions. The terrigenous material supply to the site is therefore not linearly related to the sea-level changes.

The high abundance of Indus-derived clay minerals originating from the Himalayas (illite and chlorite) in both the turbidite sequence as well as the pelagic sequence suggests that the source and supply of clay minerals to the Indus Fan remained constant over last 525 ka.

Recommendations for future work:

During past 1500 years centennial-scale natural climate oscillations such as Little Ice Age and Medieval Warm Period affected broad areas of Earth. It appears that these century-scale climate oscillations were not only restricted to the high latitudes but also have involved a significant perturbations in tropical ocean temperatures and monsoon rainfall. To argue the role of tropical oceans on the global climate we need to generate centennial time scale resolution marine and terrestrial paleoclimate records with more spatial coverage from tropics. Such kind of records will enable us to answer whether tropics or high latitudes kick the start of abrupt climate changes on global scale.

Agnihotri R, Sarin MM, Somayajulu BLK, Jull AJT, Burr GS (2003). Late Quaternary biogenic productivity and organic carbon deposition in the eastern Arabian Sea. *Palaeogeogr. Palaeoclima. Palaeoecol.*, 197, 43-60.

Alley RB, Meese DA, Shuman AJ, Gow AJ, Taylor KC, Grootes PM, White JWC, Ram M, Waddington ED, Mayewski PA, Zielinski GA (1993). Abrupt accumulation increase at the Younger Dryas termination in the GISP2 ice core. *Nature*, 362, 527-529.

Altabet MA, Francois R, Murray DW, Prell WL (1995). Climate-related variations in denitrification in the Arabian Sea from sediment $^{15}N/^{14}N$ ratios. *Nature*, 373, 506-509.

Altabet MA, Higginson MJ, Murray DW (2002). The effect of millennial-scale changes in Arabian Sea denitrification on atmospheric CO2. *Nature*, 415, 159–162.

Anand P, Elderfield H, Conte MH (2003). Calibration of Mg/Ca thermometry in planktonic foraminifera from a sediment trap time series. *Paleoceanography*, 18(2), 1050, doi: 10.1029/2002PA000846.

Anderson DM, Prell WL (1993). A 300 kyr record of upwelling off Oman during the late Quaternary: evidence of the Asian southwest monsoon. *Paleoceanography*, 8, 193–208.

Banakar VK, Oba T, Volvaiker AV, Kuramoto T, Yamamoto M, Minagawa M (2005). A 100,000 years climate history of the Eastern Arabian Sea: Monsoon precipitation and productivity trends. *Marine Geology*, 219, 99-108.

Bard E, Rostek F, Sonzogni C (1997). Interhemispheric synchrony of the last deglaciation inferred from alkenone palaeothermometry. *Nature*, 385, 707-710.

Barker S, Greaves M, Elderfield H (2003). A study of cleaning procedures used for foraminiferal Mg/Ca paleothermometry. *Geochem. Geophys. Geosyst.*, 4(9), 8407, doi: 10.1029/2003GC000559.

Bassinot FC, Labeyrie LD, Vincent E, Quidelleur X, Shackleton NJ, Lancelot Y (1994). The astronomical theory of climate and the age of the Brunhes-Matuyama magnetic reversal. *Earth and Planetary Science Letters*, 126, 91-108.

Baumgartner A, Reichel E (1975). The World Water Balance: Annual Global, Continental and Maritime Precipitation, evaporation and Runoff. *Elsevier Sci., New York,* 31 charts, pp.179.

Bé AWH (1960). Ecology of recent planktonic foraminifera: Part-2 Bathymetric and seasonal distributions in the Sargasso Sea off Bermuda. *Micropaleontology*, 6, 373-392.

Bé AWH (1967). Foraminifera, families: Globigernidae and Globorotaliidae, in Fiches d'identification du Zooplankton, sheet 108, (Eds.) Fraser JH, pp. 1-3 Conseil International Pour l'Exploration de la Mer, Charlottenlund, Denmark.

Bé AWH, Tolderlund DS (1971). Distribution and ecology of living planktonic foraminifera in surface waters of the Atlantic and Indian Oceans; The Micropaleontology of the Oceans, Funnel BM, Riedel WR (Eds.) Cambridge Univ. Press, London, 105-149.

Berger A (1977). Long-term variations of the Earth's orbital elements. *Celestial Mech.*, 15, 53-74.

Berger A (1978). Long-term variations of daily insolation and Quaternary climatic changes. *J. Atmos. Sci.*, 35, 2362–2367.

Berger A, Loutre MF (1991). Insolation values for the climate of the last 10 million years. *Quaternary Science Reviews,* 10, 297-317.

Berger WH, Smetacek VS, Wefer G (1989). Ocean productivity and paleoproductivity – an overview. In: Berger WH, Smetacek VS, Wefer G (Eds.) *Productivity of the Ocean: Present and Past.* J Wiley & Sons, Chichester, pp 1-34.

Bhushan R, Dutta K, Somayajulu BLK (2001). Concentrations and burial fluxes of organic and inorganic carbon on the eastern margins of the Arabian Sea. *Marine Geology*, 178, 95–113.

Biscay PE (1965). Mineralogy and sedimentation of recent deep sea clay in the Atlantic Ocean and adjacent seas and oceans. *Geol Soc Amer Bull.*, 76, 803-832.

Bond G, Kromer B, Beer J, Muscheler R, Evans M, Showers W, Hoffmann S, Lotti-Bond R, Hajdas I, Bonani G (2001). Persistent solar influence on North Atlantic climate during the Holocene. *Science*, 294, 2130-2136.

Bond G, Showers W, Cheseby M, Lotti R, Almasi P, deMenocal P, Priore P, Cullen H, Hajdas I, Bonani G (1997). A pervasive millennial-scale cycle in North Atlantic Holocene and glacial climates. *Science*, 278, 1257-1266.

Bond G, Showers W, Elliot M, Evans M, Lotti R, Hajdas I, Bonani G, Johnson S (1999). The North Atlantic's 1-2 kyr climate rhythm: relation to Heinrich Events, Dansgaard/Oeschger cycle and the Little Ice Age. In: Clark P, Webb R, Keigwin L (Eds.), *Mechanism of Global Climate Change at Millennial Time Scales,* Geophysical Monograph Series, American Geophysical Union, Washington, DC, 112, 35-58.

Bouma AH, Colemen JH, Stelting CE, Kohl B (1989). Influence of relative sea level changes on the construction of the Mississippi fan. *Geo-Marine Letters* 9, 161-170.

Boyle EA (1988). Cadmium: chemical tracer of deepwater Paleoceanography. *Paleoceanography*, 3, 471-489.

Boyle EA (1992). Cadmium and $\delta^{13}C$ paleochemical ocean distributions during the Stage 2 Glacial Maximum. *Ann. Rev. Earth Planet. Sci.*, 20, 245-287.

Boyle EA, Keigwin LD (1982). Deep circulation of the North Atlantic over the last 200,000 years: Geochemical evidence. *Science*, 218, 784-786.

Bradley RS (1999). Paleoclimatology: Reconstructing climates of the Quaternary. (Eds.) Dmowska R, Holton JR International Geophysics Series. pp. 613.

Brady HB (1884). Report on the foraminifera dredged by H. M. S. Challenger, during the years 1873-1876. *Rept. Voy. Challenger, Zool,* 9, pp. ii-xxi, 1-814, pls. 1-115.

Brink KR, Arnone P, Coble C, Flagg B, Jones J, Kindle CL, Phinney D, Wood M, Yentsch, young D (1998). Monsoons boost biological productivity in the Arabian Sea EOS. *Trans Amer Geophy Union*, 27, 168-169.

Broecker WS (1982). Glacial to interglacial changes in ocean chemistry. *Progr. Oceanogr.*, 11, 151-197.

Broecker WS (2003). Does the trigger for abrupt climate change reside in the ocean or in the atmosphere? *Science*, 300, 1519-1522

Broecker WS, Peng T–H (1982). *Tracers in the sea.* Eldigio Press, New York, pp. 690.

Broecker WS, Peng T–H (1993). What caused the glacial to interglacial CO2 change? In: Heimann M (Eds.). *The Global Carbon Cycle.* Springer, Berlin Heidelberg, New York, 95-115.

Budziak D, Schneider RR, Rostek F, Muller P, Bard E, Wefer G (2000). Late Quaternary insolation forcing on total organic carbon and C37 variations in the Arabian Sea. *Paleoceanography*, 15, 307– 321.

Bush AGB, Philander SGH (1998). The role of ocean-atmosphere interactions in tropical cooling during the last glacial maximum. *Science*, 279, 1341-1344.

Cane MA (1998). A role for the tropical Pacific. *Science*, 282, 59-61.

Charles CD, Wright JD, Fairbanks RG (1993). Thermodynamic influences on marine carbon isotope record. *Paleoceanography*, 8, 691-697.

Chauhan OS (1999). Monsoon variability during late Pleistocene–Holocene in the southeastern Arabian Sea. *Indian Journal of Marine Sciences*, 28 (1), 99–101.

Chodankar AR, Banakar VK, Oba T (2005). Past 100 ky surface salinity-gradient response in the Eastern Arabian Sea to the summer monsoon variation recorded by δ 18O of *G. sacculifer. Global and Planetory Change*, 47, 135-142.

Clark PU, Marshall SJ, Clarke KCG, Hosteller WS, Licciardi MJ, Teller JT (2001). Freshwater forcing of abrupt climate change during the last glaciation. *Science*, 293, 283-287.

Clemens S, Prell W, Murray D, Shimmield G, Weedon G (1991). Forcing mechanism of the Indian Ocean monsoon. *Nature*, 353, pp-720-725.

Clemens SC, Prell WL (2003). A 350,000 year summer-monsoon multi-proxy stack from the Owen Ridge, northern Arabian Sea. *Mar. Geol.*, 201, 35-51.

Clement AC, Seager R, Cane MA (1999). Orbital controls on the El Nino/Southern Oscillation and the tropical climate. *Paleoceanography*, 14, 441-456.

CLIMAP Project members (1981). Seasonal Reconstructions of the Eatrh's Surface at the last Glacial Maximum. *Geol. Soc. Amer. Map and Chart Series MC-36.*

Cobb KM, Charles CD (2001) A central tropical Pacific coral demonstrates Pacific, Indian, and Atlantic decadal climate connections. *Geophysical Research Letters*, 28, 2209-2212.

Colin C, Bertaux J, Turpin L, Kissel C (2001). Dynamique de l'érosion dans le bassin versant de l'Irrawaddy au cours des deux derniers cycles climatiques (280–0 ka), Comptes Rendus de l'Académie des Sciences Paris. 332, 483–489.

Colin C, Turpin L, Bertauxc J, Desprairies A, Kissel C (1999). Erosional history of the Himalayan and Burman ranges during the last two glacial–interglacial cycles. *Earth and Planetary Science Letters,* 171, 646-660.

Craig H (1965). The measurement of oxygen isotope paleotemperature. In: *Proceedings of he Spoleto Conference on stable isotope in Oceanographic studies and paleotemperatures*. Consiglio Nazionale delle Ricerche Laboratoriodi Geologia Nucleare, Pisa, 3-24.

Croll J (1867). On the eccentricity of the Earth's orbit, and its physical relations to the glacial epoch. *Philosophical Magazine*, 33, 426-445.

Cullen JL, Prell WL (1984). Planktonic foraminifera of the northern Indian Ocean: distribution and preservation in surface sediments. *Mar. Micropaleontol.*, 9, 1-52.

Curry WB, Duplessy JC, Labeyrie LD, Shackleton NJ (1988). Changes in the distribution of δ 13C of deep water ∑CO2 between the last glaciation and the Holocene. *Paleoceanography*, 3 (3), 317-341.

Curry WB, Lohmann GP (1982). Carbon isotopic changes in benthic foraminifera from the western South Atlantic: Reconstruction of glacial abyssal circulation patterns. *Quat. Res.*, 18, 218-235.

Curry WB, Ostermann DR, Guptha MV, Ittekkot V (1992). Foraminiferal production and monsoonal forcing in the Arabian Sea: evidence from sediment traps. In: Summerhayes CP, Prell WL, Emeis K-C (Eds.) Upwelling system: Evolution since the early Miocene. *Geol. Soc. Spec. Publ.*, 64, 93-106.

d'Orbigny A (1826). Tableau methodique de la classe de cephalopods. *Ann. Sci. Nat. Paris Ser.*, 1-7, 245-314.

Dahl AK, Oppo DW (2006). Sea surface temperature pattern reconstructions in the Arabian Sea. *Paleoceanograpy,* 21, PA1014, doi: 10.1029/2005PA001162.

Damuth JE (1975). Quaternary climate change as related by calcium carbonate fluctuations in western equatorial Atlantic sediments. *Deep-Sea Research,* 22, 725-743.

Damuth JE (1975). Quaternary climate change as revealed by calcium carbonate fluctuations in western equatorial Atlantic sediments. *Deep-Sea Res. Part A,* 22, 725-743.

Dansgaard, W., et al., Evidence for general instability of past climate from a 250-kyr ice-core record. *Nature,* 364, 218-220 (1993).

Darbyshire M (1967). The surface waters off the coast of Kerala, south-west India. *Deep-Sea Res.,* 14, 295–320.

de Garidel-Thoron T, Beaufort L, Linsley BK, Dannenmenn S (2001). Millennial-scale dynamics of the east Asian winter monsoon during the last 200000 years. *Paleoceanography,* 16, 491-502.

Defant A (1961). *Physical oceanography,* vol. I. Oxford: Pergamon Press.

Dekens PS, Lea DW, Pak DK, Spero HJ (2002). Core top calibration of Mg/Ca in tropical foraminifera: refining paleo-temperature estimation. *Geochem. Geophys. Geosys.* 3, 1022, 10.1029/2001GC000200.

deMenocal PB (2001). Cultured response to climate change during the Late Holoene. *Science,* 292, 667-673.

Denton GH, Karlen W (1973). Holocene climatic variations: their pattern and possible cause. *Quaternary Research,* 3, 155-205.

Duplessy JC (1982). Glacial to interglacial contrast in the northern Indian Ocean. *Nature,* 295, 464-498.

Duplessy JC, Be AWH, Blanc PL (1981). Oxygen and Carbon isotopic composition and biogeographic distribution of planktonic foraminifera in the Indian Ocean. *Paleogeography, Paleoclimetology, Paleoecology,* 33, 9-46.

Eggins SM, Sadekov A, Deckker PDe (2004). Modulation and daily banding of Mg/Ca in orbulina universa tests by symbiont photosynthesis and respiration: a

complication for seawater thermometry? *Earth and Planetary Science Letters*, 225, 411-419.

Elderfield H, Ganssen G (2000). Past temperatures and $\delta^{18}O$ of surface ocean waters inferred from foraminiferal Mg/Ca ratios. *Nature*, 405, 442-445.

Emeis K-C, Anderson DM, Kroon D, Schulz-Bull D (1995). Sea-surface temperatures and history of monsoon upwelling in the northwestern Arabian Sea during the last 500,000 years. *Quart. Res.*, 43, 355-361.

Emerson S, Bender M (1981). Carbon fluxes at the sedimentwater interface of the deep-sea—calcium-carbonate preservation. *Journal of Marine Research*, 39 (1), 139–162.

Emiliani C (1954). Depth habitats of some species of pelagic foraminifera as indicated by oxygen isotopic ratios. *American Jour. Science*, 252, 149-158.

Emiliani C (1955). Pleistocene temperatures. *J. Geol*, 63, 538-578.

Emiliani C (1966). Paleotemperature analysis of Caribbean cores, P6304-8 and P6304-9 and a generalized temperature curve for the past 425,000 years. *Jour. Geology*, 74, 109-126.

Epstein S, Buchsbaum R, Lowenstam HA, Urey HC (1953). Revised carbonate-water isotopic temperature scale. *Geol. Soc. America Bull.*, 64, 1315-1325.

Fairbanks RG (1989). A 17,000-year glacio-eustatic sea-level record: influence of glacial melting rates on the Younger Dryas event and deep-ocean circulation, *Nature*, 342, 637–642.

Feely MH, Moore TC Jr, Loutit ST, Bryant WR (1990). Sequence stratigraphy of Mississippi fan related to oxygen isotope sea level index. *AAPG Bulletin* 74, 407-474.

Fischer AF, Weller R, Rudnick ADL, Eriksen C, Lee C, Brink MK, Fox CA, Leben RR (2002). Mesoscale eddies, coastal upwelling, and the upper-ocean heat budget in the Arabian Sea. *Deep-Sea res. II*, 49, 2231-2264.

Fleitmann D, Burns SJ, Mudelsee M, Neff U, Kramers J, Mangini A, Matter A (2003). Holocene Forcing of the Indian Monsoon Recorded in a Stalagmite from Southern Oman. *Science*, 300, 1737-1739.

Folk RL (1968). Petrology of sedimentary rocks. Hemphills, University Station, Austin, Texas 170 pp.

Fontugne MR, Duplessy JC (1986). Variations of the monsoon regime during the upper Quaternary: Evidence from carbon isotopic record of organic matter in north Indian Ocean sediment cores. *Palaeogeogr. Palaeoclimatol. Palaeoecol.*, 56, 69-88.

Gadgil S (2003). The Indian monsoon and its variability. *Annual Review Earth and Planetary Science*, 31, 429-467.

Ganeshram RS, Pederson TF, Calvert SE, McNeill GW, Fontugne MR (2000). Glacial–interglacial variability in denitrification in the world's oceans: causes and consequences. *Paleoceanography*, 15, 361–376.

Gasse F (2000). Hydrological changes in the African tropics since the last glacial maximum. *Quaternary Science Reviews*, 19, 189-211.

Gasse F (2001). Hydrological changes in Africa. *Science*, 292, 2259-2260.

Goodbred SL Jr, Kuehl SA (2000). Enormous Ganges-Brahmaputra sediment discharge during strengthened early Holocene monsoon. *Geology*, 28, 1083–1086.

Govil P, Naidu PD, Radhika TK (2004). Major turbidity flows in the western Indus Fan between 290 and 360 ka BP. *Current Science*, 87(14), 1597-1600.

Griffin JJ, Windom H, Goldberg ED (1968). The distribution of clay minerals in the world oceans. *Deep Sea Research*, 15, 433-459.

Gupta AK (2004). Origin of agriculture and domestication of plants and animal linked to early Holocene climate amelioration. *Current Science*, 87 (1), 54-59.

Gupta AK, Anderson DM, Overpeck JT (2003). Abrupt changes in the Asian southwest monsoon during the Holocene and their links to the North Atlantic Ocean. *Nature*, 421, 354-356.

Guptha MVS, Naidu PD, Haake BG, Schiebel R (2005). Carbonate and Carbon fluctuations in the Eastern Arabian Sea over 140ka: Implications on productivity changes? *Deep-Sea Research II* 52, 1981-1993

Hasternath S, LAMB PJ (1979). Climatic Atlas of the Indian Ocean Part 1, Surface Circulation and Climate University of Wisconsin Press, Madison, pp. 97.

Haug GH, Günther D, Peterson LC, Sigman DM, Hughen KA, Aeschlimann B (2003). Climate and the Collapse of Maya Civilization. *Science,* 299 (5613), 1731-1735.

Hays JD, Imbrie J, Shackleton NJ (1976). Variations in the Earth's orbit: pacemaker of the ice ages. *Science*, 194, 1121-1132.

Hemleben C, Spindler M (1983). Recent advances in research on living planktonic foraminifera, *Utrecht Micropaleontological Bulletins*, 30, 141–170.

Herbert TD, Schuffert JD, Anderson D, Heusser L, Lyle M, Mix A, Ravelo AC, Stott LD, Herguera JC (2001). Collapse of the California current during glacial maxima linked to climate change on land. *Science*, 293, 71.

Holeman JN (1968) Sediment yield of major rivers of the world. *Water Resources Res.* 4, 737-747.

Hong Y, Hong B, Lin Q, Zhu Y, Shibata Y, Hirota M, Uchida M, Leng X, Jiang H, Xu H, Wang H, Yi L (2003). Correlation between Indian Ocean summer monsoon and North Atlantic climate during the Holocene. *Earth and Planetary Science Letters*, 211, 371–380.

Imbrie J, Kipp N (1971). A new micropaleontological method for quantitative paleoclimatology: application to a late pleistocene caribbean core. In: Turekian KK (eds.). *The late Cenozoic glacial ages*, Yale Univ. Press, New Haven, 71-181.

Islam SR (1959). The Indus Submarine Canyon. *Oriental Geogr* 3(1), 101-104 (East Pakistan Geograph. Soc., Dacca)

Islam SR, (1959) The Indus submarine canyon. *Pakistan Geographical Review*, XIV, 32-34.

Ivanochko TS, Ganeshram RS, Brummer G-JA, Ganssen G, Jung SJA, Moreton SG, Kroon D (2005). Varitions in tropical convection as a n amplifier of global climate change at the millennial scale. *Earth and Planetary Science Letters*, 235, 302-314.

Ivanova E (1999). Late Quaternary monsoon history and paleoproductivity of the western Arabian Sea. *Ph.D. dissertation, Free Univ., Amstrerdam.*

Ivanova E, Schiebel R, Singh AD, Schmiedl G, Niebler H-S, Hemleben Ch (2003). Primary production in the Arabian Sea during the last 135 000 years. *Palaeogeography, Palaeoclimatology, Palaeogeology*, 197, 61–82.

Jennerjahn T, Ittekkot V, Arz H, Behling H, Pa¨tzold J, Wefer G (2004). Asynchrony of preserved terrestrial and marine signals of climate change in the tropics during the Heinrich events. *Science*, 306, 2236–2239.

Kineast M, Stephanie SK, Stephen EC, Timothy IE, Mollenhauer G, Francois R, Mix AC (2006). Eastern Pacific cooling and Atlantic overturning circulation during the last deglaciation. *Nature*, 443, 846- 849.

Kolla V, Coumes F (1987). Morphology, internal structure, seismic stratigraphy and sedimentation of Indus Fan. *Am Assoc Petrol Geol Bull,* 71, 650-677.

Kolla V, Henderson L, Biscay PE (1976). Clay mineralogy and sedimentation in the western Indian Ocean. *Deep-Sea Research,* 23, 949-961.

Kolla V, Kostecki JA, Robison F, Biscaye PE, Ray PK (1981). Distribution and origin of clay-minerals and quartz in surface sediments of the Arabian sea. *J. Sediment Pertol,* 51(2), 563-569.

Kominz MA, Heath GR, Ku T-L, Pisias NG (1979). Brunhes time scales and the interpretation of climate change. *Earth and Planetary Science Letters*, 45, 394-410.

Konta J (1985). Mineralogy and chemical maturity of suspended matter in major rivers sampled under the SCOPE/UNEP project. Mitteilungen aus dem geologisch-paleontologischen Institut, University of Hamburg , Heft 58, 557-568.

Koumes F, Kolla V (1982). Indus Fan: Seismic Structure, channel migration and sediment-thickness in the Upper Fan. *Marine Geology and Oceanography of Arabian Sea and coastal Pakistan*, (eds.). Haq, B.U and Milliman, J.D. Scientific and Academic Editions, 101-110.

Kroon D, Ganssen G (1989). Northern Indian Ocean upwelling cells and stable isotope composition of living planktonic foraminifers. *Deep Sea Research*, 36, 1219-1236.

Kroopnick P (1980). The distribution of 13C in the Atlantic Ocean. *Earth and Planetary Science Letters*, 49, 469-484.

Kroopnick PM (1985). The distribution of 13C of total CO2 in the world oceans. *Deep sea Research*, 32 (1), 57-84.

Kudrass HR, Hofmann A, Doose H, Emeis K, Erlenkeuser H (2001). Modulation and amplification of climatic changes in the northern hemisphere by the Indian summer monsoon during the past 80 k.y. *Geology*, 29, 63-66.

Lea DW (2001). Paleoclimate: Ice ages, the California current, and Devis Hole. *Science*, 293, 59-60.

Lea DW, Martin PA, Pak DK, Spero HJ (2002). Reconstructing a 350 ky history of sea level using planktonic Mg/Ca and oxygen isotope from records from a Cocos Ridge core. *Quaternary Science Review*, 21, 283-293.

Lea DW, Mashiotta TA, Spero HJ (1999). Controls on magnesium and strontium uptake in planktonic foraminifera determined by living culturing. *Geochimica et Cosmochimica Acta* 63, 2369-2379.

Lea DW, Pak DK, Peterson LC, Hughen KA (2003). Synchroneity of Tropical and High-Latitude Atlantic Temperatures over the Last Glacial Termination. *Science*, 301, 1361–1364.

Lea DW, Pak DK, Spero HJ (2000). Climate impact of late quaternary equatorial Pacific sea surface temperature variations. *Science*, 289, 1719-1724.

Lear CH, Rosenthal Y, Slowey N (2002). Benthic foraminiferal Mg/Ca-paleothermometry: a revised core-top calibration. *Geochimica et Cosmochimica Acta* 66, 3375-3387.

Levitus S, Boyer TP (1994). World Ocean Atlas 1994. Temperature, vol. 4. NOAA Atlas NESDIS, 4. US Department of Commerce, Washington, DC, pp. 117.

Levitus S, Burgett R, Boyer TP (1994). World Ocean Atlas 1994. Salinity. NOAA Atlas NESDIS, 3, US Department of Commerce, Washington, DC, pp. 99.

Lindzen RS, Hou AYJ (1988). Hadley circulations for zonally average heating centered off the equator. *Atmos. Science,* 45, 2416-2427.

Lisitzen AP (1972). Sedimentation in the world ocean, Society of Economic Paleontologists and Mineralogists Special Publication, No. 17, Tulsa, OK, 218 pp.

Lyle M, Murray DW, Finney BP, Dymond J, Robbins JM, Brooksforce K (1988). The record of late Pleistocene biogenic sedimentation in the eatserntropical Pacific Ocean. *Paleoceanography*, 3, 39-59.

Mackensen A, Bickert T (1999). Stable Carbon Isotopes in Benthic Foraminifera: Proxies of Deep and Bottom Water Circulation and New Production. In: Fischer G, Wefer G (eds.). *Use of Proxies in Paleoceanography: Examples from the South Atlantic.* Springer-Verlag Berlin Heidelberg, 229-254.

Mackensen A, Hubberten H-W, Bickert T, Fischer G, Futterer DK (1993). The $\delta^{13}C$ in benthic foraminifera tests of *Fontbotia wuellerstorfi* (Schwager) relative to the $\delta^{13}C$ of dissolved inorganic carbon in southern Ocean Deep Water: Implications for glacial ocean circulation models. *Paleoceanography*, 8, 587-610.

Malmgren BA, Nordlund U (1996). Application of artificial neural networks to chemostratigraphy. *Paleoceanography*, 11, 505-512.

Malmgren BA, Nordlund U (1997). Application of artificial neural networks to paleoceanographic data. *Palaeogeogra. Palaeoclimatol. Palaeoecologi.,* 136, 359-373.

Manely PL, Flood RD (1988). Cyclic sediment deposition within Amazon deep-sea fan. AAPG Bulletin. 72, 912-925

Manghnani V, Morrison JM, Xie L, Subrahmanyam B (2002). Heat transports in the Indian Ocean estimated from TOPEX/POSEIDON altimetry and model simulations. *Deep Sea Research,* Part II, 49, 1459-1480.

Martin J M, Burton JD, Eisma D (1981). River inputs to Ocean systems, United Nations Press, Geneva, Switzerland, pp. 384.

Martinson DG, Pisias NG, Hays JD, Imbrie J, Moore TC, Shackleton NJ (1987). Age dating and the orbital theory of the ice ages: development of a high resolution 0 to 300,000-year chronostratigraphy. *Quaternary Research*, 27, 1-29.

Mashiotta TA, Lea DW, Spero HJ (1999). Glacial-interglacial changes in subantarctic sea surface temperature and δ^{18}O-water using foraminiferal Mg. *Earth Planet. Sci. Lett.* 170(4), 417-432.

Mayewski PA, Rohling EE, Stager JC, Karlen W, Maasch KA, Meeker LD, Meyerson EA, Gasse F, Kreveld SV, Holmgren K, Lee-Thorp J, Rosqvist G, Rack F, Staubwasser M, Schneider RR, Stieg EJ (2004). Holocene climate variability. *Quaternary Research*, 62, 243-255.

McCorkle DC, Keigwin LD, Corliss BH, Emerson SR (1990). The influence of microhabitats on the carbon isotopic composition of deep-sea benthic foraminifera. *Paleoceanography*, 5, 161-185.

McCrea JM (1950). On the isotopic chemistry of carbonates and a paleotemperature scale. *J. Chem. Phys.*, 18, 849-857.

Meeker LD, Mayewski PA (2002). A 1400-year high-resolution record of atmospheric circulation over the North Atlantic and Asia. *Holocene*, 12, 257-266.

Milankovitch MM (1941). Canon of insolation and the ice-age problem. Beograd: Konglich Serbische Akademie. [English translation by the Israel Program for Scientific Translations, Published for the US department of Commerce, and the National Science, Foundations, Washington, DC (1969).]

Milliman JD, Quraishee GS, Beg MAA (1984) Sediment discharge from the Indus River to the Ocean: Past, Present and Future. In: Haq, B.U. & Milliman, J.D. (eds.). Marine Geology and Oceanography of the Arabian Sea and Coastal Pakistan. Van Nostrand Reinhold, New York, 65-70

Molinari RL, Olson D, Reverdine G (1990). Surface current distributions in the tropical Indian Ocean derived from complications of surface buoy trajectories. *Journal of Physical Oceanography*, 95, 7217-7238.

Montegut CD, Vialard J, Shenoi SSC, Shankar D, Durand F, Ethe C, Madec G (2007). Simulated seasonal and interannual variability of mixed layer heat budget in the northern Indian Ocean. *Journal of Climate* (in press).

Murray DW, Prell WL (1992). Late Pliocene and Pleistocene climatic oscillations and monsoon upwelling recorded in sediments from the Owen Ridge, northwestern Arabia Sea. In: C.P. Summerhayes et al. Upwelling Systems: Evolution since the Early Miocene, Geological Society, [London], pp. 301–321 Special Publication 64.

Murray RW, Leinen M (1996). Scavenged excess aluminium and its relationship to bulk titanium in biogenic sediment from the central equatorial Pacific Ocean. *Geochim. Cosmochim. Acta,* 60, 3869-3878.

Mutti E, Normark WR (1987) Comparing examples of modern and ancient turbidite systems: Problems and concepts. In: Leggett JK, Zuffa GG (Eds) Marine clastic sedimentology. Graham and Trotman, London, 1-38

Naidu AS, Mowatt TC, Somayajulu BLK, Rao KS (1985). Characteristics of clay minerals in the bed loads of major Rivers of India. Mitteilungen aus dem geologisch-paleontologischen, Institut, University of Hamburg, Heft 2, 559-568.

Naidu AS, Shankar R (1999). Palaeomonsoon history during the late quaternary: results of a pilot study on sediments from the laccadive trough, southeastern Arabian Sea. *J. Geol. Soc. India* 53, 401–406.

Naidu PD (1991). Glacial to interglacial contrasts in the calcium carbonate content and influence of Indus discharge in two eastern Arabian Sea cores. *Palaeogeogr. Palaeoclimatol. Palaeco.,* 86, 255-263.

Naidu PD (1996). Onset of an arid climate at 3.5 ka in tropics: Evidence from monsoon upwelling record. *Current Science,* 71, 715-718.

Naidu PD (1998). Driving forces of Indian summer monsoon on Milankovitch and sub-Milankovitch time scales: A review. *J. Geol. Soc. India,* 52, 257–272.

Naidu PD (2004). Isotopic evidences of past upwelling intensity in the Arabian Sea. *Global Planet. Change,* 40, 285-293.

Naidu PD, Malmgren BA (1995). A 2,200 years periodicity in the Asian monsoon system. *Geophys. Res. Lett.,* 22, 2361-2364.

Naidu PD, Malmgren BA (1996). A high-resolution record of late Quaternary upwelling along the Oman Margin, Arabian Sea based on planktonic foraminifera. *Paleoceanography*, 11, 129–140.

Naidu PD, Malmgren BA (2005). Seasonal sea surface temperature contrast between the Holocene and last glacial period in the western Arabian Sea (Ocean Drilling Project Site 723): Modulated by monsoon upwelling. *Paleoceanography*, 20, doi: 10.1029/2004PA001078.

Naidu PD, Malmgren BA, Bornmalm L (1993). Quaternary history of calcium carbonate fluctuations in the western equatorial Indian Ocean (Somali Basin). *Palaeogeogr. Palaeoclimatol. Palaeco.*, 103. 21-30.

Naini BR, Kolla V (1982). Acoustic character and thickness of sediments of the Indus Fan and the continental margin of western India. *Marine Geology*, 47, 181-195.

Nair RR, Ittekkot V, Manganini SJ, Ramaswamy V, Haake B, Degens ET, Desai BN, Honjo S (1989). Increased particulate flux to the deep ocean related to monsoon. *Nature*, 338, 749-751.

Neff U, Burns SJ, Mangini A, Mudelsee M, Fleitmann D, Matter A (2001). Strong Coherence between solar variability and the monsoon in Oman between 9 and 6 kyr ago. *Nature*, 411, 290-293.

Nigam R (1990). Palaeoclimatic implications of size variation in *Orbulina universa* in a core from the North Indian Ocean. *Current Science*, 59, 46-47.

Nigam R, Khare N (1999). Spatial and temporal distribution of foraminifera in sediments off the central west coast of India and use of their test morphologies for the reconstruction of palaeomonsoonal precipitation. *Micropaleontology*, 45, 1-15.

Niitsuma N, Naidu PD (2001). History of Monsoon. *Encyclopedia of Marine Sciences*, 1841-1849.

Nurnberg D (1995). Magnesium in tests of Neogloboquadrina pachyderma sinistral from high northern and southern latitudes. *J. Foram. Res.*, 25, 350-368.

Nurnberg D, Bijma J, Hemleben C (1996a). Assessing the reliability of magnesium in foraminiferal calcite as a proxy for water mass temperatures. *Geochim. Cosmochim. Acta* 60 (5), 803 – 814.

Nurnberg D, Bijma J, Hemleben C (1996b). Assessing the reliability of magnesium in foraminiferal calcite as a proxy for water mass temperatures. *Geochim. Cosmochim. Acta* 60 (13), 2483-2484.

O'Brien SR, Mayewski PA, Meeker LD, Meese DA, Twickler MS, Whitlow SI (1995). Complexity of Holocene climate as reconstructed from a Greenland ice core. *Science*, 270, 1962-1964.

Oberhuber JM (1988). An atlas based on COADS data set. *Max Planck Institute for Meteorology Rep 15: Hamburg, Germany.*

Ortiz JD, O'Connell SB, DelViscio J, Dean W, Carriquiry JD, Marchitto T, Zheng Y, van Geen A (2004). Enhanced marine productivity off western North America during warm climate intervals of the past 52 ky. *Geology*, 32 (6), 521–524.

Overpeck JT, Anderson DM, Trumbore S, Prell W (1996). The southwest Indian monsoon over the last 18,000 years. *Climate Dynamics*, 12, 213–225.

Owen R (1867). On the dental character of genera and species, chiefly of fisher from the lower main seam and shales of coal. *North umberland, Trans. Odent. Soc. Gt. Br.*, 5, 323-376, pls 1-15.

Parker WR, Jones TR (1865). On some foraminifera from the North Atlantic and Arctic Oceans including Davis straits and Baffin's Bay. *Royal Soc. London, Phil. Trans,* 155, 325-441.

Pattan JN, Masuzawa T, Naidu PD, Parthiban G, Yamamoto M (2003). Productivity fluctuations in the southeastern Arabian Sea during the last 140 ka. *Palaeogegraphy Palaeoclimatology Palaeoecology*, 193, 575-590.

Peeters F, Beyerle U, Aeschbach-hertig W, Holocher J, Brennwald MS, Kipfer R (2003). Improving noble gas based paleoclimate reconstruction and groundwater dating using 20Ne/22Ne ratios. *Geochimica et Cosmochimica Acta,* 67 (4), 587-600.

Peeters F, Ivanova E, Conan S, Brummer GJ, Ganssen G, Troelstra S, van Hinte J (1999). A size analyses of planktonic foraminifera from the Arabian Sea. *Marine Micropaleontology*, 36, 31-63.

Pierrehumbert RT (2000). Climate change and the tropical Pacific: The sleeping dragon wakes. *Proceedings of National Academy of sciences*, 97, 1355-1358.

Pisias N G (1976). Late Quaternary sediment of the Panama Basin: sedimentation rates, periodicities, and controls of carbonate and opal accumulation. *Mem.—GeoL Soc. Am.*, 145, 375-391.

Pisias NG, Martinson DG, Moore Jr TC, Shackleton NJ, Prell W, Hays J, Boden G (1984). High resolution stratigraphic correlation of benthic oxygen isotopic records spanning the last 300,000 years. *Marine Geology*, 56, 119-136.

Pitulko VV, Nikolsky PA, Girya EYu, Basilyan AE, Tumskoy VE, Koulakov SA, Astakhov SN, Pavlova EYu, Anisimov MA (2004). The Yana RHS Site: Humans in the Arctic Before the Last Glacial Maximum. *Science*, 303 (5654), 52-56.

Prell WL (1984). Variation of monsoonal upwelling: a response to changing solar radiation. In: Hansen JE, Takahashi T (eds.). *Climatic Processes and Climate sensitivity. Am. Geophys. Union, Maurice Ewing Ser.*, 5, 48-57.

Prell WL (1985). The stability of low-latitude sea-surface temperature: an evaluation of the CLIMAP reconstruction with emphasis on the positive SST anomalies. *Dept. Energy Tech Report* TR-025, Washington, DC.

Prell WL, Campo EV (1986). Coherent response of Arabian Sea upwelling and pollen transport of late Quaternary monsoonal winds. *Nature*, 323, 526-528.

Prell WL, Curry WB (1981). Faunal and isotopic indices of monsoonal upwelling: western Arabian Sea. *Oceanologica Acta,* 4, 91-98.

Prell WL, Hutson WH (1979). Zonal temperature-anomaly maps of Indian Ocean surface waters: Modern and ice-ages patterns. *Science*, 206, 454-456.

Prell WL, Imbrie J, Martinson DG, Morley JJ, Pisias NG, Shackleton NJ, Streeter HF (1986). Graphic correlation of oxygen isotope stratigraphy: application to the Late Quaternary. *Paleoceanography*, 1, 137-162.

Prell WL, Kutzbach JE (1987). Monsoon variability over the past 150,000 years. *J. Geophys. Res.*, 92, 8411-8425.

Prell WL, Kutzbach JE (1992). Sensitivity of the Indian monsoon to forcing parameters and implications for its evolution. *Nature,* 360, 647-652.

Prell WL, Murry DW, Clemens SC (1992). Evolution and variability of the Indian Ocean summer monsoon: Evidence from the western Arabian Sea drilling program. *Geophysical Monograph*, 70, 447–469.

Prell WL, Niitsuma N (1989). Ocean Drilling Program. College Station Texas (Eds.) *Proceedings of Ocean Drilling Program, Initial Reports* 117: 319-384

Prins MA, Postma G (2000). Effect of climate, sea level, and tectonics unraveled for last deglaciation turbidite records of the Arabian Sea. *Geology*, 28(4), 372-378.

Prins MA, Postma G, Cleveringa J, Cramp A, Kenyon NH (2000). Controls on terrigenous sediment supply to the Arabian Sea during Later Quaternary: The Indus Fan. *Marine Geology*, 169, 327-349.

Raja R, Saraswati PK, Iwao K (2007). A field-based study on variation in Mg/Ca and Sr/Ca in larger benthic foraminifera. *Geochemi. Geophys. Geosy.*, 8 (10), Q10012, doi:10.1029/2006GC001478.

Rao RR, Molinari RL, Festa JF (1989). Evolution of the climatological near-surface thermal structure of the tropical Indian Ocean: 1. description of mean monthly mixed-layer depth and sea surface temperature, surface current and surface meteorological fields. *Journal of Geophysical Research,* 94, 10801-10815.

Rao VP, Rao BR (1995). Provenance and distribution of clay minerals in the sediments of the western continental shelf and slope of India. *Cont. Shelf Res.*, 15, 1757-1771.

Rixen T, Haake B, Ittekkot V, Guptha MVS, Nair RR, Schlüssel P (1996). Coupling between SW monsoon-related surface and deep ocean processes as discerned from continuous particle flux measurements and correlated satellite data. *J. Geophys. Res.*, 101, 28569–28582.

Rosenthal Y, Boyle EA, Slowey N (1997). Temperature control on the incorporation of magnesium, strontium, fluorine and cadmium into benthic foraminiferal shells from Little Bahama Bank: prospects for thermocline paleoceanography. *Geochimica et Cosmochmica Acta* 61, 3633-3643.

Rosenthal Y, Lohman GP, Lohman KC, Sherell RM (2000). Incorporation and preservation of Mg in Globigerinoides sacculifer: Implications for

reconstructing the temperature and 18O/16O of sea water. *Paleoceanography*, 15, 135.

Rostek F, Ruhland G, Bassinot FC, Muller PJ, Labeyrie LD, Lancelot Y, Bard E (1993). Reconstructing sea surface temperature and salinity using δ18O and alkenone records. *Nature*, 364, 319-321.

Rozanski K, Araguas-Araguas L, Gonfiantini R (1992). Isotopic patterns I modern global precipitation. In: Climate Change in Continental Isotopic Records (Eds.) Swart PK, Lohmann KC, McKenzie J, Savin S, Washington, DC: American Geophysical Union. 1-36.

Russell AD, Emerson S, Nelson BK, Erez J, Lea DW (1994). Uranium in foraminiferal calcite as a recorder of seawater uranium concentrations. *Geochimica et Cosmochimica Acta*, 58, 671-681.

Saher MH, Jung SJA, Elderfield H, Greaves MJ, Kroon D (2007). Sea surface temperatures of the western Arabian Sea during the last deglaciation. *Paleoceanography*, 22, PA2208, doi: 10.1029/2006PA001292.

Saraswat R, Nigam R, Weldeab S, Mackensen A, Naidu PD (2005). A first look at past sea surface temperatures in the equatorial Indian Ocean from Mg/Ca in foraminifera. *Geophysical Research Letters*, 32, L24605, doi:10.1029/2005GL024093

Sarkar A, Ramesh R, Bhattacharya SK, Rajagopalan G (1990). Oxygen isotope evidence for a stronger winter monsoon current during the last glaciation. *Nature,* 343, 549-551.

Sarkar A, Ramesh R, Somayajulu BLK, Agnihotri R, Jull AJT (2000). High resolution Holocene monsoon record from the eastern Arabian Sea. *Earth Planet Sci. Lett.,* 177, 209-218.

Schneider RR, Miller PJ, Acheson R (1999). Atlantic alkenone sea surface temperature records: Low versus mid latitudes and differences between hemispheres, in reconstructing Ocean history: A window in to the Future, (Eds.) Abrantes F, Mix AC, Kluwer Acad., Norwell, Mass., pp. 33-56.

Schott FA, McCreary JP-Jr (2001). The monsoon circulation of the Indian Ocean. *Prog. Oceanogr.*, 51, 1-123.

Schott, G. 1935. Geographie des Indischen und Stillen Ozeans. Verlag von C. Boysen. Hamburg, pp. 413.

Schulz H, Von Rad U, Ittekkot V (2002). Planktic foraminifera, particle flux and oceanic productivity off Pakistan, NE Arabian Sea: Modern analogues and application to the palaeoclimatic record, In: The tectonic and climatic Evolution of the Arabian Sea Region, (Eds:) Clift PD et al., *Geol. Soc. Spec. Publ.*, 195, 499-516.

Schulz HS, Von Rad U, Erlenkeuser H (1998). Correlation between Arabian Sea and Greenland climate oscillations of the past 110, 000 years. Nature, 393, 54- 57.

Seager R, Zebiak SE, Cane MA (1988). A model of the tropical Pacific sea surface temperature climatology. *J. Geophys. Res.*, 93, 1265-1280.

Seltzer GO, Rodbell DT, Baker PA, Fritz SC, Tapia PM, Rowe HD, Dunbar RB (2002). Early warming of tropical South America and the last glacial-interglacial transition. *Science*, 296, 1685-1686.

Shackleton NJ (1977). The oxygen isotope stratigraphic record of the late Pleistocene. Phil. Trans. Royal Society of London, B280, 169-179.

Shackleton NJ, Berger A, Peltier WR (1990). An alternative astronomical calibration of the lower Pleistocene timescales based on ODP site 677. Trans. Royal Society of Edinburgh, Earth Science, 81, 251-261.

Shackleton NJ, Hall MA, Line J, Cang S (1983). Carbon isotope data in core V19-30 (Carenegie Ridge, south of the Panama Basin) confirm reduced carbon dioxide concentrations in the ice age atmosphere. *Nature*, 306, 319-322.

Shackleton NJ, Opdyke ND (1973). Oxygen-isotope and paleomagnetic stratigraphy of equatorial Pacific core V28-239: oxygen isotope temperatures and ice volumes on a 105 year and 106 year scale. *Quaternary Research*, 3, 39-55.

Shackleton NJ (2000). A 100,000 year ice-age cycle identified and found to lag temperature, carbon-dioxide, and orbital eccentricity. *Science*, 289, 1897-1902.

Sharma S, Joachimiski M, Sharma M, Tobschall HJ, Singh IB, Sharma C, Chauhan MS, Morgenroth G (2004). Late glacial and Holocene environmental changes in Ganga plain, northern India. *Quat. Sci. Rev.*, 23, 145– 159.

Shenoi S, Saji P, Almeida A (1999). Near-surface circulation and kinetic energy in the tropical Indian Ocean derived from Lagrangian drifters. *Journal of Marine Research*, 57, 885-907.

Shetye SR, Shenoi SSC, Gouveia AD, Michael GS, Sundar D, Nmpoothiri G (1991). Wind driven coastal upwelling along the western boundary of the Bay of Bengal during the southwest monsoon. *Continental Shelf Research*, 11, 1397-1408.

Shimmield GB, Mowbray SR (1991). The inorganic geochemical record of the northwest Arabian Sea: A history of productivity variation over the last 400 ka from sites 722 and 724. In: Prell WL, Niitsuma et al., Proc. Ocean Drilling Programme, Scientific Results 117, College Station, TX, pp. 409-429.

Shimmield GB, Mowbray SR, Weedon GP (1990). A 350 ka history of the Indian southwest monsoon-evidence from the deep sea cores, northwest Arabian Sea. *Trans. R. Soc. Edinburgh Earth Sci.*, 81, 289-299.

Sigman DM, Boyle EA (2000). Glacial/interglacial variations in atmospheric carbon dioxide. *Nature*, 407, 859-869.

Sirocko F, Garbe-Schonberg D, Deve C (2000). Processes controlling trace element geochemistry of Arabian Sea sediments during the last 25,000 years. *Global and Planetary Change*, 26, 217-303.

Sirocko F, Garbe-Schonberg D, McIntyre A, Molfino B (1996). Teleconnection between the subtropical monsoon and high latitude climates during the last deglaciation. *Science*, 272, 526-529.

Sirocko F, Lange H (1991). Clay mineral accumulation rates in the Arabian Sea during the Late Quaternary. *Marine Geology*, 97, 105-119.

Sirocko F, Sarnthein M (1989). Wind-Borne deposits in Northwestern Indian Ocean: record of Holocene sediments versus modern satellite data. In: Leinin M, Sarnthein M (Eds.), Paleoclimatology and Paleometeorology: Modern and past patterns of glacial transports.-NATO ASI series C. Math, Phys, Sci, Kluwer Acedemic Publishers, Dordrecht. pp. 401-433.

Sirocko F, Sarnthein M, Erlenkeuser H, Lange H, Arnold M, Duplessy JC (1993). Century scale events in monsoon climate over the past 24,000 years. *Nature*, 364, 322-324.

Spero HJ, Lea DW (1996). Experimental determination of stable isotope variability in Globigerina bulloides: implications for paleoceanographic reconstructions. *Mar. Micropaleontol.* 28, 231–246.

Spero HJ, Williams DF (1988). Extracting environmental information from planktonic foraminiferal $\delta^{13}C$ data. *Nature*, 335, 717-719.

Staubwasser M, Sirocko F, Grootes PM, Segl M (2003). Climate change at the 4.2 ka BP termination of the Indus Valley civilization and Holocene south Asian monsoon variability. *Geophys. Res. Lett.*, 30(8), 1425, doi: 10.1029/2002GL016822.

Stott L, Cannariato K, Thunell R, Haug GH, Koutavas A, Lund S (2004). Decline of surface temperature and salinity in the western tropical Pacific Ocean in the Holocene epoch. *Nature*, 431, 56–59.

Stow DAV (1985). Deep-sea clastics: Where are we and where are we going, In: Brenchely PJ, Williams BPJ. (Eds.). Sedimentology: recent developments and applied aspects: Blackwell Scientific Publications, Oxford pp 67-94.

Tiwari M, Ramesh R, Somayajulu BLK, Jull AJT, Burr G S (2005). Early deglacial (19–17 ka) strengthening of the northeast monsoon. *Geophys. Res. Lett.*, 32 L19712.

Toggweiler JR, Carson S, Bjornsson H (1999). Response of the ACC and the Antarctic pycnocline to a meridional shift in the southern hemisphere westerlies. *Eos Trans. AGU,* Ocean Sci. Meet. Suppl, OS286, 80 (49).

Trenberth K, Branstator G, Karoly D, Kumar A, Lau NC, Ropelewski C (1988). Progress during TOGA in understanding and modeling global teleconnections associated with tropical sea surface temperatures. *J. Geophys. Res.*, 103, 14291-14324.

Urey HC (1948). Oxygen Isotopes in nature and in the laboratory. *Science*, 108, 489-496.

Varkey MJ, Murty VSN, Suryanarayana A (1996). Physical oceanography of the Bay of Bengal and Andaman Sea. In: Ansell AD, Gibson RN, Barnes M (Eds.), Oceanography and Marine Biology: an Annual Review, 34. UCL Press, pp. 1–70.

Vincent E (1976). Planktonic foraminifera, sediments and oceanography of the Late Quaternary SW Indian Ocean. Allan Hancock Monogra. *Marine Biology*, 9, 1-235.

Vincent E, Berger WH (1981). Planktonic foraminifera and their use in paleoceanography. In: Emiliani C (Eds.) *The Sea*, Wiley-Interscience, New York, pp. 1025-1119.

Visser K, Thunell R, Stott L (2003). Magnitude and timing of temperature change in the Indo-Pacific Warm Pool during deglaciation. *Nature*, 421, 152-154.

Wang B, Clemens S, Liu P (2003). Contrasting the Indian and East Asian monsoons implications on geologic time scale. *Marine Geology*, 201, 5–21.

Wang X, Auler AS, Edwards L, Cheng H, Cristalli PS, Smart PL, Richards DA, Shen C-C (2004). Wet periods in northeastern Brazil over the past 210 ka linked to distant climate anomalies. *Nature*, 432, 740–743.

Wang YJ, Cheng H, Edwards RL, An ZS, Wu JY, Shen C-C, Dorale JA (2001). A high-resolution absolute-dated late Pleistocene monsoon record from Hulu Cave, China. *Science*, 294, 2345-2348.

Wang YJ, Cheng H, Lawrence Edwards R, He Y, Kong X, An Z, Wu J, Kelly MJ, Dykoski CA, Li X (2005). The Holocene Asian Monsoon Links to solar changes and north Atlantic climate. *Science*, 308, 854-857.

Wang Z, Hu R, Mysak LA, Blanchet J-P, Feng J (2004), A parameterization of solar energy disposition in the climate system. *Atmosphere-Ocean*, 42 (2), 113–125.

Warren BA (1966). Medieval Arab references to the seasonally reversing currents of the north Indian Ocean. *Deep-Sea Research*, 13, 167-171.

Wasserman PD (1989). Neural Computing Theory and Practice, (Eds.) Hoboken NJ, pp. 230, Von Nostrand Reinhold.

Weaver CE (1989). Clays, muds and shales. Developments in sedimentology. Elsevier Amsdam, pp 819.

Webb A (2002). Statistical Pattern Recognition, 2nd (Eds.) Hoboken NJ, pp. 496, John Wiley.

Webster PJ (1987)."The Elementary Monsoon". Monsoons, J. Wiley Co., (Eds., Fein and Stephens), 3-32.

Wefer G, Berger WH, Bijma J, Fisher G (1999). Clues to Ocean History: a brief overview of proxies. In: Fischer G, Wefer G (eds.). Use of proxies in Paleoceanography: Examples from the South Atlantic. *Springer-Verlag Berlin Heidelberg*, 1-68.

Weimer P (1990). Sequence stratigraphy facies geometrics, and depositional history of the Mississippi fan, Gulf of Mexico. *AAPG Bulletin*, 74, 425-453.

Weller RA, Fischer AS, Rudnick DL, Eriksen CC, Dickey TD, Marra J, Fox C, Ben LR (2002). Moored observations of upper-ocean response to the monsoons in the Arabian Sea during 1994-1995. *Deep-Sea Res. II*, 49, 2195-2230.

Wells JT, Coleman JM (1982). Deltaic morphology and sedimentology, with special reference to the Indus River Delta, Marine Geology and Oceanography of Arabian Sea and Coastal Pakistan (Eds.). Haq BU, Milliman JD, Scientific and Academic Editions, New York, 85-100.

Weninger B, Jöris O, Danzeglocke U (2006). Calpal-Cologne Radiocarbon Calibration and Palaeoclimate Research Package, Universität zu Köln, Institut für Ur-und Frühgeschichte Radiocarbon Laboratory.

Windom HL (1975). Eolian contributors to marine sediments. *J. Sedimentology Petrology.*, 45, 520-529.

Wyrtki K (1973). Physical oceanography of the Indian Ocean. Vol. 3 of Ecological studies: analysis and synthesis. In B. Zeischel, & S. A. Gerlach (Eds.), Biology of the Indian Ocean (pp. 18-36). London: Chapman and Hall Ltd.

Zahn R, Pederson TF (1991). Late Pleistocene evolution of surface and mid-depth hydrography at the Oman Margin: Planktonic and benthic isotope records at site 724. *Proc. Ocean Drill. Program Sci. Results*, 117, 291-308.

Zhang J (1985). Living planktonic foraminifera from the eastern Arabian Sea. *Deep-Sea Research*, 32, 789-798.

Govil P, Naidu PD, Radhika TK (2004)
Major turbidity flows in the western Indus Fan between 290 and 360 kyr.
***Current Science*, 87, 1597-1600.**

Major turbidity flows in the Western Indus Fan between 290 and 360 kyr

Pawan Govil, P. Divakar Naidu* and T. K. Radhika

National Institute of Oceanography, Dona Paula, Goa 403 004, India

Calcium carbonate ($CaCO_3$), aluminium (Al), titanium (Ti), and terrigenous matter analyses were carried on the Ocean Drilling Programme Site 720A from the Indus Fan in the Arabian Sea. $CaCO_3$, Al, Ti and terrigenous matter values range from 4.5 to 74.4%, 1.4 to 7.8%, 0.03 to 0.4% and 5.5 to 66.7%, respectively. High $CaCO_3$ (40–60%) in association with low values of Al, Ti and terrigenous matter from 0 to 290 kyr (0 to 18 mbsf) and low $CaCO_3$ (< 10%) with high values of Al, Ti and terrigenous matter suggest that $CaCO_3$ fluctuations at this site were controlled by terrigenous dilution. Low Al, Ti and terrigenous matter percentages from 0 to 290 kyr and strikingly high values from 290 to 360 kyr reveal that the supply of terrigenous matter to the Indus Fan was significantly higher during 290 to 360 kyr (18 to 28 mbsf depth) due to massive turbidity flows triggered by slumping.

INDUS is one of the largest rivers in terms of drainage area, river discharge and sediment load. It drains an area of c.1 × 10^6 km^2 from the western Himalayas with sediment discharge of about 400 × 10^6 metric tons of sediment per year[1]. The sediment transported by the river is deposited in the Arabian Sea as the Indus Fan, one of the largest deep-sea fans in the world, totalling c.5 × 10^6 km^2. Terrigenous input from the Indus river dominates sediments in the northern Arabian Sea. Sediments are characterized by coarse size, low calcium carbonate content and an abundance of quartz and feldspar[2]. The Persian Gulf and Red Sea are not considered to be important sources of sediment to the Indus shelf, but significant contributions may be derived from the dust-bearing winds blowing-off Africa in summer and northern India in winter[3].

Sediment discharged by the Indus river into the northern Arabian Sea may be transported farther offshore, accumulate on the continental shelf offshore of the delta, or may be transported by long shore currents to the southeast. Much of the coarse sediment is carried directly offshore to the Indus Fan by way of the Indus submarine canyon[4]. The Fan sedimentary sequences have been deposited since about late Oligocene or early Miocene as a consequence of Himalayan uplift and sea-level lowerings[5].

The peak discharge of Indus river occurs during summer months as a result of seasonal glacial melting and increased run-off generated by the summer monsoon. The rate of sediment discharge to the Fan has varied through time, depending upon the climatic and monsoon condition in the Asian

*For correspondence. (e-mail: divakar@darya.nio.org)

subcontinent. Therefore, the present communication is aimed to addresses changes in terrigenous material supply to the Indus Fan during the Late Quaternary Period.

Ocean Drilling Programme (ODP) site 720A is located on the western part of the middle Indus Fan at a water depth of 4045 m (Figure 1). Calcium carbonate ($CaCO_3$) was estimated by using gasometric technique. For the analyses of aluminium (Al) and titanium (Ti), finely powdered, overnight oven-dried (at 105 ± 5°C) sample of 0.3 g was transferred to PTFE beakers and added 20 ml HF, 5 ml HNO_3, 2 ml $HClO_4$ and evaporated on a hotplate. The incipiently dried digest was dissolved and brought to volume (50 ml) with 10 ml of HCl in 1 : 1 ratio. Repeating the digestion steps until the clear solutions were obtained ensured complete digestion. The 50 ml solutions of the samples and (MAG-1) standard are analysed for major and minor elements on a Perkin Elmer® Plasma-400 sequential ICP-AES. The analyses were accurate and precise to within 5%.

Terrigenous matter (wt%) was estimated using Ti-based normative calculation[6] and assuming that the terrigenous matter of the sediment is almost similar to average Post-Archean Australian Shale : Terrigenous matter (wt%) = $(Ti_{samp}/Ti_{paas}) \times 100$.

The chronology of the core is based on biostratigraphy. The ages were assigned based on the first appearance of *Emiliania huxleyi* and the last occurrence of *Pseudoemiliania lacunose* (Table 1). The chronology adopted in this study may differ to some extent compared to the chronology based on isotopes. Therefore, to avoid chronological ambiguity we also have referred major events in terms of core depth in metres below sea floor (mbsf).

The calcium carbonate content varied from 4.5 to 74.4%. Higher $CaCO_3$ values (>30%) were noticed from 0 to 290 kyr, strikingly minimum $CaCO_3$ values (< 10%) were recorded from 290 to 360 kyr (Figure 2). The accumulation of calcium carbonate on the sea floor is mainly controlled by the surface-water biological production, rate of dissolution during its journey through the water column as well as on the sea floor and dilution by the non-carbonate fraction and terrigenous matter[7].

The ODP Site 720A was drilled at a water depth of 4045 m which is above the calcium carbonate compensation depth; therefore dissolution of calcium carbonate factor can be ruled out. Further the foraminifera fragments data also confirm that calcium carbonate dissolution was insignificant. No evidences exist regarding the fourfold change in productivity in the Arabian Sea over the last 400 kyr[8]. Productivity and dissolution seem to have not played a major role in shaping the carbonate fluctuations at this site. Therefore, we suggest that calcium carbonate changes were controlled by terrigenous dilution.

Al and Ti content in the marine sediment mainly derives from continental origin supplied through eolian and fluvial pathways. Therefore, Al and Ti have been commonly used as geochemical indicators to discover the content of aluminosilicate detritus of continental origin[9]. At this site, Al and Ti content vary from 1.4 to 7.8% and 0.03 to 0.4% respectively (Figure 3). Both Al and Ti show low values from 0 to 290 kyr and high values from 290 to 360 kyr. Low Al and Ti values from 0 to 290 kyr coincide with high calcium carbonate, and high Al and Ti values corresponding with low calcium carbonate suggest that terrigenous material supply from the Indus river was strikingly higher from 360 to 290 kyr. Lowest calcium carbonate content and highest Al, Ti and terrigenous matter values between 360 and 290 kyr (18 to 28 mbsf depth) regime suggest massive turbidity flows to the Indus Fan (Figures 2 and 3).

Table 1. Chronological list of faunal events used in the study for ODP Site 720A

Event	Depth (mbsf)	Age (kyr)
Emiliani huxleyi	4.0	190
Pseudoemiliani lacunosa	46.5	490

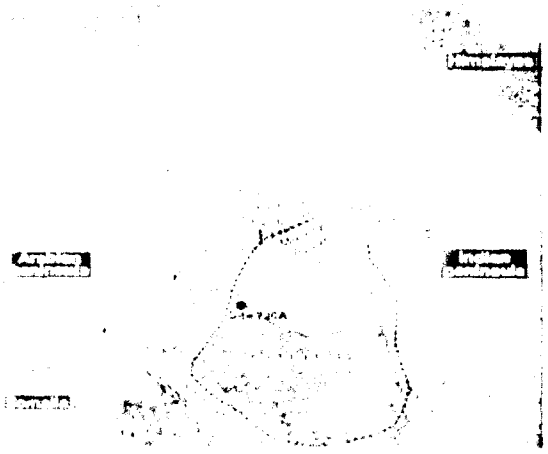

Figure 1. Bathymetry and physiography of Indus Fan and location of ODP Site 720A (modified from Prins *et al.*[10]).

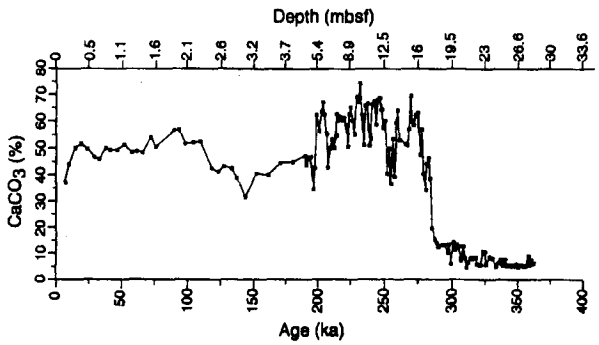

Figure 2. Fluctuations of calcium carbonate (wt%) at ODP Site 720A.

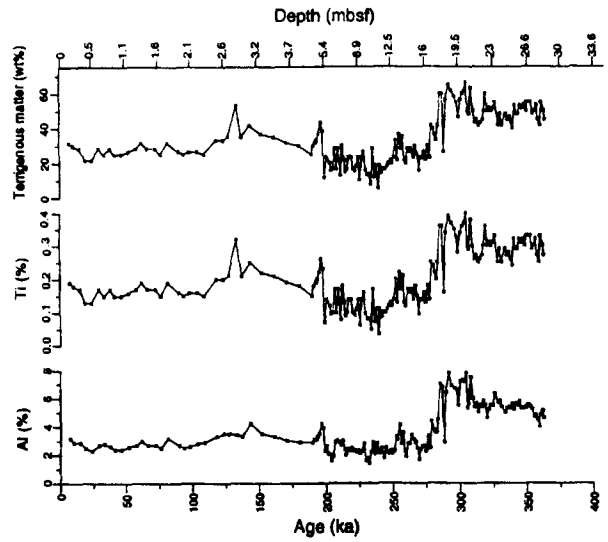

Figure 3. Fluctuations of aluminium, titanium and terrigenous matter at ODP Site 720A.

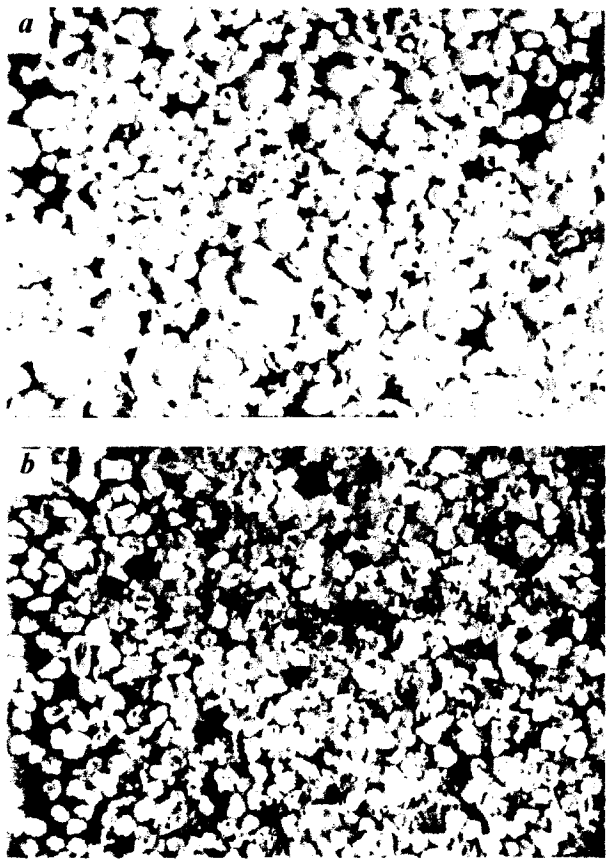

Figure 4. Photograph depicting (*a*) carbonate-rich coarse fraction from 0 to 290 kyr intervals (0–18 mbsf depth) and (*b*) terrigenous detritus material-rich fraction from 290 to 360 kyr (18–28 mbsf depth).

Examination of coarse fraction shows that above 18 mbsf corresponding to 290 kyr interval samples mostly contain foraminifer ooze and terrigenous material (Figure 4 *a*); however below 18 mbsf interval, samples show only turbidity silts and sands (Figure 4 *b*). This observation also supports massive turbidity flows below 290 kyr.

Our data do not show any major turbidity flows from 290 kyr to the Holocene. However, we do admit that the present study cannot rule out minor turbidite sedimentation of a few centimetres thickness within the main feeder channel and Indus Canyon. This kind of turbidite sedimentation was noticed on the eastern part of the Indus Fan during the Last Glacial Maximum when the sea level was low[10]. A sharp decrease in turbidity frequency during the late Holocene is observed on the upper continental slope, the deep slope basin and the abyssal plain[10]. Along the Makaran Margin, the change in turbidity frequency appears to have taken place synchronously irrespective of physiographic settings.

Sediment transport by turbidity currents is the dominant process on deep-sea fan systems whereby terrigenous sediment is transported from the continents and continental margins to the deep sea. The rate of terrigenous sediment input to the deep sea is controlled by mechanisms including sea level and climate changes, and tectonic activity[11]. Apart from these processes, autocyclic mechanisms include slumping resulting in channel plugging and sediment build-up within channels, and as a consequence of these sedimentary processes, neither a major sea-level drop[12] nor a strong tectonic activity occurred around 290 kyr[11]. Therefore, we attribute that the major turbidity flow consisting of silts and sands reached the core location due to slumping of thick sediment built-up within the channel leeves without any trigger by allocyclic mechanisms.

Studies on the ODP Site 720A reveal that the down core variations of calcium carbonate were controlled by dilution of terrigenous matter. The terrigenous material supply to the Indus Fan through the Indus river varied over the years. Low terrigenous material supply from 290 kyr through Holocene and higher terrigenous material supply from 290 to 360 kyr is noticed. Highest terrigenous supply to the Indus Fan between 290 and 360 kyr would suggest massive turbidity flows to the Indus Fan system. This kind of major turbidity flow was not noticed from 290 kyr onwards. The autocyclic mechanism would have caused such kind of thick turbidity deposition of about 10 m in the Indus Fan during Late Quaternary Period.

1. Wells, J. T. and Coleman, J. M., Deltaic morphology and sedimentology, with special reference to the Indus River Delta. *Marine Geology and Oceanography of Arabian Sea and Coastal Pakistan* (eds Haq, B. U. and Milliman, J. D., Scientific and Academic Editions, New York, 1982, pp. 85–100.
2. Naini, B. R. and Kolla, V., Acoustic character and thickness of sediments of the Indus Fan and the continental margin of western India. *Mar. Geol.*, 1982, **47**, 181–195.
3. Sirocko, F. and Sarnthein, M., Wind-borne deposits in the Northwestern Indian Ocean: record of Holocene sediments versus modern satellite data. *Paleoclimatology and Paleometeorology: Modern*

and Past Patterns of Global Atmospheric Transport (eds Leinen, M. and Sarnthein, M.), NATO, ASI Ser. C. 282. Kluwer, Dordrecht, 1989, pp. 401–433.
4. Islam, S. R., The Indus submarine canyon. *Pak. Geogr. Rev.*, 1959, **XIV**, 32–34.
5. Koumes, F. and Kolla, V., Indus Fan: Seismic structure, channel migration and sediment-thickness in the Upper Fan. *Marine Geology and Oceanography of Arabian Sea and Coastal Pakistan* (eds Haq, B. U. and Milliman, J. D.), Scientific and Academic Editions, New York, 1982, pp. 101–110.
6. Murray, R. W. and Leinen, M., Scavenged excess aluminium and its relationship to bulk titanium in biogenic sediment from the central equatorial Pacific Ocean. *Geochim. Cosmochim. Acta*, 1996, **60**, 3869–3878.
7. Damuth, J. E., Quaternary climate change as related by calcium carbonate fluctuations in western equatorial Atlantic sediments. *Deep-Sea Res.*, 1975, **22**, 725–743.
8. Prell, W. L., Murray, D. W., Clemens, S. C. and Anderson, D. M., Evolution and variability of the Indian Summer Monsoon: Evidence from western Arabian Sea Drilling Program. *Geophys. Monogr.*, 1992, **70**, 447–469.
9. Pattan, J. N., Masuzawa, T., Naidu, P. D., Parthiban, G. and Yamamoto, M., Productivity fluctuations in the southeastern Arabian Sea during the last 140 ka. *Paleogeogr. Paleoclimatol. Paleoecol.*, 2003, **193**, 575–590.
10. Prins, M. A., Postma, G., Cleveringa, J., Cramp, A. and Kenyon, N. H., Controls on terrigenous sediment supply to the Arabian Sea during late Quaternary: the Indus Fan. *Mar. Geol.*, 2000, **169**, 327–349.
11. Clift, P. D., Carter, A., Krol, M. and Kirby, E., Constraints on India–Eurasia collision in the Arabian Sea region taken from the Indus Group, Ladakh Himalaya, India. *Geological Soc,, London, Spec. Publ.*, 2002, **195**, 97–116.
12. Glennie, K. W., Singhvi, A. K., Lancaster, N. and Teller, J. T., The tectonic and climatic evolution of the Arabian Sea region. *Geol. Soc., London, Spec. Publ.*, 2002, **195**, 301–316.

ACKNOWLEDGEMENTS. The samples were provided by Ocean Drilling Program, which is sponsored by the U.S. National Science Foundation and participating countries under management of Joint Oceanographic Institutions. This is National Institute of Oceanography Contribution No. 3921.

Received 4 May 2004; revised accepted 26 July 2004

Govil P, Naidu PD (2008)

Late Quaternary changes in depositional processes along the western margin of the Indus Fan.

***Geo-Marine Letter*, 28, 1-6.**

Geo-Mar Lett (2008) 28:1–6
DOI 10.1007/s00367-007-0083-1

ORIGINAL

Late Quaternary changes in depositional processes along the western margin of the Indus Fan

P. Govil · P. D. Naidu

Received: 6 September 2006 / Accepted: 23 April 2007 / Published online: 12 June 2007

Abstract Detailed sedimentological, geochemical and isotopic analyses were carried out on sediment samples from ODP Site 720A on the Indus Fan, Arabian Sea. High values of calcium carbonate associated with low values of Al and Ti from 0 to 375 ka, and low values of calcium carbonate along with high values of Al and Ti from 375 to 525 ka represent two distinct sedimentary sequences. The sediments deposited from 525 to 375 ka correspond to a turbidite sequence, characterized by a high terrigenous input of coarse-grained sediments composed mostly of sand and silt. The sediments deposited from 375 ka to the present day comprise a pelagic sequence, consisting of pelagic material and clay. The major turbidity flow between 375 and 525 ka resulted in the greatest development of the Indus Fan during the late Quaternary. Most of the active channels were buried by 375 ka, followed by deposition of mainly pelagic sequences since then. Enrichment of an Indus-derived Himalayan clay mineral assemblage (illite and chlorite) in both the turbiditic and pelagic sequences reveals that the source and supply of clay minerals to the Indus Fan were the same during pre- and post-turbidite deposition. At ODP Site 720A, Al, Ti and terrigenous material do not show any systematic changes with respect to glacial and interglacial periods, suggesting that sea-level changes are not directly responsible for the terrigenous material supply to this site. Rather, a major switch in distributary channels away from the western margin of the Indus Fan is suggested.

P. Govil · P. D. Naidu (✉)
National Institute of Oceanography,
Dona Paula 403004 Goa, India
e-mail: divakar@nio.org

Present address:
P. Govil
National Centre for Antarctic and Ocean Research,
Vasco da Gama 403804, Goa, India

Introduction

The initiation of Indus Fan deposition is thought to have begun in Oligocene to early Miocene times, when the Indian and Arabian plates collided. The Indus Fan, which is 1,500 km long and has a maximum width of 960 km, is the most extensive physiographic feature in the Arabian Sea. The fan is bounded by the Indian continental margin/Chagos–Laccadive Ridge in the east, the Owen–Murray Ridge in the west, and the Mid-Indian Ridge (Carlsberg Ridge) in the south (Fig. 1).

The primary source of sediments to the Indus Fan is derived from the Indus River, which drains the arid to semi-arid western Himalaya Mountains, with headwaters at elevations greater than 4,000 m and a catchment area of ca. 1×10^6 km^2. Peak discharge occurs during the summer months as a result of seasonal glacier melting and the increased runoff generated by the summer monsoon rainfall (Milliman et al. 1984). Sediment discharge of the Indus River varied in the range 435–675 million t before 1950 (Holeman 1968). After construction of dams at several places, sediment discharge was reduced to 50 million t (Milliman et al. 1984). Sediments supplied by the Indus River to the northern Arabian Sea may be distributed on the inner shelf as well as in the offshore. However, much of the coarse sediment is carried directly offshore to the Indus Fan through the Indus Submarine Canyon (Islam 1959).

The lithostratigraphy of Ocean Drilling Program (ODP) Site 720A shows two units: unit I, from 0 to 18 mbsf (metres below seafloor), is composed of pelagic nanofossil ooze, with a non-carbonate component consisting primarily of quartz and clay minerals. Unit II, from 18 mbsf to the bottom of the hole, is dominated by turbidite facies, comprising interbedded silty clays, silty sands, and sands which commonly occur in fining-upward sequences on scales of <2 to >50 cm (Prell and Niitsuma 1989).

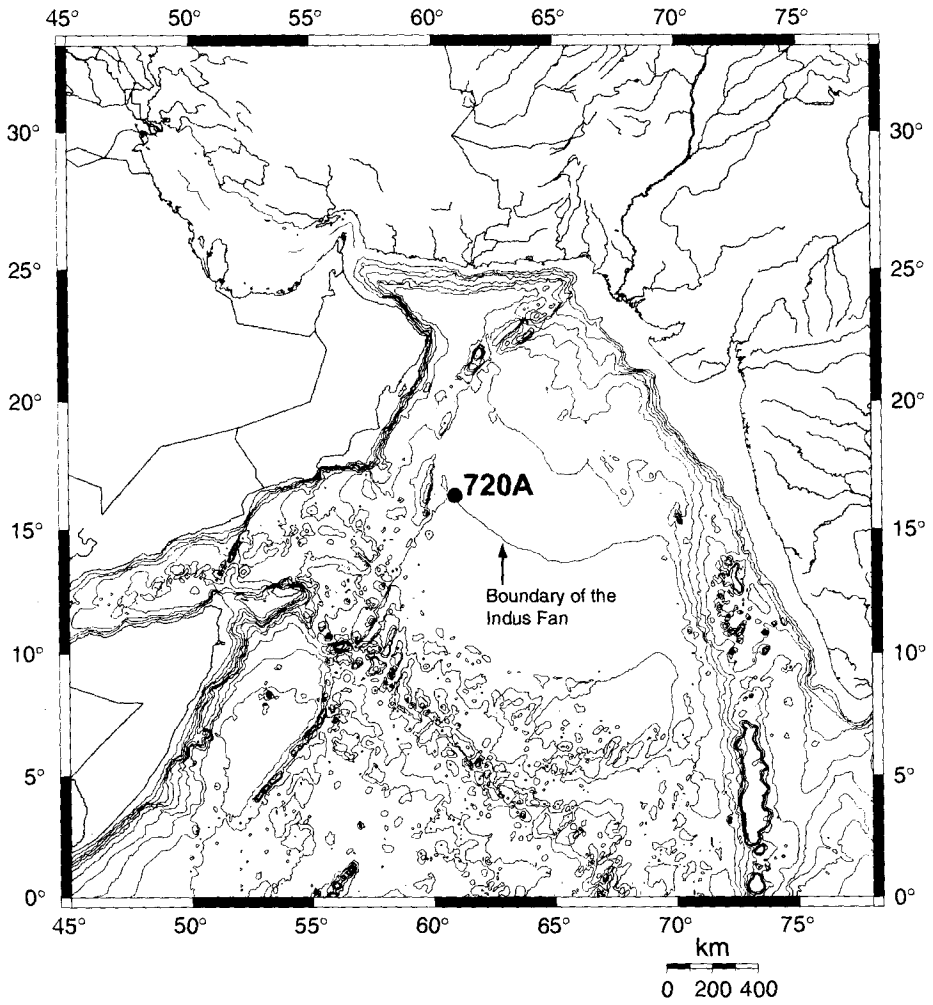

Fig. 1 Bathymetry and physiography of the Indus Fan and location of ODP Site 720A

Earlier work identified a major turbidite sequence of the late Quaternary between 18 to 28 mbsf (Govil et al. 2004). In the present study, detailed analyses of oxygen isotopes of planktic Foraminifera, grain size and clay mineralogy were carried out to investigate the depositional history of the Indus Fan over the last 525 ka. The aim was to identify sediment sources and potential factors controlling sediment supply to the Indus Fan.

Materials and methods

ODP Site 720A is located on the westernmost part of the middle Indus Fan at a water depth of 4,050 m (Fig. 1). Clay mineral composition was determined on the <2-μm fraction of the sediment, which was separated on the basis of Stokes' Law of settling. The separated clay aliquots were treated with 5 ml acetic acid and 10 ml hydrogen peroxide to remove carbonate and organic matter respectively. The aliquots were then washed several times with de-ionized water to remove excess reagents and decanted. Oriented slides were prepared by pipetting 1 ml of the concentrated clay suspensions onto glass slides, following the procedures of Rao and Rao (1995). The slides were allowed to dry in air.

X-ray diffraction measurements were then carried out on these slides from 3 to 35° 2θ at 0.05° 2θ/s, by means of a Philips X-ray diffractometer (1840 model) using nickel-filtered Cu Kα radiation. The instrument was calibrated by running internal silica standards. The slides were subsequently exposed to ethylene glycol vapour at 100 °C for 1 h and rescanned under the same instrumental settings. In order to differentiate the kaolinite and chlorite peaks, the slides were also scanned from 24 to 26° 2θ at 0.01° 2θ/s. Following Biscaye (1965), the peak areas of 14 Å of smectite were multiplied by 1, 10 Å of illite by 4, and 7 Å of kaolinite and chlorite by 2.

Grain-size measurements were carried out on the carbonate- and organic-free sediments, with a Malvern laser particle size analyser (Master-Sizer 2000). Size classification is according to the Wentworth scale (Folk 1968).

Calcium carbonate contents were estimated by using the gasometric technique. Aluminium (Al) and titanium (Ti) were analysed by means of ICP-AES, according to the analytical procedure described in Govil et al. (2004).

Oxygen isotope analyses were performed on tests of *Globigerinoides ruber* (250–355 μm size fraction). For this purpose, 10–15 specimens from each selected sample (cf. below) were crushed and the material ultrasonically cleaned in ethanol. Cleaned foraminifer samples were transferred into V-vials and loaded into a Gilson Auto Sampler for acidification online. The CO_2 evolved in the reaction was transferred cryogenically to the inlet of a gas ratio stable isotope mass spectrometer using routine procedures, and the sample gas was compared to an internal standard gas sequentially 10 times. The isotopic composition of the evolved CO_2 gas is recorded as ‰ deviation from Peedee Belemnite (PDB). The analytical precision, estimated from repeated analyses of unroasted NBS-19 carbonate reacted under conditions identical to that of the foraminiferal samples, was 0.07‰.

Oxygen isotope analyses were carried out up to 18 mbsf, the reconstructed chronology being based on the isotope stage boundaries up to 11 described in Bassinot et al. (1994). Oxygen isotopic analyses were not carried out below 18 mbsf, due to insufficient number of Foraminifera specimens. Therefore, by using the linear sedimentation rate within isotope stage 11, we extrapolated the ages further down in the core. A discrepancy was observed when comparing the oxygen isotope chronology with an earlier chronology based on nanofossil dating (Govil et al. 2004). Since the chronology based on oxygen isotope boundaries is better constrained than that derived from biostratigraphy, we relied on the former in the present study (Fig. 2).

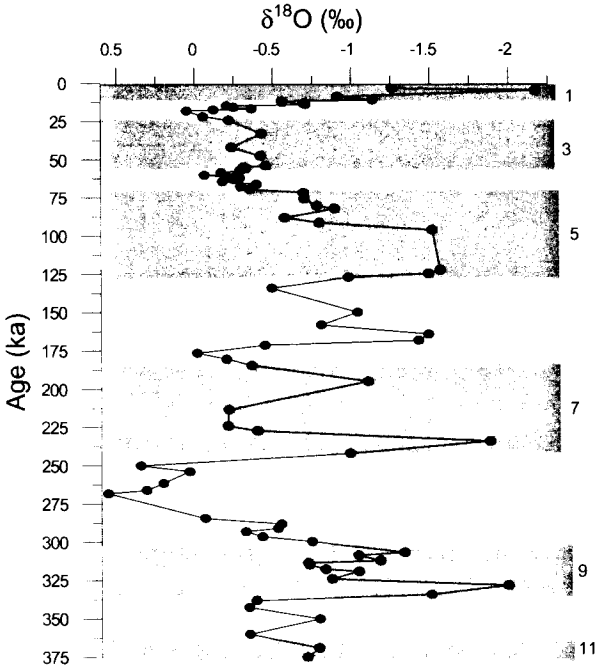

Fig. 2 Chronology of ODP Site 720A based on $\delta^{18}O$ stratigraphy. Interglacial isotope stages are highlighted by *dark shades* and are *labelled*

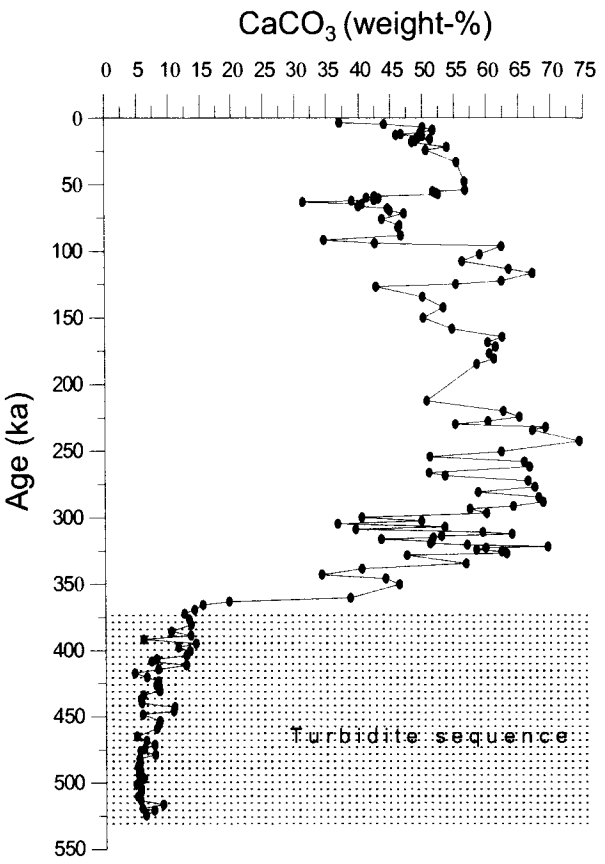

Fig. 3 Calcium carbonate fluctuations at ODP Site 720A during the late Quaternary. Note the strong reduction in calcium carbonate from 375 ka onwards

Results

The calcium carbonate ($CaCO_3$) content varied from 4.5 to 74.4%. Higher $CaCO_3$ values (>30%) occur from 0 to 375 ka whereas strikingly low $CaCO_3$ values (<10%) mark the period from 375 to 525 ka (Fig. 3). $CaCO_3$ fluctuations at the study site are presumably controlled by terrigenous "dilution." Thus, high terrigenous material supply (mostly sand and silt) between 375 and 525 ka has reduced the overall $CaCO_3$ content (cf. below).

The aluminium (Al), titanium (Ti), and terrigenous matter contents vary from 1.4 to 7.8%, 0.03 to 0.4%, and 5.5 to 66.67% respectively (Fig. 4). Low Al, Ti and terrigenous matter contents between 0 and 375 ka (Fig. 4) coincide with high $CaCO_3$ contents (Fig. 3) whereas high Al, Ti and terrigenous matter contents (Fig. 4) correspond to low $CaCO_3$ contents between 375 and 525 ka (Fig. 3), suggesting that terrigenous material supply from the Indus Fan was considerably higher from 375 to 525 ka. The higher terrigenous material supply to the Indus Fan during the period 375–525 ka would result from an increased turbidity flow.

From 375 ka onwards, a predominantly pelagic sequence was deposited. Evidently, two distinct types of sedimentary sequences characterize the western part of the Indus Fan over the last 525 ka. From 525 to 375 ka, a turbidite sequence occurs, which is dominated by sand and coarser silt. By contrast, the younger pelagic sequence consists of finer silt and clay (Fig. 5). The mean grain size of the sediment also documents large variations between the turbidite and pelagic sequences at the study site. The turbidite sequence shows mean grain sizes varying strongly from 86 to 107 μm whereas the mean grain sizes of the pelagic sequence are more uniform at <13.3 μm (Fig. 6).

Four clay minerals were recorded at the site. Of these, illite (60–77%) is the dominant, followed by kaolinite (10–25%), chlorite (3–16%) and smectite (traces to 7%; Fig. 7). The distribution patterns of clay minerals in the pelagic and the turbidity sequences are very similar (Fig. 7).

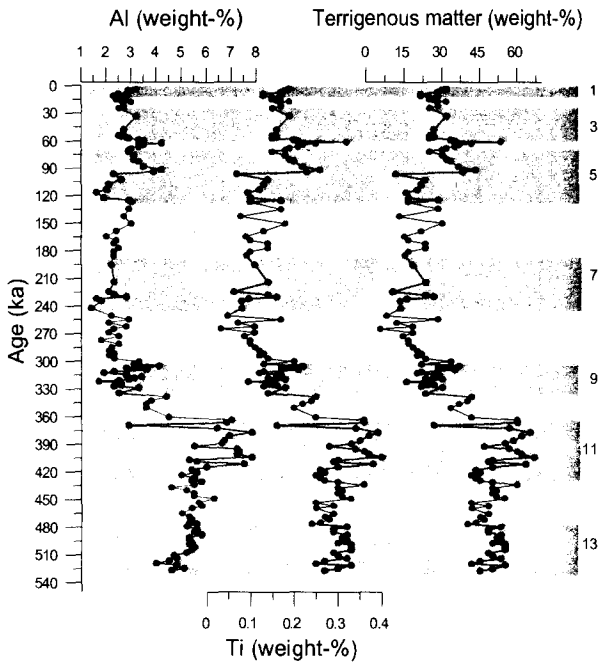

Fig. 4 Variations in Al, Ti and terrigenous matter at ODP Site 720A. Higher contents of Al, Ti and terrigenous matter occur from 375 to 525 ka. Interglacial isotope stages are highlighted by *dark shades* and are *labelled*

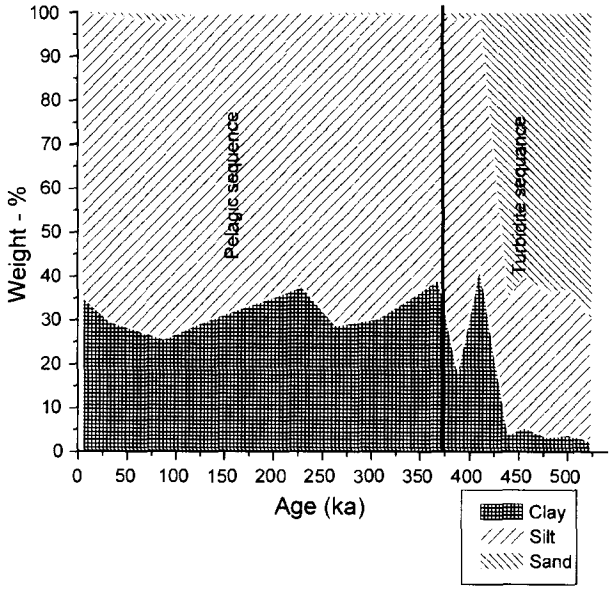

Fig. 5 Downcore fluctuations in sand, silt and clay at ODP Site 720A. The turbidity sequence is generally dominated by sand and coarser silt, the pelagic sequence by clay and finer silt

Discussion

Turbidity currents are the major mechanism by which sediment is supplied to deep-sea fan systems. The intensity and frequency of the terrigenous material supply varies in response to sea-level changes. In the Arabian Sea, sea-level fall activates submarine fans due to an increase in sediment transport from the rivers across the shelf towards the deeper parts of the basin (Prins and Postma 2000), via submarine canyons cut into the continental margin. Terrigenous sediment can thus easily be transported to the deep-sea fans via these channels. By contrast, during sea-level rise towards high stands, sediment is increasingly trapped on the shelf platform, rather than being transported to the deep-sea basin (Stow 1985; Mutti and Normark 1987). For example, turbidite sedimentation on the Amazon Fan, Mississippi Fan, and the Indus Fan is influenced by such changes in sea level (Manely and Flood 1988; Bouma et al. 1989; Weimer 1990; Feely et al. 1990; Prins et al. 2000).

The deposition of the pelagic sequence on the Indus Fan clearly reflects a decrease in clastic influx to the site, rather than an increase in the pelagic sedimentation rate. This decrease in clastic influx may have been caused by local mechanisms. For example, a sea-level high stand would have reduced the clastic flux to the Indus Fan. This pattern is observed in the Holocene sediments of the Indus Fan, which consist of foraminiferal marls and oozes (Kolla and

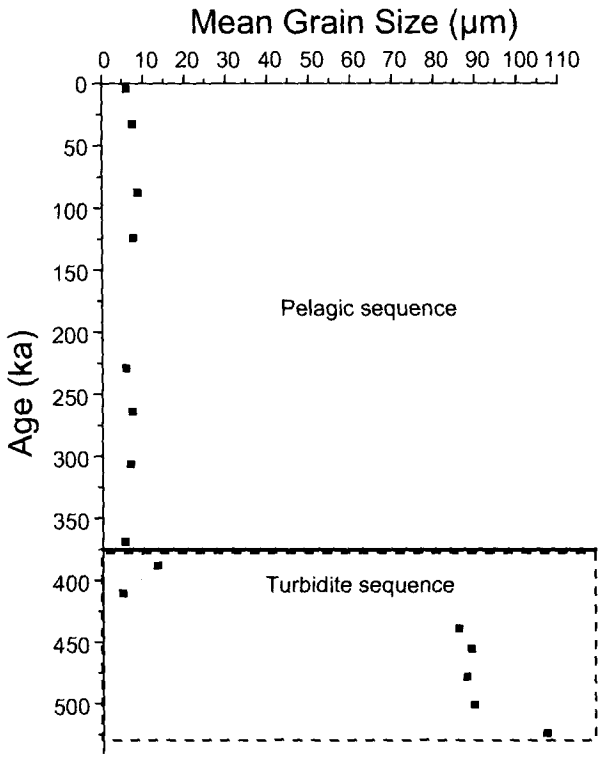

Fig. 6 Variations in mean grain size (μm) at ODP Site 720A

Coumes 1987). Analogously, higher terrigenous input to the Arabian Sea during glacials were attributed to low sea-levels stands (Gupta et al. 2005). However, such a sea-level rise and fall does not explain the reduction of terrigenous material in the Indus Fan from 375 ka onwards, because

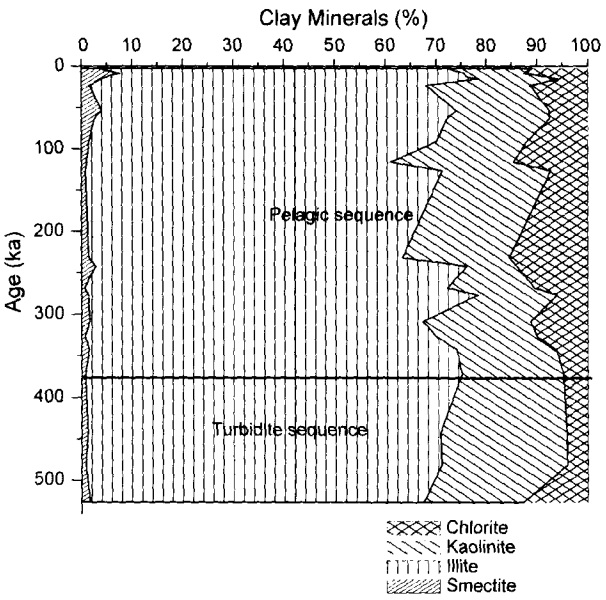

Fig. 7 Variations in clay mineral content at ODP Site 720A. The distribution patterns of clay minerals in the turbidite and pelagic sequences are very similar

terrigenous proxies such as Al and Ti do not show any systematic variation corresponding to glacial and interglacial periods at this site. We therefore invoke another local mechanism which would facilitate the deposition of the pelagic sequence from 375 ka onwards.

The abandonment of active channels or burial of previously active channels by 375 ka may have been responsible for the deposition of predominantly pelagic sediments on the elevated levees. This mechanism would be local in extent and would enable pelagic sediments to accumulate over several sea-level cycles. We thus suggest that channel switching and abandonment of active channels resulted in the deposition of the pelagic sequence from 375 ka onwards. As a consequence, the terrigenous material supply to the study area was reduced from 375 ka to the present day, the general decrease in turbidite deposition being a result of channel switching away from the site, rather than an actual decrease in turbidite activity. In fact, a major eastward shift of active channel deposition during the late Pleistocene was noted for the Indus Fan by Kolla and Coumes (1987). In general, turbidite deposition rates are twice as high on the Indus Fan than on the distal Ganges Fan. These high accumulation rates are consistent with accelerated uplift and erosion in the Indus source area (Prell and Niitsuma 1989).

Clay mineral contents have been used to characterize the sediment provinces of the world oceans (Biscaye 1965; Windom 1975). The clay minerals in sediments of the Arabian Sea are derived from various sources, e.g. river run-off from India, dust contributed from Africa, Arabia, Pakistan and northern India, as well as from basalts on the mid-ocean ridges (Kolla et al. 1981; Naidu et al. 1985). To date, however, most have not been related to any specific source areas and transport pathways. High percentages of illite and chlorite are usually associated with cold climates, and are physical and mechanical weathering products (Kolla et al. 1976). The formation of kaolinite, by contrast, is favoured by warm and humid climates, being strongly controlled by the intensity of continental hydrolysis (Griffin et al. 1968). Chlorite is a high-latitude clay mineral produced by weathering under arid, cold climatic conditions (Weaver 1989).

Throughout the Arabian Sea, kaolinite contents show little variation and, therefore, this mineral could originate more or less uniformly from all the major sediment source areas in the region (Sirocko and Lange 1991). Kaolinite can hence not serve as a palaeoclimatic tracer mineral in the Arabian Sea.

Illite and chlorite, on the other hand, are dominant clay minerals at the ODP 720A study site and hence characterize the Indus sedimentary province (Konta 1985; Rao and Rao 1995). In the present study, the finding that the distribution patterns of clay minerals in the pelagic and the turbidity

sequences are very similar suggests that the main source of clay minerals on the Indus Fan is of Himalayan origin, the material being supplied by the Indus River. In addition to the Indus Fan, very subordinate amounts of clay minerals may also have been derived from an aeolian source located on the Arabian Peninsula.

Conclusions

At ODP Site 720A, calcium carbonate and elemental contents (Al and Ti) as well as grain-size analysis data reveal a turbidite sequence from 525 to 375 ka which is overlain by a pelagic sequence from 375 ka to the present day. We infer that most channels were buried by 375 ka, which caused the distributary channels to switch away from the site. This, in turn, resulted in a general decrease in turbidite deposition at the study site, rather than indicating a decrease in terrigenous supply to the Indus Fan as a whole. The high abundance of Indus-derived clay minerals originating from the Himalayas (illite and chlorite) in both the turbidite as well as the pelagic sequence suggests that the source and supply of clay minerals to the Indus Fan remained constant over the last 525 ka.

Fluctuations in calcium carbonate content at the study site can be explained by terrigenous material "dilution". In the pelagic sequence, calcium carbonate is diluted largely by clay whereas, in the turbidite sequence, "dilution" is by sand and silt. Al, Ti and terrigenous material do not show any consistent responses to glacial and interglacial climatic conditions at this site. At ODP Site 720A on the western margin of the Indus Fan, terrigenous material supply is therefore not linearly related to sea-level changes.

Acknowledgements We thank Mr. B. R. Rao for his help in clay mineral analyses. Comments by two anonymous reviewers and Prof. Burg Flemming, Editor-in Chief, have helped to improve the paper. The samples were provided by the Ocean Drilling Program, which is sponsored by the U.S. National Science Foundation and participating countries under the management of the Joint Oceanographic Institutions. This is National Institute of Oceanography Contribution 4250.

References

Bassinot FC, Labeyrie LD, Vincent E, Shackleton NJ, Lancelot Y (1994) The astronomical theory of climate and age of the Brunhes–Matuyama magnetic reversal. Earth Planet Sci Lett 126:91–108

Biscaye PE (1965) Mineralogy and sedimentation of recent deep sea clay in the Atlantic Ocean and adjacent seas and oceans. Geol Soc Amer Bull 76:803–832

Bouma AH, Colemen JH, Stelting CE, Kohl B (1989) Influence of relative sea level changes on the construction of the Mississippi fan. Geo Mar Lett 9:161–170

Feely MH, Moore TC Jr, Loutit ST, Bryant WR (1990) Sequence stratigraphy of the Mississippi fan related to oxygen isotope sea level index. AAPG Bull 74:407–474

Folk RL (1968) Petrology of sedimentary rocks. Hemphills, University Station, Austin, TX

Govil P, Naidu PD, Radhika TK (2004) Major turbidity flows in the western Indus Fan between 290 and 360 ka BP. Curr Sci 87 (14):1597–1600

Griffin JJ, Windson H, Goldberg ED (1968) The distribution clay materials in the world ocean. Deep-Sea Res 15:433–459

Gupta MVS, Naidu PD, Haake BG, Schiebel R (2005) Carbonate and carbon fluctuations in the Eastern Arabian Sea over 140 ka: implications on productivity changes? Deep-Sea Res II 52:1981–1993

Holeman JN (1968) Sediment yield of major rivers of the world. Water Resour Res 4:737–747

Islam SR (1959) The Indus Submarine Canyon. Oriental Geogr 3 (1):101–104

Kolla V, Coumes F (1987) Morphology, internal structure, seismic stratigraphy and sedimentation of the Indus Fan. AAPG Bull 71:650–677

Kolla V, Henderson L, Biscaye PE (1976) Clay mineralogy and sedimentation in the western Indian Ocean. Deep-Sea Res 23:949–961

Kolla V, Kostecki JA, Robison F, Biscaye PE, Ray PK (1981) Distribution and origin of clay-minerals and quartz in surface sediments of the Arabian Sea. J Sediment Petrol 51(2):563–569

Konta J (1985) Mineralogy and chemical maturity of suspended matter in major rivers sampled under the SCOPE/UNEP project. Mitteilungen aus dem geologisch-paläontologischen Institut, University of Hamburg. Heft 58:557–568

Manely PL, Flood RD (1988) Cyclic sediment deposition within Amazon deep-sea fan. AAPG Bull 72:912–925

Milliman JD, Quraishee GS, Beg MAA (1984) Sediment discharge from the Indus River to the ocean: past, present and future. In: Haq BU, Milliman JD (eds) Marine geology and oceanography of the Arabian Sea and coastal Pakistan. Van Nostrand Reinhold, New York, pp 65–70

Mutti E, Normark WR (1987) Comparing examples of modern and ancient turbidite systems: problems and concepts. In: Leggett JK, Zuffa GG (eds) Marine clastic sedimentology. Graham and Trotman, London, pp 1–38

Naidu AS, Mowatt TC, Somayajulu BLK, Rao KS (1985) Characteristics of clay minerals in the bed loads of major Rivers of India. Mitteilungen aus dem geologisch-paläontologischen Institut, University of Hamburg. Heft 2:559–568

Prell WL, Niitsuma N (1989) Ocean Drilling Program. College Station, TX.Ocean Drill Program Proc Initial Rep 117:319–384

Prins MA, Postma G (2000) Effect of climate, sea level, and tectonics unraveled for last deglaciation turbidite records of the Arabian Sea. Geology 28(4):372–378

Prins MA, Postma G, Cleveringa J, Cramp A, Kenyon NH (2000) controls on terrigenous sediment supply to the Arabian Sea during Later Quaternary: the Indus Fan. Mar Geol 169:327–349

Rao VP, Rao BR (1995) Provenance and distribution of clay minerals in the sediments of the western continental shelf and slope of India. Cont Shelf Res 15:1757–1771

Sirocko F, Lange H (1991) Clay-mineral accumulation rates in the Arabian Sea during the late Quaternary. Mar Geol 97:105–119

Stow DAV (1985) Deep-sea clastics: where are we and where are we going. In: Brenchely PJ, Williams BPJ (eds) Sedimentology: recent developments and applied aspects. Blackwell, Oxford, pp 67–94

Weaver CE (1989) Clays, muds and shales. Developments in Sedimentology 44. Elsevier, Amsterdam

Weimer P (1990) Sequence stratigraphy facies geometrics, and depositional history of the Mississippi fan, Gulf of Mexico. AAPG Bull 74:425–453

Windom HL (1975) Eolian contributions to marine sediments. J Sediment Petrol 45(2):520–529

Abstracts:

- ✓ **Govil P,** Naidu PD (2003). *"Variability of Terrigenous Sediment Supply to the Indus Fan during last 360 kyr"* in abstract volume of the 40th Annual Convention and National Symposium of the Indian Geophysical Union.

- ✓ **Govil P,** Radhika TK (2004). *"Late Quaternary Variations in Planktonic Foraminifera Faunas at the ODP Site 720 in the Arabian Sea"* 41st Annual Convention and National Symposium of the Indian Geophysical Union at N.G.R.I. Hyderabad.

- ✓ **Govil, P.,** Naidu PD, Mulitza S (2006). *"Synchronous δ18O changes in Bay of Bengal sediment core and Greenland Ice Core"* at the 3rd Annual Convention of the Asia Oceania Geosciences Society at Singapore.

- ✓ **Govil P,** Naidu PD, Mulitza S, Kuhnert H (2006). *"Paleo Sea Surface Salinity and Paleo Sea Surface Temperature changes in Bay of Bengal: Implications on Global Climate Changes"* published in AGU Fall Meeting (American Geophysical Union) at San Francisco.

- ✓ **Govil P,** Naidu PD (2007). *"Sea Surface Temperature Changes in the Eastern Arabian Sea,"* XXI Indian Colloquium on Micropalaeontology and Stratigraphy, at BSIP, Lucknow.

- ✓ **Govil P,** Naidu PD (2008). *"Early Deglacial Warming in the Arabian Sea and Bay of Bengal"* published in "International Conference on Terrestrial Planets Evolution through Time" at Physical Research Laboratory, Ahemdabad.